Kashmir Journal of Geology (KJG)

Volume 13, 2021

Institute of Geology
University of Azad Jammu and Kashmir
Muzaffarabad, Pakistan

Publisher: Institute of Geology, University of Azad Jammu and Kashmir, Muzaffarabad, Pakistan

KASHMIR JOURNAL OF GEOLOGY (KJG)

Aim and Scope

The Institute of Geology is one of the pioneer institutes of the University of Azad Jammu and Kashmir (UAJ&K), Pakistan. It was established as Department of Geology in 1973. Currently, the Institute offers BS, MS and PhD degree programs in Applied Geology. The Institute is engaged in exploring the natural resources of the country to play its role in the socio-economic uplift of the country.

The Kashmir Journal of Geology (KJG) initially started in the year 1983 and had successfully published twelve print volumes. The journal got popular among the national and international geoscientific community, however, due to some unavoidable circumstances the journal has been discontinued since 1994.

The Institute of Geology, UAJ&K has revived the journal with the same name (Kashmir Journal of Geology) which aims to provide the most complete and reliable source of information on current development in the field of Geosciences. The journal is set to publish quality research articles covering broad areas of Geosciences on annual basis both in print and online volumes to make them freely available to researchers worldwide.

EDITORIAL BOARD

Publisher: Institute of Geology, University of Azad Jammu and Kashmir, Muzaffarabad, Pakistan

ADVISORY BOARD

FOREWORD

I am extremely pleased to foreword this volume of the Kashmir Journal of Geology (KJG) being published by the Institute of Geology, University of Azad Jammu and Kashmir.

The Kashmir Journal of Geology (KJG) reflects the most comprehensive and reliable source of information on current development in the field of Geosciences by publishing quality research articles covering broad areas of Geosciences. Its purpose is to promote excellence and stimulates the minds engaged in teaching and learning.

Kashmir Journal of Geology forms a valuable addition to the existing body of knowledge and will provide new insight to the university students, researchers of Geosciences, geological investigators and scholars of other contiguous sciences about the variety of earth science related questions and applications.

As the Vice-Chancellor of the University of Azad Jammu and Kashmir, I am extremely proud of the work being done by the editorial board of the Kashmir Journal of Geology who pool their knowledge, skills, and expertise to make the publication of this journal possible.

Prof. Dr. Muhammad Kaleem Abbasi
Vice Chancellor
University of Azad Jammu & Kashmir

CONTENTS

Articles

KASHMIR JOURNAL OF GEOLOGY (KJG)
www.kjg.ajku.edu.pk

The factors of psychometric lightness from loess-paleosol stratigraphy and their environmental significance

Wanyi Zhang[1,*], Jinjiao Yao[1], Jiapeng Cheng[1], Renchao Wan[1], Na Yang[1], Yunhan Tao[1], Chengjun Zhang[1]

[1]School of Earth Sciences & Key Laboratory of Mineral Resources in Western China (Gansu Province), Lanzhou University, Lanzhou, 730000, China.

*Corresponding author:
zhangwanyi@lzu.edu.cn

Received: 10 March 2021
Accepted: 12 August 2021
Published Online: 27 December 2021

Abstract

The psychometric lightness of sediments in different environments such as lakes, loess-paleosols and topsoils is not only influenced by carbonate, organic matter, compounds of the different valence of iron, but also have obvious correlations with magnetization rate, pollen, sediment particles, heavy metal elements, weathering, and others. In this study, the analysis of carbonate, organic matter and major elements content of loess-paleosol strata in Caofeng from Pingliang and Nuanquanshan from Longxi in Gansu showed that the psychometric lightness value L* of loess-paleosol strata in Nuanquanshan has a good correlation with the organic matter content and the psychometric yellow-blue chromaticness value b*, while there is no obvious correlation with the carbonate content. On the other hand, it has moderate correlations with SiO_2, Na_2O and Na_2O+K_2O, and moderate-weak correlations with Al_2O_3, K_2O, chemical index of alteration (CIA) and the paleoclimate index C. There are good correlations between L* and b* in the loess-paleosol section from Caofeng. Moderate-weak correlations are presented between total organic carbon (TOC) content in sediments, Al_2O_3 and paleoclimate index C, while weak correlations are recorded between L* values and SiO_2, Na_2O, K_2O, Na_2O+K_2O and also in weathering index CIA. No correlations are detected between L* and carbonate content. The study indicates that different amount of precipitation leading to differences in the mineral weathering such as feldspar and mica, the sediment formation, the redox properties of the environment, and trace element components, which are intrinsic factors affecting L* during the formation of loess-paleosols. The formation of clay minerals and their content have significant impacts on L* during weathering. L* can possibly be increased in arid areas where the surface of sediment particles covers with carbonate minerals.

Keywords: arid areas; loess-paleosol; psychometric lightness value L*; psychometric yellow-blue chromaticness value b*; organic matter; clay minerals

1. Introduction

The sediment colour models were recognized as valuable sources of paleoclimate evolution since 1990s, when the International Commission on Illumination L*a*b* (CIEL*a*b*, 1976) epochromatic system chromaticity index was used to record millennial-scale climatic environmental changes in marine sediments of the Atlantic Ocean. Researchers have conducted a large number of studies on oceans, loess-paleosol and lakes to gain insight into the environmental indicator significance of chromaticity indexes, psychometric lightness value (L*), psychometric red-green chromaticness (a*) and psychometric yellow-blue chromaticness value (b*, Balsam et al., 1991; Nagao and Nakashima, 1992; Jakobsson et al., 2000; Andrews et al., 2002; Chen et al., 2002; Helmke et al., 2002; Gao et al., 2017; Fang et al., 1999; Porter, 2000; Wang et al. 2015; Chen et al., 2016; Chen et al., 2018; Song et al., 2005; Wu and Shen, 2009; Chen et al., 2016; Moernaut et al., 2017; Du et al., 2019). Gao et al. (2017) even used the sediment chromaticity values a* and b* to distinguish between terrestrial and marine environments. The chromaticity index has also been applied to the study of modern environmental pollution with good results in recent years (Ren et al., 2009).

Nagao and Nakashima (1992) concluded from a study of Atlantic deep-sea sediments that calcium carbonate determines the whiteness of the psychometric lightness value L*, organic matter determines the blackness of value L*; furthermore, redox conditions have a large effect on value L*. The value a* is related to pelagic sediments (grain size factor), manganese carbonate ($MnCO_3$); it is also allied to iron oxides and hydroxides in calcareous turbidites, and colour-bearing minerals containing divalent iron. The value b* is controlled by the hydroxides of iron in calcareous turbidites. A large number of studies have indicated that the values L*, a* and b* from sediments in different environments such as lakes, loess-paleosols and topsoils are not only influenced by carbonates, organic matter and compounds with the different valence of Fe but also have an obvious correlation with magnetic susceptibility, pollen, sediment particles, heavy metal elements and weathering (Chen et al., 1993; Yang and Ding, 2003; Li and Wu, 2004; Ren et al., 2009; Wu and Shen, 2009; He et al., 2010).

The loess-paleosol formation is directly related to sediment source and climate; minerals under specific climatic conditions play a role in determining the colour of loess-paleosols (Nesbitt and Yong, 1982; Guan, 1992; Ji et al., 2001; Chen et al., 2002; Xu and Yang, 2002; Sun et al., 2011). Chemical and biological weathering can alter the structure of the parent mineral; the characteristics of sediment elemental composition can reflect the transformation process (Hao and Guo, 2001; Xu and Yang, 2002; Li and Wu, 2004). Therefore, the knowledge of the relationship between chromaticity indexes L*, a*, b* and the main elements of loess-paleosols can provide insight into the environmental indicator significance of chromaticity indexes and the formation process of loess-paleosols. In this paper, researchers analyze the chromaticity of loess strata from Longxi and Pingliang in the central part of Loess Plateau to further understand the main controlling factors and environmental significance of chromaticity indexes in areas with certain climatic differences.

2. Study region and sample collection

Samples were collected from Nuanquanshan in Longxi and Caofeng in Pingliang, Loess Plateau (Fig. 1). Longxi has an annual precipitation of 415 mm, an average annual temperature of 8 ℃, and a frost-free period of 100-160 days. It is a temperate semi-arid zone in the loess hilly-gully region with less precipitation, sufficient sunshine and large temperature differences, belonging to the temperate continental climate (Ma, 2019). Pingliang is located at the intersection of Shaanxi, Gansu and Ningxia provinces with a monsoonal continental climate, belonging to the Jingwei cold temperate sub-humid zone. The vertical difference in climate is obvious due to the influence of topography and altitude. The region has four distinct seasons, with an average annual temperature of 10 ℃, 1981 hours of sunshine, 476.5 mm of annual precipitation and 163 days of the frost-free period (Ma, 2018).

Nuanquanshan loess-paleosol section is located in the second terrace on the south bank of Weihe River in Dongpu Village, Wenfeng Town, Longxi county (34º52′49.82″N, 104º34′44.16″ E, 1730 m±a.s.l.). 0-10 cm is a light grey argillaceous silt layer, containing abundant modern plant roots; 10-30 cm is grey-white with lumpy calcareous argillaceous silt layer; 30-146 cm is a well-sorted light yellow silt layer with quasi-lamellar structure; fine gravel (<1 cm) occasionally appeared with uneven distribution pattern. 80-120 cm is an inceptisols layer with some porcelain fragments. 146-214 cm is a dark grey thick-bedded silty mud layer with a large number of wormholes and occasional single grains of gravel. Grey clumps are occasionally seen in the middle of the layer and irregular thinly-bedded brick-red muddy silt with plenty of black charcoal particles at the bottom; 214-354 cm (bottom unseen) is a well-sorted grey-white thinly-bedded silt layer with horizontal bedding.

Caofeng loess-paleosol section is located in loess tableland of Qiaojiazhuang, Caofeng Town, Pingliang City (35º30′21.16", 106º55′43.67", 1469 m± a.s.l.). 0-60 cm is a dark grey silty mud layer with abundant modern plant root and high organic matter content. 60-92 cm is a greyish-yellow silty mud layer with fewer plant roots. 92-166 cm is a well-sorted light yellow massive muddy silt layer with small crystals of gypsum in the middle of this layer. 166-242 cm (bottom unseen) is a well-sorted greyish-yellow

massive muddy silt layer.

Samples were collected at 2 cm intervals in each section for environmental index analysis in the laboratory. 178 samples (NQS-1-1~NQS-3-70) were collected from the Nuanquanshan loess-paleosol section with a total thickness of 354 cm. A total of 121 (CF2019-1~121) samples were taken from the

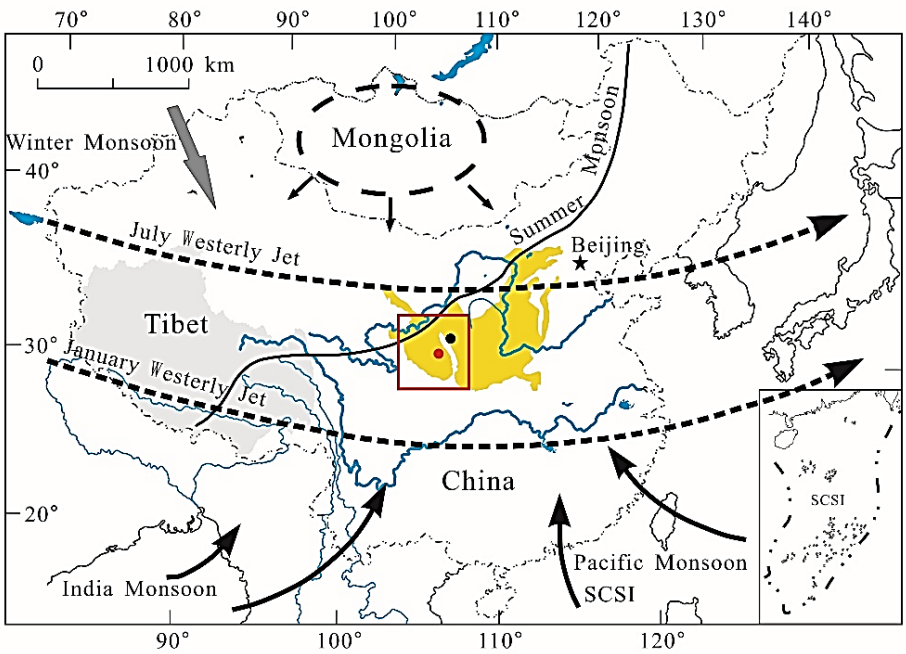

Fig. 1: The range of the Chinese Loess Plateau and the locations of Nuanquanshan and Caofeng loess sections. The black dot represents the Caofeng section in Pingliang; the red dot represents the Nuanquanshan section in Dingxi.

Caofeng loess-paleosol section with a thickness of 242 cm.

3. Methods

The carbonate content was determined by treating sediment samples with dilute HCl and measuring the generated CO_2 volume. The error is less than ±1%. The total organic carbon content (TOC) was determined by the antititration method with dense sulphuric acid and potassium dichromate. The error is less than ±0.5%.

The dried sample was ground to 75 μm before X-ray fluorescence (XRF) measurement. Approximately 4 g sample from the previous step was filled into the presser and an appropriate amount of boric acid was then added from the surround. The sample was pressed into a round block with a diameter of 4 cm and a thickness of 8 mm under the pressure of 30 t/m^2 for 20 seconds. The pressed samples were measured for elemental compositions in Philips Magix (PW2403) XRF spectrometer with an operating temperature of 30±0.05°C and an analytical error of 2%. The analyzed elements are from Be to U. The data were analyzed by the Super Q quantitative software package.

Samples were dried and ground to approximately 0.18 mm. 2-3 g was placed after sieving on a white reference colour plate. After being compacted and flattened, three areas were randomly taken for chromaticity measurements with a Minolta SPAD-503 soil colorimeter from Japan. The Munsell CIEL*a*b* (1976) colour system was applied, and the measured values were averaged to obtain the values of each parameter L*, a* and b* of soil colour. The chromaticity calibration was performed on a white reference plate before measurement. The instrument can measure L* between 0 and 100, and a* and b* between ±60. Positive a* values are biased towards red and negative values towards green, whereas positive b* values are biased towards yellow, negative values towards blue.

4. Results

Sediment colour is greatly influenced by grain size, humidity, mineral composition, etc. (He et al., 2010). The higher is the humidity, the lower is the lightness. The lightness values generally decrease by 20-25 from completely dry to semi-wet soils; when the grain size is less than 45 μm, the sediment colour is uniform and stable (Yang et al., 2001). In this study, values of chromaticity parameters were not affected by grain size and humidity since the samples were dried and ground before the measurement.

Values L*, a* and b* from the Nuanquanshan section (Fig. 2) are 48.3-63.3, 5.1-8.2 and 16.4-25.1 respectively. The carbonate contents range from

10.9% to 20.8 % with increasing values between 184 cm and 218 cm, an abrupt decrease at 184 cm, and thereafter remained relatively constant. The TOC content varies from 2.6% near the top to 1.3% around 30 cm in the soil layer where modern plants are developed and human impact are intensive; it changes from 0.6% to 1.1% in the loess layer (30 cm-146 cm); between 146 cm and 214 cm, the TOC is changing from 0.8% to 2.7%; from 214 cm to 354 cm, TOC contents are between 0.3% and 0.9%.

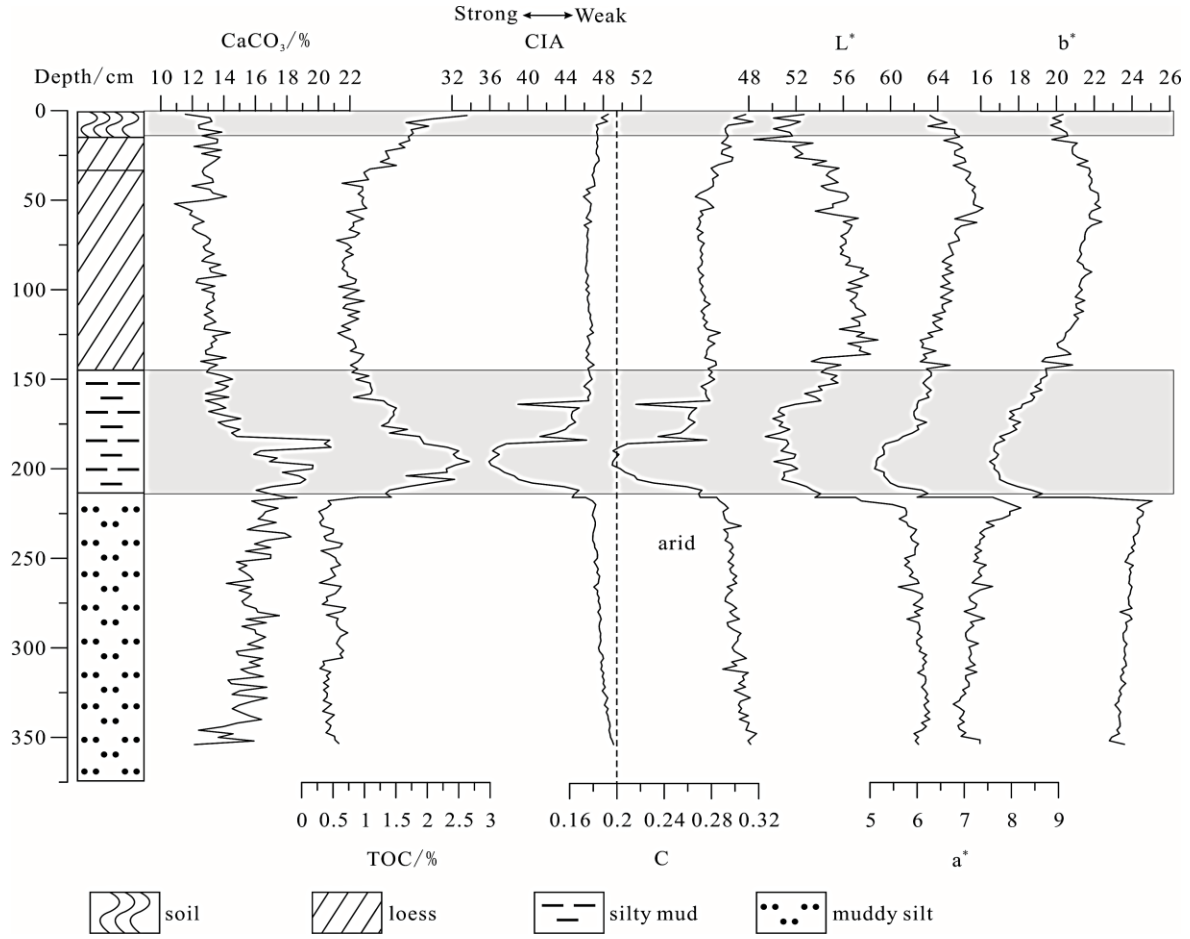

Fig. 2: The analysis results of the CaCO3, TOC content, CIA, the paleoclimate index C and colour chromaticness of Nuanquanshan Loess-Paleosol in Longxi, Gansu.

Values L*, a* and b* from the Caofeng section (Fig. 3) are 50.5-62.4, 7.0-8.9, 18.8-24.0 respectively. The carbonate contents vary from 11.3% to 14.9%. The peak is recorded at the depth of 76 cm. The TOC content varies from 2.5% near the top to 1.0% around 30 cm; it changes from 0.1% to 0.9% between 30 cm and 242 cm.

The chemical weathering index $CIA=Al_2O_3/(Al_2O_3+CaO+Na_2O+K_2O)$ can reflect the loss of soluble elements K, Na, Ca, Mg, etc. during the weathering process (Nesbitt and Yong, 1982); Al and Fe can eventually be enriched into oxides. The CIA value is not only in direct proportion to the degree of weathering into clay minerals but also in direct proportion to the intensity of weathering. CIA values between 50 and 65 reflect a low degree of weathering, indicate a cold and dry climate. CIA values varying from 65 to 85 reflect a moderate degree of weathering, indicate a warm and humid climate while CIA values changing between 85 and 100 reflect a strong degree of weathering, indicating a hot and humid climate (Nesbitt and Yong, 1982). According to the results of elemental analysis, the CIA value of the Nuanquanshan section ranges from 35.9 to 45.1, with a low degree of weathering; the CIA value of the Caofeng section varies from 40.6 to 46.6, with a moderate degree of weathering. Guan (1992) suggested that the paleoclimate can be reconstructed by the paleoclimate index $C=\Sigma(Fe+Mn+Cr+V+Co+Ni)/\Sigma(Ca+Mg+Sr+Ba+Na+K)$. Greater C values indicate wetter conditions and lower C values indicate drier conditions: $C\leq0.2$, extreme dry climate; $0.2<C\leq0.4$, dry climate; $0.4<C\leq0.6$, semi-dry climate; $0.6<C\leq0.8$, semi-humid climate; $0.8<C\leq1.0$, humid climate. The paleoclimatic index C values from the Nuanquanshan section and Caofeng section are from 0.2 to 0.3, which represent arid climate conditions.

The paleoenvironmental evolutions from the Nuanquanshan section and Caofeng section are presented in Figures 2 and 3, respectively. Generally, the Loess Plateau is poorly vegetated and weakly weathered, associated with a dry and cold climate.

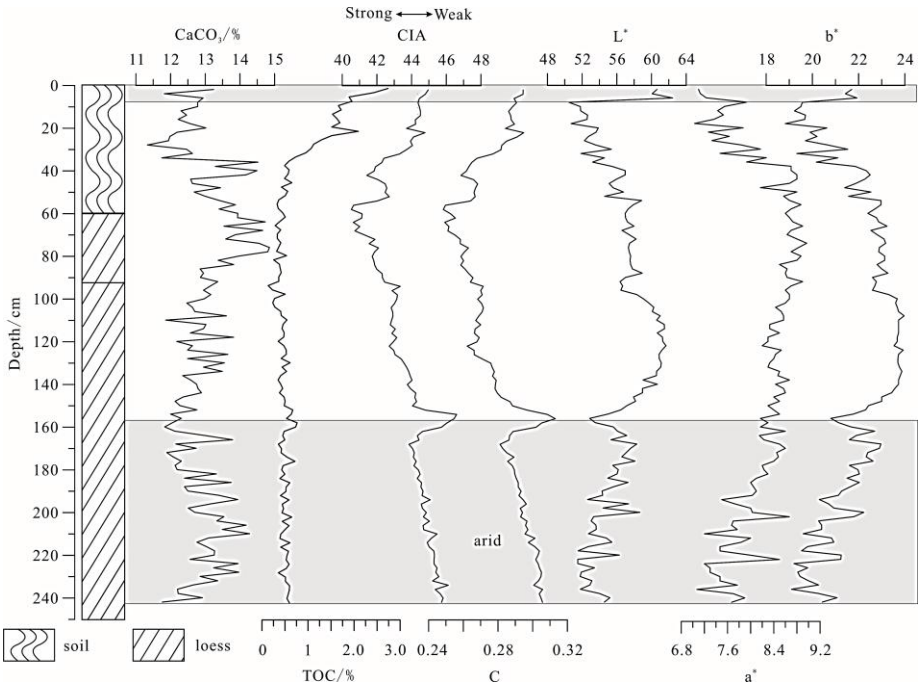

Fig. 3: The analysis results of the CaCO3, TOC content, CIA, the paleoclimate index C colour chromaticness of Caofeng Loess-Paleosol in Pingliang, Gansu.

5. Discussion

Figure 4 reflects the correlation between L* and the carbonate content, the TOC content and the elemental content in sediments from the Nuanquanshan section. L* shows a good correlation with the TOC content (r=0.90), while there is no significant correlation with the carbonate content. On the other hand, it has a moderate correlation with the content of SiO_2, Na_2O and Na_2O+K_2O (r=0.81-0.72) and has a moderate-weak correlation with the content of Al_2O_3 and K_2O, weathering index CIA and paleoclimate index C (r=0.67-0.50).

Figure 5 shows a moderate-weak correlation (r=0.54-0.53) between L* and the TOC content, Al_2O_3 content and paleoclimate index C in the Caofeng section, while there is no correlation with the carbonate content. It has a weak correlation (r=0.27-0.46) with contents SiO_2, Na_2O, K_2O, Na_2O+K_2O and weathering index CIA. In Figures 4 and 5, L* from both sections has a negative correlation with the TOC content and a positive correlation with Na_2O. Furthermore, the correlation between L*and contents SiO_2, Al_2O_3, K_2O, Na_2O+K_2O, weathering index CIA and paleoclimate index C from two sections are showing the opposite pattern.

The correlation between L* and the TOC content is more significant in both sections, particularly in the Nuanquanshan section, while the correlation between the lightness L* value and the carbonate content is weak. However, in Figure 4, if we exclude the soil humus layer and the sediments with high TOC content formed by the back-swamp environment, there is also a positive correlation between the carbonate content and L* in the remaining samples (Fig. 4). There is no correlation between the carbonate content and L* in the Caofeng section. L* was mainly influenced by the organic matter in sections from Zhaosu in Xinjiang, Jingyuan area in Gansu, Danfengchafang village in southern Shaanxi and Xiaoshu in Zhoujiashan, Nanjing (Shi et al., 2012; Li et al., 2014; Gao et al., 2015; Liu et al., 2015). It was also reported that L* in the Zhaosu section and the Jingyuan section were also influenced by the calcium carbonate formation mechanism (Shi et al., 2012; Li et al., 2014). It is suggested that the carbonate content in the loess-paleosol section also has some impact on L*. The correlation between the carbonate content and L* is less obvious under the stronger leaching (Liu et al., 2015). At the same time, the chromaticity index of the sediment, such as peat with high organic matter content formed in marsh environments may not be an obvious indicator of environmental information due to more complex chromogenic substances.

Shields and Paul (1968) and Krishnan et al. (1981) concluded that organic matter is the most important factor leading to the dark soil colour. It was

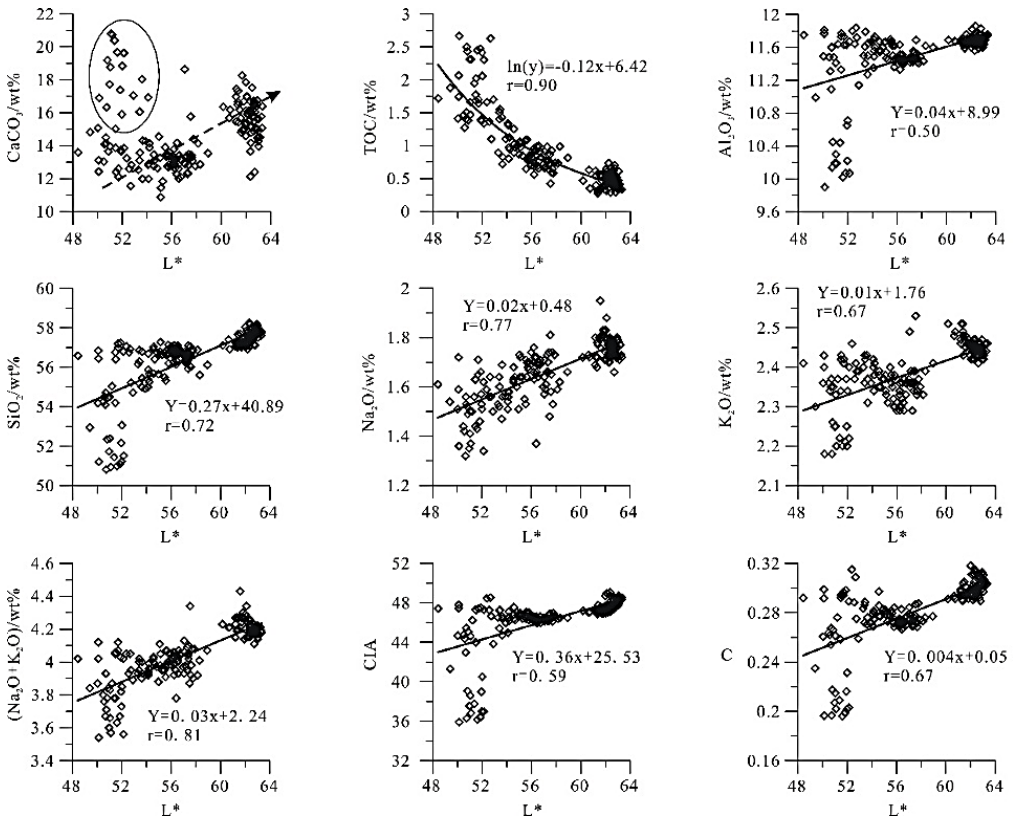

Fig. 4: The correlation between lightness L* and geochemical parameters in the Nuanquanshan loess section, Longxi.

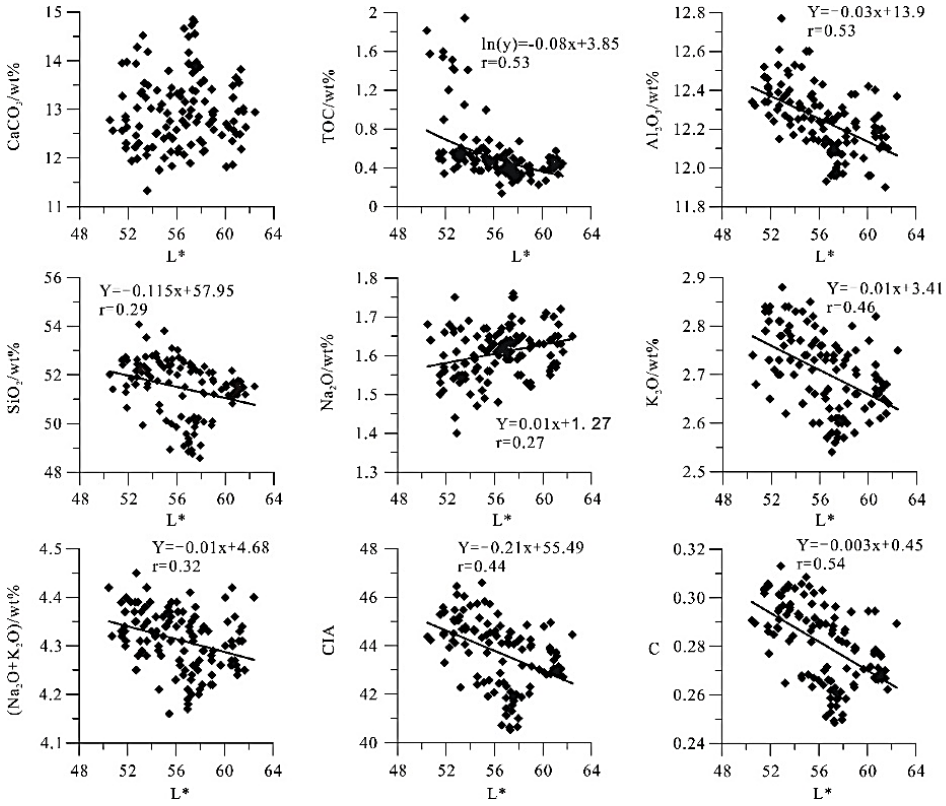

Fig. 5: The correlation between lightness L* and geochemical parameters in the Caofeng loess section, Pingliang.

found that the lightness of the soil Munsell colour system was linearly correlated with the content of organic matter or organic carbon, and the correlation coefficient varied with soil development in different areas, reaching to 0.9 or even higher. The organic matter content in soil is influenced by the ecological environment; better vegetation is conducive to the formation of high organic matter soil under suitable water-heat conditions (Shields and Paul, 1968; Krishnan et al., 1981). In the Loess Plateau, regional precipitation and temperature affect the development of vegetation, the degree of leaching and weathering of rocks and minerals. By analyzing the colour of topsoil in different areas, L* values showed a significant negative correlation with precipitation and an insignificant correlation with temperature (Yang et al., 2001; Song et al., 2016). In contrast, Ji et al. (2013) suggested that soil chromaticity was not only related to rainfall but also had a good correlation with altitude and temperature. According to Yang et al. (2001), L* is closely related to organic matter accumulation, humus processes and carbonation processes; and the relationship with climate exists only in the temperate humid-arid area. Different minerals play an important role in the chromaticity of sediments because they have specific colours. Weathering leads to clayization of minerals such as feldspar; clay minerals with different colours were formed under different weathering intensities, parent rock types, acidic and alkaline media, and temperature. Besides, the clay absorbs iron-oxide components during weathering, leading to the variation in lightness, darkness and reddish-brown tones on the surface of feldspar (Li and Wu, 2004).

The weathering products of the rocks are related to the type of parent rock and the intensity of weathering. Compared with the parent rock, the weathering products have lower SiO_2 and K_2O content and higher content of oxides such as Al_2O_3 and Fe_2O_3 (Shang et al., 2005). The weathering of the parent rocks, containing mainly quartz and sodium-calcium feldspar series, formed clay minerals mainly with halloysite and kaolinite, followed by illite; the weathering of black mica mainly formed mica-vermiculite; the weathering of potassium feldspar formed illite, ilmenite/montmorillonite mixed layer and chlorite minerals (Shang et al., 2005). The sodium-calcium feldspar series and potassium feldspar not only differ greatly in rock colour but also change greatly in Na and K ion content. Precipitation leaching experiments on loess in northwest China have shown that Na^+, Ca^{2+}, Mg^{2+} and Cl^- are mainly leached out through rapid inorganic salt dissolution processes, while the leaching release of K^+ and SiO_2 is associated with slow weathering of silicate minerals (Xu and Yang, 2002). Therefore, the intensity of weathering causes differential changes in elements such as Na, K, Mg, Al_2O_3 and SiO_2 in the weathering products, resulting in differences in the colour of the final weathering products. Although sections Nuanquanshan and Caofeng are in the same arid steppe zone with C values of $0.2<C\leq0.4$, the annual rainfall of 415 mm in Nuanquanshan is slightly less than the annual rainfall of 476.5 mm in the Pingliang area. With Liupan Mountains as the boundary, there is a clear difference in the heavy minerals in the loess between the eastern and western regions. It indicates that the degree of weathering tends to weaken from east to west during the late diagenesis process (Chen and Chen, 1993). L* in Figs. 4 and 5 have obvious correlations with Na, K, Al_2O_3 and SiO_2, but the Nuanquanshan and Caofeng sections reflect the opposite characteristics of L* correlations with SiO_2, Al_2O_3, K_2O, Na_2O+K_2O, weathering index CIA, and paleoclimate index C. The study assumes that it mainly related to the intensity of weathering.

In addition, many quartz and feldspar surfaces are often covered with carbonate films due to low rainfall in arid areas (Ye, 2000). The Nuanquanshan loess-paleosol sediments are dominated by common hornblende, epidote and opaque minerals (62-82%); common hornblende has clayization of illite on its surface, and epidote is heavily weathered (Wen et al., 1982). It indicates that with the increase of SiO_2 and Al_2O_3 content in the Nuanquanshan loess-paleosol stratum, the carbonate and purer illite covering the surface of the particles lead to the increase of L*; while in the Caofeng stratum, where weathering is stronger, the relatively large leaching effect leads to quartz and clay mineral particles not only without the covering of carbonate and other minerals but also due to the contamination of other trace chromogenic elements in the claying process, resulting in L* decreasing with increased SiO_2, Al_2O_3 content. For example, Ren et al. (2009) revealed a negative correlation between Cu, Pb, Zn and L* in the sediments of the low, middle and high tidal flats of Chongming Island, with correlation coefficients up to r_{Cu}=-0.97, r_{Pb}=-0.88 and r_{Zn}=-0.98.

Field observation shows that the lower part of the Nuanquanshan section is mainly composed of silt with low mud content, well sorted and rounded; the horizontal bedding is well developed. It indicates a weak hydrodynamic environment. The analysis results reveal high L* values and low TOC content in the lower part (Fig. 4). The lower TOC content is related to the dilution effect of the higher coarse-grained quartz and feldspar particle content of the sediment. It suggests that sediment lightness values increase significantly with lower clay content and cleaner surfaces of quartz and feldspar particles. Balsam et al. (1999) also found in their study of marine sediments that lightness values decrease with higher clay content. Therefore, in general, increasing clay mineral content in sediments has a greater effect on L* values.

It has been shown that L* is largely controlled by the colour component a* and b* during loess accumulation in the loess-paleosol sections from Zhaosu and Pamir Plateau (Li et al., 2014; Chen et al., 2018). L* in the loess-paleosol sequence in the last

glacial-interglacial cyclone of the Chaona section in Lingtai County, Gansu Province are influenced by the hematite/goethite ratio (Wang et al., 2015). Figure 6 shows the correlation among L*, a*, b* and a*/b* values in the Nuanquanshan and Caofeng section: a moderate-weak degree of correlation among L*, a* and a*/b*, a strong correlation between L* and b*; especially, the correlation between L* and b* in the more humid Caofeng section is better than that in the relatively arid Nuanquanshan section. Since a* and b* are related to divalent and trivalent Fe, they can indicate the redox status of the environment. It suggests that the arid area, in general, has less rainfall and higher temperature, but relatively higher rainfall may lead to enhanced weathering and thus more iron oxide formation during clayization.

6. Conclusion

The purpose of the current study was to determine the correlation between chromaticity indexes L*, a*, b* and geochemical parameters including the carbonate content, the TOC content and major element content of loess-paleosols sections in Caofeng and Nuanquanshan in Gansu. The study shows that the TOC content, mineral composition and b* are the main factors affecting chromaticity.

The TOC content of loess-paleosol strata in relatively arid areas has a good correlation with L*. However, in the sediments with high TOC content formed in the soil humus layer, back-swamp and other environments, L* is not efficient for indicating the deposition environment. The high content of clay minerals in the loess-paleosol stratum can significantly reduce the lightness value L*. The correlation between the carbonate content of loess-paleosol strata and L* is not obvious and is related to the leaching effect of more rainfall. However, arid areas can result in an increase in lightness values due to the carbonate minerals covering the surface of sediment particles. The loess-paleosol stratum in the arid area is influenced by the environmental medium, and the increase in oxidation increases can result in a better correlation between L* and b*.

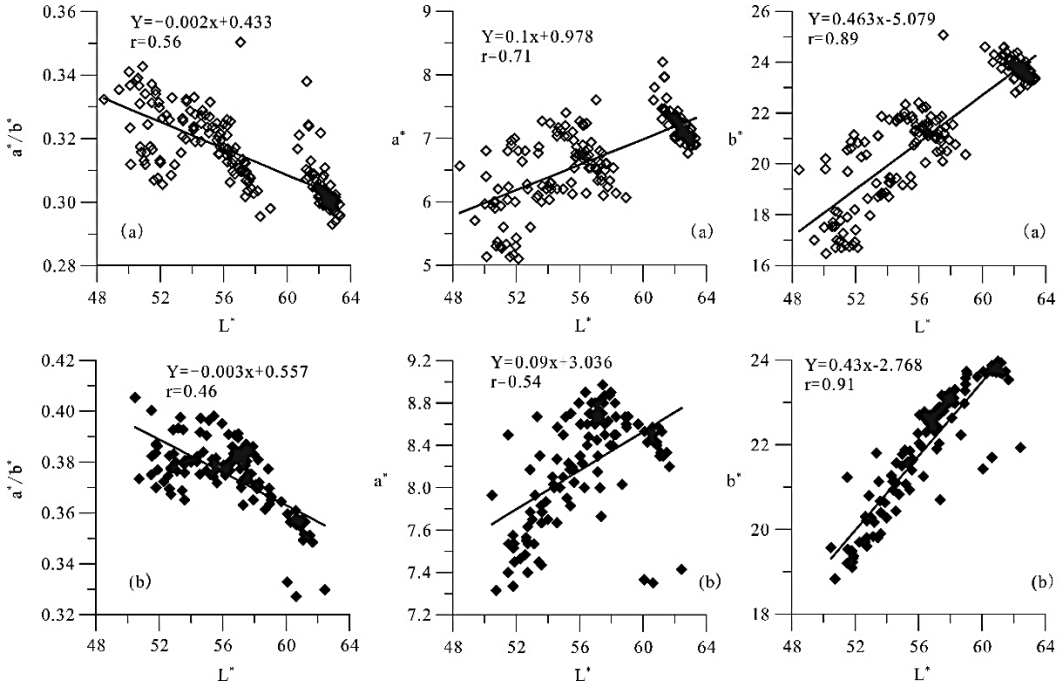

Fig. 6: The relationship among L* and a*, b*, a*/b* of the loess-paleosol sections Nuanquanshan (a) and Caofeng (b).

Acknowledgement

We wish to thank Dr. Xiaoyu Wang, Dr. Rong Fan, Mingwei Liao, Wenbin Huang, Jinlei Fan, Yang Liu, Meigeng Yu, Yuanxin Li, Xiaohu Liu, Miao Yin, Jiaxin Zhang for help during the field trip. We furthermore acknowledge the critical comments and suggestions by the anonymous reviewers, and the editor Dr. Muhammad Basharat and Dr. Fahad Hameed who helped to improve the manuscript. The research was supported by the Fundamental Research Funds for the Central Universities, Lanzhou University (2022019zr46) and the National Natural Science Foundation of China (41571177).

References

Andrews, J.T., Barber, D.C., 2002. Dansgaard-Oeschger events: is there a signal off the Hudson Strait Ice Stream? Quaternary Science Reviews, 21(1), 443-454.

Balsam, W.L., Deaton, B.C., Damuth, J.E., 1991. Evaluating optical lightness as a proxy for

carbonate content in marine sediment cores. Marine Geology, 161, 141-153.

Balsam, W.L., Deaton, B.C., Damuth, J.E., 1999. Evaluating optical lightness as a proxy for carbonate content in marine sediment cores. Marine Geology, 161, 141-153.

Chen, F.H., Jia, J., Chen, J.H., Li, G.Q., Zhang, X.J., Xie, H.C., Xia, D.S., Huang, W., An, C.B., 2016. A persistent Holocene wetting trend in arid central Asia, with wettest conditions in the late Holocene, revealed by multi-proxy analyses of loess-paleosol sequences in Xinjiang, China. Quaternary Science Reviews, 146, 134-146.

Chen, G.Y., Chen, F.H., 1993. A study on heavy mineral compositions of Jiuzhoutai loess profile, Lanzhou. Journal of Lanzhou University (Natural Sciences), 29(4), 257-267 (in Chinese with English abstract).

Chen, J., Ji, J.F., Balsam, W., Chen, Y., Liu, L.W., An, Z.S., 2002. Characterization of the Chinese loess-palesol stratigraphy by whiteness measurement. Palaeogeography Palaeoclimatology Palaeoecology, 183(3/4), 287-297.

Chen, J., Yang, T.B., Zeng, B., He, Y., Ji, Q, 2018. Chroma characteristics and its paleoclimatic significance in Pamir Loess section，China. ActaASedimentologicaSinica, 36(2), 333-342 (in Chinese with English abstract).

Du, D.D., Muhammad, S.M., Dembele, B., Zhang, C.J., 2019. Paleoclimatic changes reflected by diffuse reflectance spectroscopy since Last Glacial Maximum from Selin Co Lake sediments, central Qinghai-Tibetan Plateau. Arid Land Geography, 42(3), 551-558 (in Chinese with English abstract).

Fang, X.M., Pan, B.T., Guan, H.D., Li, J.J., 1999. A study of the millennial-scale instability of summer monsoon in Lanzhou since about 60 ka. Chinese Science Bulletin, 44(4), 436-439 (in Chinese).

Gao, F., Xu, Q.M., Yuan, G.B., Yang, J.L., Fan, Y.L., Liu, W.D., Zhao, J.J., 2017. Sedimentary environment evolution of borehole TZ02 in the northern Bohai Bay during late Cenozoic. Quaternary Sciences, 37(3), 667-678 (in Chinese with English abstract).

Gao, P.K., Pang, J.L., Huang, C.C., Zhou, Y.L., Bian, H.Y., Wang, L.B., Wang, X.J., 1992. Chroma characteristics and its significances of the Chafangcun Loess-paleosol profile in southeast Shaanxi, China. Acta Sedimentologica Sinica, 33(3), 537-542 (in Chinese with English abstract).

Guan, Y.Z., 1992. The element, clay mineral and depositional environment in Horqin sand land. Journal of Desert Research, 12(1), 9-15 (in Chinese with English abstract).

Hao, Q.Z., Guo, Z.T., 2001. A quantitative study of the intensity of weathering soil formation in the loess-paleosol sequence since 1.2 Ma and the evolution of summer monsoon in East Asia. Science in China, 31(6), 520-528 (in Chinese).

He, L., Sun, YB., An, Z.S., 2010. Changing color of Chinese loess: controlling factors and paleoclimatic significances. Geochemica, 39(5), 447-455 (in Chinese).

Helmke, J.P., Schulz, M., Bauch, H.A., 2002. Sediment-Color record from the Northeast Atlantic reveals patterns of millennial-scale climate variability during the past 500 000 years. Quaternary Research, 57, 49-57.

Jakobsson, M., Løvlie, R., Al-Hanbali. H., Arnold, E., Backman, J., Mörth, M., 2000. Manganese and color cycles in Arctic Ocean sediments constrain Pleistocene chronology. Geology, 28(1), 23-26.

Ji, H.L., Zhou, W.J., Zhang, Y.P., Sha, L.Q., 2013. Relationship between soil color and climatic factors in Yunnan Journal of Yunnan University (Natural Sciences) 35, 352-358 (in Chinese with English abstract).

Ji, J.F., Balsam, W., Chen, J., 2001. Mineralogic and climatic interpretations of the Luochuan loess section (China) based on diffuse reflectance spectrophotometry. Quaternary Research, 56(1), 23-30.

Krishnan, P., Butler, B.J., Hummel, J., 1981. Close-range sensing of soil organic matter. Transactions of the ASAE, 24(2), 306-311.

Li, R.Y., Wu, L.F., 2004. Research on characteristic indexes of weathering intensity of rocks. Chinese Journal of Rock Mechanics and Engineering 22, 3830-3833 (in Chinese with English abstract).

Li, Y., Song, Y.J., Wang, Q.S., 2014. Chromaticity variation characteristics and paleoclimatic significance of the Zhaosu loess profile in Xinjiang. Journal of Earth Environment, 5(2), 67-75 (in Chinese).

Liu, F., Wang, H., Qin, Y.F., Ren, S.F., Zheng, X.M., 2015. Chroma characteristics of the Zhoujiashan Xiashu loess profile in Nanjing and its significance. Marine Geology & Quaternary Geology, 35(5), 143-151 (in Chinese with English abstract).

Ma, L.J., 2018. Analysis of suitable climatic conditions for hops cultivation in Pingliang City. Modern Agriculture Technology, 1, 222 (in Chinese with English abstract).

Ma, X.C. Spatiotemporal change of social-ecological system resilience and its influencing factors in loess hilly-gully region of central Gansu: a case study of Longxi county, Gansu province. Master thesis, Lanzhou University, 2019 (in Chinese with English abstract).

Moernaut, J., Van Daele, M., Strasser, M., Clare, M.A., Heirman, K., Viel, M., Cardenas, J., Kilian, R., de Guevara, B.L., Pino, M., Urruta, R., De Batist, M., 2017. Lacustrine turbidites produced by surficial slope sediment remobilization: a mechanism for continuous and

sensitive turbidite paleoseismic records. Marine Geology, 384, 159-176.

Nagao, S., Nakashima, S., 1992. The factors controlling vertical color variations of north Atlantic Maderia Abyssal plain sediments. Marine Geology, 109(1-2), 83-94.

Nesbitt, H.W., Yong, G.M., 1982. Early Proterozoic climates and plate motions inferred from major element chemistry of lutites. Nature, 299, 715-717.

Porter, S.C., 2000. High-resolution paleoclimatic information from Chinese Eolian sediments based on grayscale intensity profiles. Quaternary Research, 53, 70-77.

Ren, S.F., Zheng, X.M., Zhou, L.M., Zhu, L.F., Song, L.H., Wang, Y.J., Huang, D.F., 2009. A new assessment method of heavy metal pollution in tidal flat sediments using color indexes. Acta Scientiae Circumstantiae, 29(12), 2606-2615 (in Chinese with English abstract).

Shang, Y.J., Yue, Z.Q., Wang, S.J., Tu, X.B., 2005. Distinctive features of chemical components and minerals in mass and clay portions of completely decomposed granite. Chinese Journal of Geology 40, 95-104 (in Chinese with English abstract).

Shi, P.H., Yang, T.B., Tian, Q.C., Wang, J.Y., 2012. Analysis of chromaticity change characteristics and paleoclimate significance of Jingyuan loess-paleosol. Journal of Lanzhou University (Natural Sciences), 48(2), 15-23 (in Chinese).

Shields, J.A., Paul, E.A., 1968. Spectrophotometry measurement of soil color and its relationship to moisture and organic matter. Canadian Journal of Soil Science, 48, 271-280.

Song, C.H., Bai, J.F., Zhao, Y.D., Jin, H.B., Meng, Q.Q., 2005. The Color of lacustrine sediments recorded climatic changes from 13 to 4. 5 Myr in Linxia Basin. Acta Sedimentologica Sinica, 23(3), 507-513 (in Chinese with English abstract).

Song, R.Q., Zhu, Y., Lv, B., Zhang, J.Y., Zheng, Y.P., He, L., 2016. Chroma peat deposits in the hill of Fujian basin and their environmental significance. Journal of Fujian University (Natural Sciences Edition), 32(3), 116-123 (in Chinese with English abstract).

Sun,Y., He, L., Liang, L., An, Z.S., 2011. Changing color of Chinese loess: Geochemical constraint and paleoclimatic significance. Journal of Asian Earth Sciences, 40(6), 1131-1138.

Wang, Q.S., Song, Y.J., Li, J.J., Zhao, Z.J., Rong, P., 2015. Characteristics of color in Chaona section and its paleoclimatic significance during the Last Glacial-interglacial cycle. Scientia Geographica Sinica, 35(11), 489-494 (in Chinese with English abstract).

Wen, Q.Z., Zheng, H.H., Han, J.H., Wang, J.D., Lin, S.M., Qiao, Y.L., Wei, Y.L., Diao, G.Y., 1982. Loess of Longxi basin in Gansu province. Scientia Geographica Sinica, 2(8), 202-209 (in Chinese with English abstract).

Wu, J., Shen, J., 2009. Paleoenvironmental and paleoclimatic changes reflected by diffuse reflectance spectroscopy and magnetic susceptibility from Xingkai Lake sediments. Marine Geology & Quaternary Geology, 29(3), 123-131 (in Chinese with English abstract).

Xu, H., Yang, X., 2002. Releasing of major elements from loess leached by rain. Soil and Environmental Sciences 11(1), 38-41 (in Chinese with English abstract).

Yang, S.L., Ding, Z.L., 2003. Color reflectance of Chinese loess and its implications for climate gradient changes during the last two glacial-interglacial cycles. Geophysical Research Letters, 30(20), 158-161.

Yang, S.L., Fang, X.M., Li, J.J., An, Z.S., Chen, S.Y., 2001. Qualitative to semi-quantitative relationship study between topsoil color and climate. Science in China (Series D), 31, 175-181 (in Chinese).

Ye, W., 2000. The mineral characteristics of loess and depositing environment in Yili area, Xinjinag. Arid Zone Research, 17(4), 1-10 (in Chinese with English abstract).

Table 1: The data analysis from Nuanquanshan section.

Sample-Nuquanshan	L*	a*	b*	$CaCO_3$%	TOC	CIA	C
NQS-1-1	52.68	6.28	20.35	11.56	2.63	48.52	0.31
NQS-1-2	50.10	6.40	19.80	13.11	2.07	47.79	0.30
NQS-1-3	52.37	6.63	20.27	13.24	1.66	48.44	0.32
NQS-1-4	51.50	6.23	19.70	12.40	2.02	47.25	0.29
NQS-1-5	50.10	6.80	20.20	12.44	1.74	47.44	0.29
NQS-1-6	51.47	6.80	20.53	13.87	1.78	47.30	0.29
NQS-1-7	51.70	6.90	20.60	12.61	1.70	47.39	0.29
NQS-1-8	48.43	6.57	19.77	13.60	1.72	47.42	0.29
NQS-1-9	53.43	6.87	21.10	13.58	1.55	47.29	0.29
NQS-1-10	51.70	6.97	20.87	12.11	1.64	47.41	0.30
NQS-1-11	52.13	6.80	20.83	13.85	1.34	47.27	0.29
NQS-1-12	52.57	6.80	20.87	12.60	1.36	47.26	0.29
NQS-1-13	51.90	7.00	21.13	13.75	1.39	47.49	0.30
NQS-1-14	54.57	7.03	21.67	13.45	1.25	47.56	0.30
NQS-1-15	53.40	6.77	21.10	13.11	1.51	47.20	0.29
NQS-1-16	55.63	6.97	21.73	12.76	1.09	47.03	0.28
NQS-1-17	54.83	7.13	21.80	12.64	0.99	47.02	0.28
NQS-1-18	54.57	7.10	21.70	12.76	1.02	46.82	0.29
NQS-1-19	55.07	7.03	21.87	13.27	1.06	46.98	0.28
NQS-1-20	55.57	7.10	21.87	13.33	0.65	47.07	0.28
NQS-1-21	54.13	7.23	21.73	11.98	0.97	47.11	0.28
NQS-1-22	54.67	7.17	21.80	13.12	0.97	46.22	0.28
NQS-1-23	56.20	7.23	22.20	13.31	0.90	46.59	0.27
NQS-1-24	56.43	7.23	22.23	14.17	0.99	45.91	0.27
NQS-1-25	56.23	7.20	22.23	12.93	0.96	46.34	0.28
NQS-1-26	55.10	7.20	22.03	10.87	0.98	46.72	0.28
NQS-1-27	55.13	7.40	22.33	11.45	1.04	46.64	0.28
NQS-1-28	53.63	7.27	21.87	11.99	0.72	46.62	0.27
NQS-1-29	55.27	7.03	21.73	11.84	0.85	46.39	0.27
NQS-1-30	57.27	6.80	21.77	12.29	0.99	46.20	0.27
NQS-1-31	56.00	7.27	22.40	12.75	0.82	46.76	0.27
NQS-1-32	56.73	6.93	21.87	12.11	0.83	45.98	0.27
NQS-1-33	56.57	6.83	21.63	12.02	0.76	46.41	0.27
NQS-1-34	56.37	6.80	21.53	12.33	0.92	46.34	0.27
NQS-1-35	55.80	6.87	21.50	12.86	0.85	46.27	0.27
NQS-1-36	56.20	6.90	21.50	13.15	0.56	46.38	0.27
NQS-1-37	56.23	6.67	21.33	13.06	0.73	46.36	0.27
NQS-1-38	55.73	6.70	21.27	12.69	0.79	46.28	0.27
NQS-1-39	56.00	6.73	21.23	12.83	0.70	46.33	0.27
NQS-1-40	55.77	6.77	21.33	13.38	0.82	46.25	0.27

Continued…

Sample-Nuquanshan	L*	a*	b*	CaCO3%	TOC	CIA	C
NQS-1-41	56.53	6.63	21.23	12.87	0.69	46.23	0.27
NQS-1-42	56.57	6.53	21.10	12.61	0.65	46.29	0.27
NQS-1-43	56.20	6.73	21.40	13.79	0.68	46.22	0.27
NQS-1-44	57.70	6.60	21.47	13.10	0.65	46.12	0.27
NQS-1-45	57.43	6.77	21.87	13.19	0.73	46.18	0.27
NQS-1-46	58.13	6.53	21.53	14.14	0.73	46.41	0.27
NQS-1-47	57.30	6.60	21.33	12.37	0.87	46.30	0.27
NQS-1-48	56.43	6.70	21.27	12.24	0.85	46.15	0.27
NQS-1-49	57.60	6.50	21.20	13.43	0.59	46.47	0.27
NQS-1-50	56.27	6.77	21.37	12.61	0.92	46.17	0.27
NQS-1-51	57.20	6.63	21.17	13.38	0.77	46.54	0.27
NQS-1-52	57.07	6.50	21.00	13.29	0.66	46.32	0.27
NQS-1-53	56.60	6.73	21.50	13.41	1.00	46.34	0.27
NQS-1-54	56.97	6.53	21.03	12.98	0.71	46.49	0.28
NQS-1-55	57.07	6.53	21.07	12.89	0.66	46.43	0.27
NQS-1-56	57.63	6.60	21.43	13.30	0.92	46.44	0.27
NQS-1-57	57.90	6.33	20.93	12.76	0.74	46.67	0.27
NQS-1-58	56.70	6.53	21.17	13.19	0.91	46.60	0.27
NQS-1-59	57.37	6.33	21.00	13.49	0.77	46.75	0.28
NQS-1-60	57.40	6.40	20.87	12.81	0.64	46.85	0.27
NQS-1-61	55.67	6.53	20.73	12.76	0.78	46.60	0.28
NQS-1-62	57.77	6.23	20.50	14.40	0.58	46.95	0.29
NQS-1-63	57.13	6.33	20.47	13.30	0.68	46.31	0.28
NQS-1-64	58.93	6.07	20.37	13.55	0.82	46.47	0.28
NQS-1-65	56.40	6.13	20.03	13.19	0.85	46.60	0.28
NQS-1-66	57.50	6.10	20.10	13.28	0.87	46.42	0.28
NQS-1-67	57.37	6.40	20.50	12.84	0.78	46.20	0.28
NQS-1-68	58.30	6.13	20.77	12.87	0.99	46.48	0.28
NQS-1-69	54.20	6.20	19.43	14.14	0.95	46.18	0.27
NQS-1-70	53.30	6.07	19.23	12.54	0.89	46.50	0.28
NQS-1-71	55.80	6.70	20.85	13.59	0.78	47.03	0.28
NQS-1-72	54.57	6.20	19.43	13.08	0.89	46.39	0.28
NQS-1-73	54.13	6.30	19.47	12.91	0.80	46.52	0.28
NQS-2-1	55.47	6.30	19.50	13.91	1.07	46.59	0.28
NQS-2-2	54.97	6.20	19.17	14.55	0.87	46.81	0.28
NQS-2-3	55.55	6.13	19.18	13.47	1.09	46.35	0.28
NQS-2-4	53.90	6.20	18.87	14.28	1.10	45.96	0.27
NQS-2-5	54.20	6.30	19.23	13.88	1.12	46.51	0.28
NQS-2-6	52.73	6.20	18.63	12.83	1.10	46.64	0.28
NQS-2-7	53.65	6.25	18.85	14.31	0.83	46.38	0.28
NQS-2-8	54.10	6.03	18.70	12.84	1.31	46.47	0.28
NQS-2-9	51.93	6.00	18.20	13.64	1.37	38.98	0.22

Continued…

Sample-Nuquanshan	L*	a*	b*	CaCO3%	TOC	CIA	C
NQS-2-10	50.70	6.00	18.13	14.13	1.51	45.45	0.27
NQS-2-11	50.50	5.93	17.53	13.04	1.46	44.76	0.26
NQS-2-12	51.03	5.93	17.77	13.95	1.47	44.62	0.26
NQS-2-13	50.03	5.97	17.50	15.07	1.41	44.67	0.26
NQS-2-14	50.87	6.20	18.10	13.65	1.38	45.07	0.27
NQS-2-15	50.58	6.00	17.70	14.09	1.27	44.37	0.26
NQS-2-16	51.47	6.03	17.90	15.02	1.68	44.00	0.26
NQS-2-17	50.67	5.90	17.53	14.50	1.40	42.97	0.25
NQS-2-18	49.40	5.70	17.00	14.83	1.88	41.30	0.23
NQS-2-19	51.20	5.60	17.27	20.72		46.23	0.28
NQS-2-20	51.37	5.33	16.80	20.38	1.95	37.76	0.21
NQS-2-21	51.10	5.27	16.70	20.80	2.32	36.83	0.20
NQS-2-22	50.73	5.30	16.70	16.33	2.50	36.29	0.20
NQS-2-23	51.97	5.30	16.93	15.90	2.41	37.00	0.20
NQS-2-24	51.83	5.17	16.80	17.39	2.48	36.38	0.20
NQS-2-25	50.13	5.13	16.47	16.90	2.67	35.91	0.20
NQS-2-26	51.60	5.13	16.73	19.66	2.45	36.15	0.20
NQS-2-27	52.13	5.10	16.70	19.62	2.30	36.97	0.20
NQS-2-28	50.97	5.30	16.93	17.72	2.32	37.53	0.21
NQS-2-29	51.03	5.30	17.00	18.76	1.66	38.59	0.21
NQS-2-30	50.80	5.37	17.00	19.19	2.43	39.05	0.22
NQS-2-31	52.00	5.43	17.40	18.85	2.06	40.51	0.23
NQS-2-32	52.90	5.60	17.97	17.05	1.70	43.84	0.26
NQS-2-33	53.40	6.10	18.70	16.05	1.40	45.42	0.27
NQS-2-34	54.10	6.23	19.27	16.93	1.34	44.97	0.27
NQS-2-35	53.60	6.00	18.77	18.04	1.43	44.70	0.27
NQS-3-1	57.05	7.60	21.70	18.64	0.92	46.12	0.28
NQS-3-2	57.53		25.07	15.77	0.42	46.87	0.29
NQS-3-3	60.17		24.60	16.36	0.47	47.19	0.29
NQS-3-4	61.23	8.20	24.27	17.44	0.40	47.08	0.29
NQS-3-5	61.37	7.97	24.60	16.65	0.27	46.95	0.29
NQS-3-6	61.33	7.97	24.57	16.48	0.32	46.85	0.29
NQS-3-7	60.73	7.80	24.30	16.17	0.35	47.06	0.29
NQS-3-8	61.37	7.47	24.27	17.32	0.29	47.16	0.29
NQS-3-9	61.50	7.63	24.40	16.20	0.32	47.13	0.31
NQS-3-10	62.20	7.43	24.37	15.50	0.51	47.02	0.29
NQS-3-11	62.00	7.33	24.30	17.85	0.50	46.93	0.29
NQS-3-12	61.70	7.43	24.07	18.26	0.36	46.89	0.29
NQS-3-13	61.83	7.33	24.10	16.68	0.39	46.88	0.29
NQS-3-14	62.37	7.33	24.17	15.95	0.65	47.07	0.30
NQS-3-15	62.10	7.23	23.97	16.97	0.61	47.10	0.30
NQS-3-16	62.07	7.37	24.10	15.37	0.31	47.33	0.30

Continued…

Sample-Nuquanshan	L^*	a^*	b^*	$CaCO_3$%	TOC	CIA	C
NQS-3-17	62.07	7.23	23.83	16.99	0.45	47.39	0.30
NQS-3-18	61.20	7.30	23.77	16.97	0.54	47.37	0.30
NQS-3-19	61.60	7.20	23.63	14.80	0.56	47.02	0.29
NQS-3-20	61.20	7.47	24.07	15.46	0.62	47.27	0.30
NQS-3-21	61.70	7.33	23.87	14.95	0.46	47.47	0.30
NQS-3-22	61.90	7.30	23.95	15.34	0.50	47.33	0.30
NQS-3-23	61.60	7.37	23.87	15.68	0.54	47.61	0.30
NQS-3-24	62.25	7.25	23.88	15.87	0.44	47.52	0.30
NQS-3-25	62.40	7.17	23.83	14.16	0.28	47.47	0.30
NQS-3-26	60.67	7.60	24.00	15.69	0.63	47.00	0.29
NQS-3-27	61.87	7.33	23.93	14.97	0.59	47.40	0.30
NQS-3-28	62.67	7.20	23.90	15.76	0.54	47.36	0.29
NQS-3-29	62.70	7.10	23.80	15.50	0.39	47.55	0.29
NQS-3-30	62.37	7.13	23.83	15.15	0.41	47.46	0.29
NQS-3-31	61.93	7.27	23.83	15.32	0.33	47.63	0.30
NQS-3-32	62.73	7.23	24.00	16.04	0.70	47.68	0.30
NQS-3-33	62.03	7.00	23.37	16.15	0.65	47.42	0.30
NQS-3-34	62.50	7.20	23.87	17.52	0.39	47.66	0.30
NQS-3-35	61.40	7.43	24.00	15.42	0.58	47.77	0.30
NQS-3-36	62.37	7.13	23.67	16.68	0.55	47.61	0.29
NQS-3-37	62.47	7.20	23.73	15.15	0.57	47.56	0.29
NQS-3-38	62.47	7.10	23.70	15.98	0.62	47.60	0.30
NQS-3-39	62.27	7.03	23.53	16.03	0.73	47.73	0.30
NQS-3-40	62.67	7.03	23.53	16.65	0.62	47.69	0.30
NQS-3-41	62.23	7.07	23.57	16.14	0.59	47.74	0.30
NQS-3-42	62.23	7.30	23.73	15.51	0.56	47.64	0.30
NQS-3-43	62.60	7.10	23.60	16.50	0.61	47.50	0.30
NQS-3-44	62.43	7.13	23.60	14.80	0.67	47.60	0.30
NQS-3-45	63.05	7.15	23.65	14.93	0.61	47.92	0.30
NQS-3-46	62.73	7.10	23.57	16.47	0.65	48.02	0.31
NQS-3-47	63.03	7.13	23.67	15.62	0.34	47.75	0.30
NQS-3-48	62.73	7.23	23.70	16.30	0.36	47.86	0.30
NQS-3-49	62.80	7.03	23.47	15.08	0.29	47.74	0.29
NQS-3-50	62.30	7.27	23.57	15.56	0.46	48.05	0.31
NQS-3-51	62.93	7.03	23.40	16.51	0.40	47.89	0.31
NQS-3-52	63.00	7.03	23.43	14.26	0.44	48.08	0.31
NQS-3-53	62.93	7.10	23.67	14.47	0.35	47.98	0.30
NQS-3-54	62.63	7.10	23.47	16.72	0.43	48.20	0.31
NQS-3-55	62.93	6.97	23.33	15.02	0.35	47.89	0.30
NQS-3-56	63.13	7.03	23.43	14.52	0.41	48.19	0.31
NQS-3-57	62.93	6.93	23.30	16.74	0.40	48.46	0.31
NQS-3-58	63.23	6.90	23.30	15.76	0.35	48.29	0.30

Continued...

Sample-Nuquanshan	L^*	a^*	b^*	$CaCO_3$%	TOC	CIA	C
NQS-3-59	62.83	6.77	23.10	14.97	0.48	48.13	0.30
NQS-3-60	63.00	6.90	23.27	14.53	0.41	48.51	0.31
NQS-3-61	63.30	7.00	23.40	15.07	0.34	48.32	0.30
NQS-3-62	62.90	6.97	23.30	15.64	0.52	48.49	0.31
NQS-3-63	63.33	6.90	23.33	16.39		48.53	0.30
NQS-3-64	62.63	7.00	23.37	14.86	0.39	48.68	0.31
NQS-3-65	63.03	6.87	23.37	13.96	0.47	48.71	0.31
NQS-3-66	62.70	6.90	23.20	12.40	0.44	48.60	0.31
NQS-3-67	62.00	7.03	23.33	14.59	0.39	48.71	0.32
NQS-3-68	62.37	6.93	22.93	13.65	0.52	48.77	0.31
NQS-3-69	62.10	7.33	22.80	15.91	0.53	48.96	0.31
NQS-3-70	62.37	7.33	23.60	12.13	0.59	49.09	0.31

KASHMIR JOURNAL OF GEOLOGY (KJG)
www.kjg.ajku.edu.pk

Provenance analysis of Early Jurassic Datta Formation, Western Salt Range, Upper Indus Basin, Pakistan

Khalid Ahmed Mirani[1], Hamad ur Rahim[1,2*] Shazia Qamar[3], Mureed Hussain[4] Waqar Ahmad[5] Muhammad Imran[1] Jawad Ahmad Jan[1]

[1]Earth Sciences Division, Pakistan Museum of Natural History, Islamabad, 44000, Pakistan.
[2]Department of Earth Sciences, Quaid-i-Azam University, Islamabad, 45320, Pakistan.
[3]Institute of Geology, University of Azad Jammu and Kashmir, Muzaffarabad, Pakistan.
[4]Department of Marine Geology, Lasbela University of Agriculture, Water and Marine Sciences, Uthal, Lasbela, Balochistan, Pakistan.
[5]Department of Earth and Environmental Sciences, Bahria University, Islamabad, Pakistan.

*Corresponding author:
hamadrahim@gmail.com

Received: 11 March 2021
Accepted: 30 August 2021
Published Online: 27 December 2021

Abstract

Rocks of the Jurassic sequence are excellently exposed in the Western Salt Range. Early Jurassic Datta Formation has been selected for detailed study. The formation is well exposed at the Nammal Gorge section. It predominately consists of sandstone with a minor amount of carbonaceous shale and marl units. The petrographic analysis has been carried out to decipher the provenance of extrabasinal sediments, tectonic setting and paleoclimate conditions present at the time of deposition of the Jurassic Datta Formation. The aforementioned analysis of twenty representative fresh samples displays the dominance of quartz, feldspar, and lithic fragments making the framework grains of the lithostratigraphic unit. The study highlights that the lithological units are mature both mineralogically and texturally, and have been classified as quartz arenite, subarkose, sublithic arenite, lithic arkose, and feldspathic lithic arenite on the basis of the QFL diagram. Quartz grains are both monocrystalline and polycrystalline while feldspars are mainly composed of plagioclase and microcline. The majority of lithic fragments like granite, chert, siltstone, shale and schist with subordinate quartzite, phyllite and volcanic fragments are present in these sandstones beds. The main cementing materials are silica, quartz while minor substitutes are clay, mud and calcite. Quartz (total)-Feldspar-Lithic fragments (QtFL) and Quartz (monocrystalline)-Feldspar-Lithic fragments (total) (QmFLt) plots mostly indicate recycled orogen field and some samples fall in mixed, while others in recycled quartzose, transitional continental and basement uplift fields of provenance. The bi-variant log-log Qt/F+R and Qp/F+R plots of sandstone samples from the Datta Formation show deposition in cold arid and semi humid climate conditions. Petrographic analysis indicates that the transitional continental region representing the sandstone may have been sourced from acidic igneous (Plutonic), sedimentary, metasediments and/or metamorphic rocks. These outcrop analogues of the mature sandstone units of the Datta Formation help delineate the exact reservoir during the exploration and exploitation of Jurassic plays of the Upper Indus Basin.

Keywords: Petrography, Paleoclimate, Tectonic framework, Jurassic Sandstone, Jurassic Plays.

1. Introduction

The provenance analysis of siliciclastic rocks is routinely used for getting an idea about source rock composition, tectonic framework and paleoclimatic conditions. The detrital mineral components of siliciclastic rocks have been executed as the main focus. Although several processes prevailed during sedimentation processes, and these considerably affect the originality of the transported sediments sourced from a specific area. However, in the reconstruction of provenance, these detrital grains are supposed to be unaffected by the physiochemical processes that prevailed during the transportation and deposition of the extrabasinal grains (Dickinson, 1985). The current study deals with the petrographic analysis of the Early Jurassic siliciclastic Datta Formation. The sedimentary unit is well exposed in Western Salt Range. The reported type locality of the Datta Formation is Datta Nala in Surghar Range (Gee, 1945; Danilchik, 1961), however, Nammal gorge is an ideal location because of excellent outcrops, well exposed upper and lower contacts, and easy access. The study area falls in topo-sheet 38 P/14 of 1:50,000 scale of Survey of Pakistan at $32^0$39'40" N and $71^0$47'25" E latitudes and longitudes respectively. It is present at 12 kilometres distance from the southeast of Mianwali city (Fig. 1). For reconstruction of the provenance, paleotectonic and paleoclimatic conditions prevailing at the time of deposition, detailed petrographic analysis was carried out of the Jurassic Datta Formation (Fig. 2). The sandstone reservoir horizons of the Datta Formation are producing in several oil fields in the Upper Indus Basin (Kadri, 1995). This study is needed to be evaluated in the context of its provenance to interpret depositional environments.

2. Geological Settings

The Salt Range and Trans Indus Ranges, Potwar and Kohat plateaus, Kalachitta, and Hazara Basin are parts of the Upper Indus Basin developed by the continuing collision between the Indian and the Eurasian Plate started in the Early Cretaceous (Kazmi and Jan, 1997; Tahirkhelli, et al., 1979; Fig. 1).

This part of the Indian Plate was on the northern extremity of the Gondwana supercontinent in the Late Precambrian time. The northern part of Pakistan was located in a passive margin of the plate, the thick Phanerozoic sedimentary cover rocks were deposited under partly restricted marginal marine conditions. The continental to shallow marine Cambrian sediments are marked by an unconformable contact with the Permian rocks. This is not confirmed whether the strata missing from Ordovician to Carboniferous in the study area were present and then got eroded, or never deposited (Ghazi, 2009; Kazmi and Abbasi, 2008).

The sedimentary rocks were deposited along the northwestern margin of the Indian plate in the Tethys Sea, which was formed due to Early Jurassic rifting within the Pangea supercontinent. Thick successions of fine grained clastics were developed into thermal subsidence of passive margin during the Early Jurassic. The passive margin conditions of the northern part of Gondwana land are widespread, as similar conditions are observed in other parts of Africa. The tectonically quiet conditions and the growth in global sea levels in Middle Jurassic have been highlighted by the deposition of extensive carbonate platforms over the area (Garzanti et al., 1996). This is followed by the thickly bedded limestones of the Samana Suk Formation.

3. Material and Methods

Detailed fieldwork was conducted in the Nammal Gorge area (Fig. 1). During the fieldwork 35 sandstone, clay and shale samples were collected based on lithological contrast. Out of 35 samples, 20 representative fresh sandstone samples were selected for petrographic analysis, covering the entire formation laterally. Slabs were prepared and impregnated to maintain their stability during grinding and further polishing processes. The samples were then heated in an oven to remove moisture and verified the setting of friable materials. The polished thin section was prepared by using the carbide grit of 600, 800 and 1000. Thin sections were studied in detail under the polarizing microscope at a magnification of 4X,10X and 20X magnification of objective lenses. The individual types of different compositions of sandstone were identified. Moreover, matrix/cement and grain ratio were studied and well documented. To identify the relative abundance of clasts/cement/matrix, the visual estimation charts of Terry and Chilingar (1955) were used. The Gazzi-Dickinson method was used for framework grains in the thin sections (Dickinson, 1970). The altered framework grains in a unit area were recognized and counted as original grains. In each thin section, more than 300 points were calculated using grid spacing in the microscope. Mineralogically, the entire constituent of the thin section was divided into three main categories comprising of: (1) Framework grains, (2) Cement/matrix, and (3) Heavy and or accessory minerals. Quartz (monocrystalline-quartz (Qm), polycrystalline-quartz (Qp) and quartz with undulose extinction (Qu), feldspar (plagioclase and alkali feldspar) and rock fragments polycrystalline quartz or cryptocrystalline quartz grains (chert) are the major framework grains and the matrix is the fine-grained detrital material that filled the interstitial spaces among the framework grains. Originally open-pore spaces filled with authigenic minerals were considered as cement. While the accessory minerals are those which cover less than 1% by volume (Boggs, 1987). For framework parameters, Dickinson (1985) and Suttner and Dutta (1986) methods are incorporated and presented in Table 1. The modal

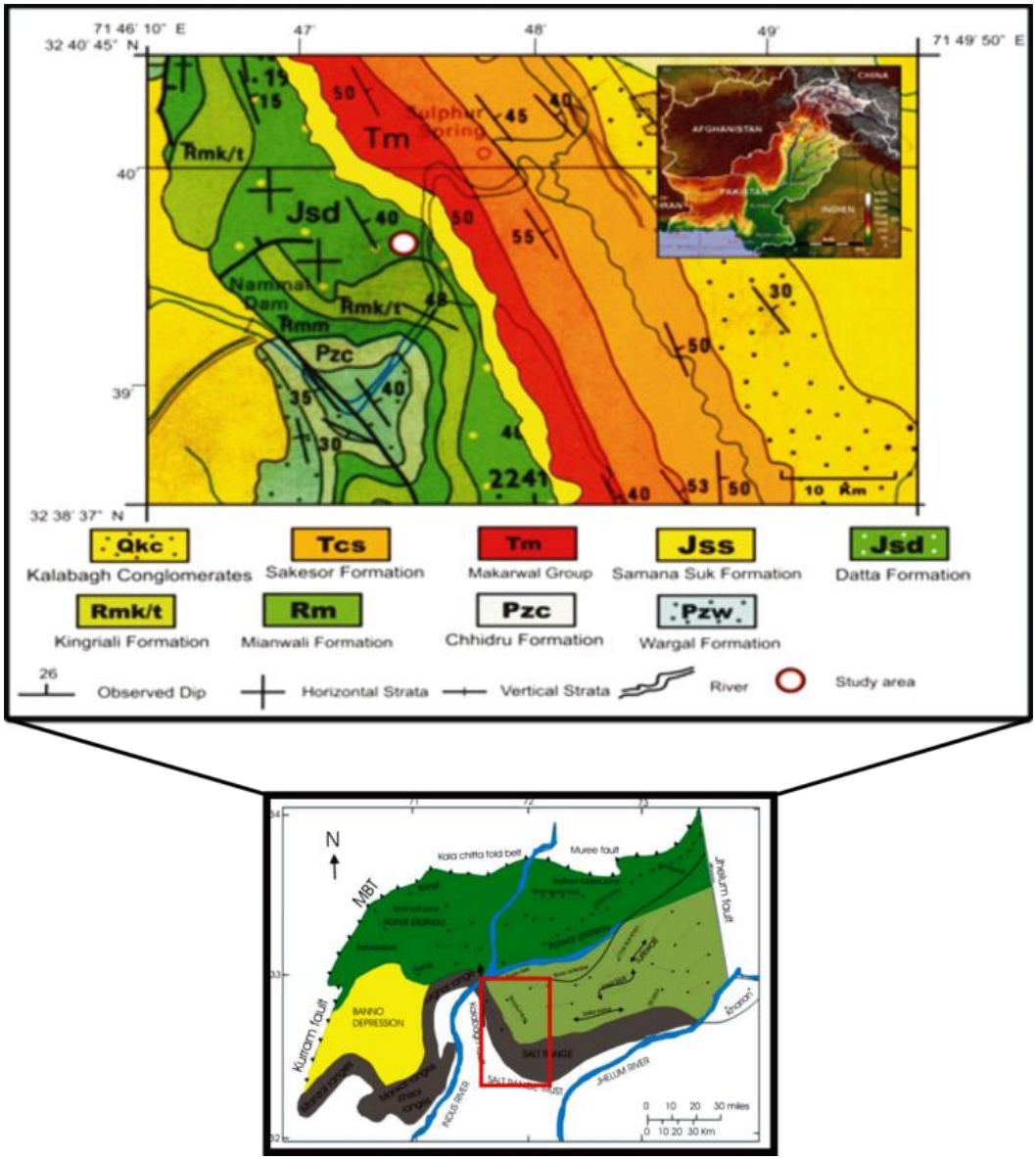

Fig. 1: The geological map of Upper Indus basin (lower figure) (modified after Khan et al., 1986) whereas the upper figure deciphers the Western Salt range (study area) as represented by a reddish box in the lower figure.

analysis data was re-calculated into percentages which are used for sandstones classification of Folk (1980) and discriminatory ternary diagrams of Dickinson (1985) were demonstrated to decipher the tectonic settings and provenance of the clastic sediments. These ternary plots are further drawn using different parameters in the isolated fields that correspond to different tectonic settings.

4. Results and Discussion

4.1 Petrographic Analysis

Datta Formation is medium to coarse-grained sandstone with sub-angular to sub-rounded and poorly to moderately sorted clasts. Quartz, feldspars, and rock fragments are the major components of the framework with smaller constituents as mica (muscovite and biotite) and accessory (heavy) minerals (zircon, tourmaline apatite and monzonite) (Fig. 3). The first component of these sandstones is quartz which id ranging from 38.6%-54%. Monocrystalline quartz clasts are more in abundance (34.4%-50.3%) as compared to polycrystalline quartz (01-7.8%). Some monocrystalline quartz grains exhibit undulatory extinction. Within polycrystalline quartz sutured boundaries are visible. Muscovite and zircon occur as an overgrowth on mono-crystalline quartz. Tourmaline inclusion can also be seen in some grains of quartz.

The second most abundant component of sandstone samples is feldspar (21.2%-39.2%) in which plagioclase is ranging from 4.1% to 18.2%, and microcline 1 to 13.4%.

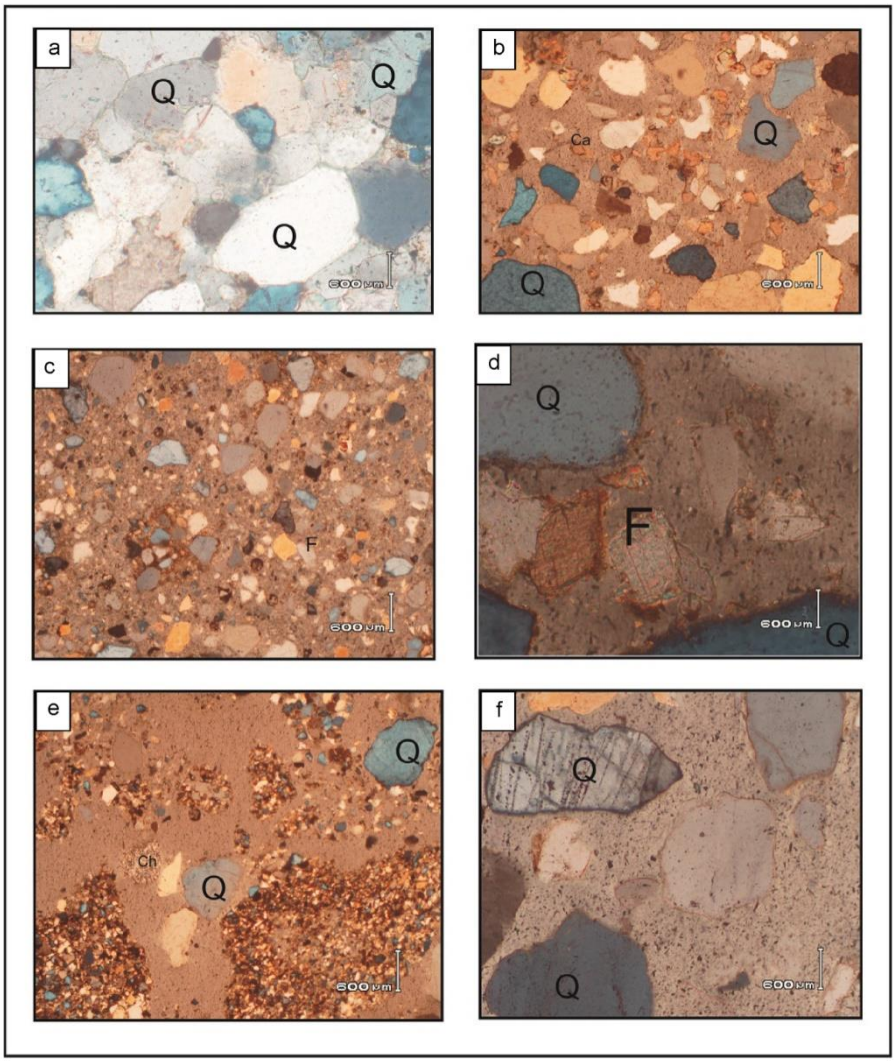

Fig. 2: Petrographic studies of the Datta Formation showing different types of grains. The main constituents are quartz (Q), feldspar (F), calcite (Ca) and chert (Ch).

Table 1: List of the terminology used in this study.

QFR	Q	Total quartzose grains (Qm + Qp)
	F	Total feldspar grains (P + K)
	R	Total rock fragments and chert
QtFL	Qt	Total quartz grains (Qm + Qp)
	F	Total feldspar grains (P + K)
	L	Total unstable lithic fragments
QmFLt	Qm	Monocrystalline quartz grains
	F	Total feldspar grains (P + K)
	Lt	Total lithic fragments
QmPK	Qm	Monocrystalline quartz grains
	P	Plagioclase feldspar grains
	K	K-feldspar grains
Qp/F+R vs Qt/F+R	Qt	Total quartz grains (Qm + Qp)
	Qp	Polycrystalline quartz grains
	F	Total feldspar grains (P + K)
	R	Total rock fragments

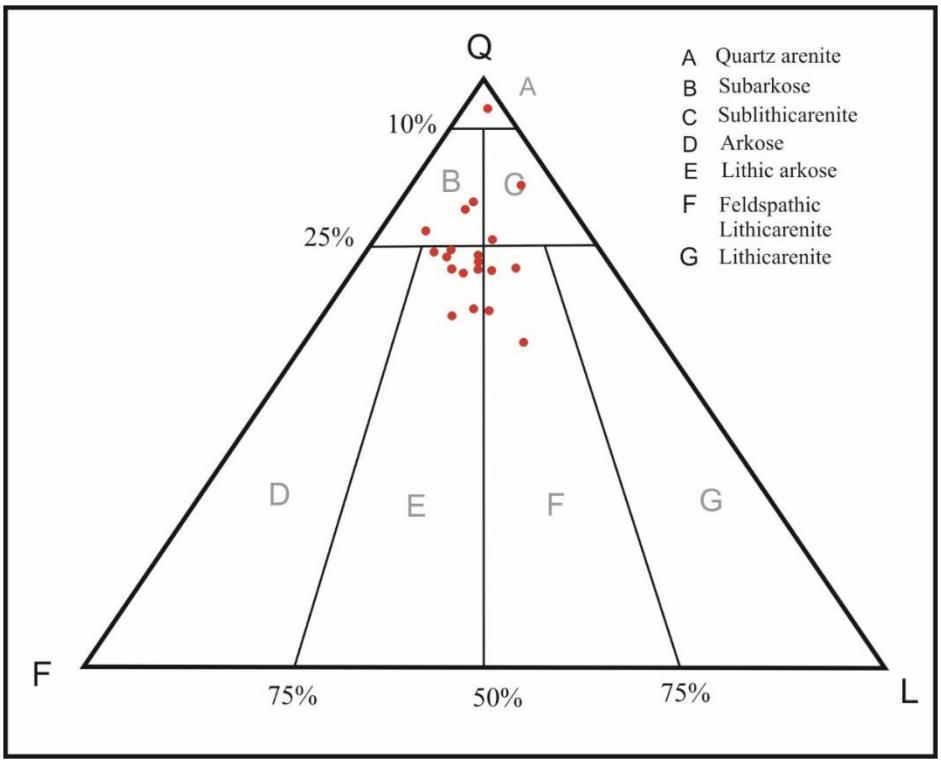

Fig. 3: QFL ternary diagram is plotted to classify the sandstones of the Datta Formation (modified after Folk, 1980).

Plagioclase is very common in different varieties of sandstone. Microcline is mostly unweathered with a few coarser grains, showing some indication of alterations along cleavage planes.

Lithic particles (09%-81.1%) show a wide variety in composition. Predominantly chert, siltstone, shale, and granite fragments are present in these sandstones. These fragments were probably derived from the Precambrian basement of the Himalayan fold-belt. Smaller amounts of mica are also identified in the form of muscovite and biotite with banded flakes. Micas are also found to be related with some of these rock fragments and minerals. It is noted that biotite is usually altered to chlorite. Flaky minerals are mainly altered and therefore, the cleavage shape is mostly wavy and broken, as well as completely absent somewhere. Other accessory minerals are calcite, aragonite, epidote, olivine, rutile, hematite, magnetite, zircon, tourmaline and garnet.

The classifications of the Datta Formation are based on petrographic studies. This study involves the evaluation of the approximate percentage of various grain types existing in a unit area usually called point count analysis. A rough approximation is developed for comparing the sandstone field of view under the microscope by percentage estimation comparison charts of Terry and Chilingar (1955). Further classification is done using Folk's (1980) sandstone classification to characterize the grains of Datta Sandstone as in Fig. 2. Based on percentage, the various types of sandstone are manifested the specific names to the rocks of framework elements as Quartz (Q), Feldspar (F) and the rock fragments (R). The Datta sandstone is classified into Quartz arenite, Subarkose, sublithic arenite, lithic arkose, and feldspathic lithic arenite types, thus pointing to their compositionally mature. However, sandstone with few numbers of lithic fragments notifies partial derivation from sedimentary or igneous rocks such as quartzite and granites (Dickinson and Suczek, 1979). The shale and siltstone rock fragments of sedimentary, most probably manifested within the basin components.

Sandstone is cemented predominantly by silica, ferruginous materials with minor substitutes of clay, mud, and calcite. Overgrowth on the quartz grains is manifested as one of the most dominant types of silica cement and it is the probable product of burial diagenesis. Along with other factors, it may also be the result of pressure solutioning, when the rock is buried and the confining fluid comes out of the pores (Folk, 1968). In quartz overgrowth, cryptocrystalline silica is most commonly precipitated enveloping the quartz grains, so that the grain and cement extinguish together under XPL (cross-polarizer light). In some cases in sandstone, the shape of original grains is defined by thin iron oxide (hematite)/clay coating between overgrowth and the grain (Ingersoll et al., 1984; Tucker, 2001). The pressure solution converts iron and calcite to ferruginous clay and mud. Ferruginous pseudo-patches are found in some places. A reddish-brown ring has been formed on the surrounding ferruginous grains by the reaction of iron

ferromagnesian materials and oxidized material. Different sizes of light dirty reddish-brown patches are observed as a result of alteration within iron-magnesium and mud. The ferruginous pseudo-patches, mud patches and iron oxide are observed in cementing materials. The grains are surrounded by pseudo-matrix, ferruginous clay, clay matrix and clay solution. The samples of the Datta Formation show moderate to highest compaction as shown by the extended and sutured contacts revealed in the petrographic study, however, the grains of the sandstone is usually found in scattered form in the matrix.

4.2 Provenance and Tectonic Framework

Tectonic framework conditions are constructed based on the assumption that the tectonic setting of an area has major control over the chemical composition of clastic sedimentary rock, especially sandstone (Dickinson, 1985). Tectonic settings effect on the mineral composition has been reported by various authors (Krynine, 1943). Several ternary diagrams are useful to create the association between detrital grain mineralogy and the tectonic framework of the area.

In the QTFL plot of Dickinson (1985) sandstones of the Datta Formation lies in the recycled orogen field (Fig. 4a). This diagram indicates the derivation of the detrital sediments from areas of the Himalayan foreland basin and sedimentation during the obduction of the Indian and Asian plates. The recycling of the orogenic belt presents the tectonic settings where the source of the sediment includes the incipient sedimentary strata with subordinate plutonic igneous rocks, which are exposed to erosion by orogenic uplift of the area. These settings include Himalayan foreland fore-thrust. Most of the studied samples are also falling in the recycled orogen field. In the QmFLt plot (Dickinson, 1985), the majority of samples lie in the mixed with some samples lying in the transitional continental, uplifted basement, and craton interior.

The triangular diagram of Q_m-F-L_t indicates recycled orogeny and mixed magmatic origin and subduction arc, respectively (Fig. 4b). Quartz and feldspars grains were originated from granitic igneous rocks with small proportions from volcanic and metamorphic rocks.

The Qm-P-K diagram (Dickinson, 1985) specifies detrital modes of the minerals present in the Datta Formation. Polycrystalline quartz and plagioclase feldspar were mainly derived from the plutonic rocks with small proportions from volcanic and metamorphic rocks. In the QmPK diagram (Dickinson, 1985) most of the samples fall near to quartz field, representing the increase in maturity or stability for sediments which suggests a continental origin (Fig. 4c).

The identified types of quartz grains propose that the source of the Datta Formation is both metamorphic and plutonic in origin. The high proportion of mono-crystalline quartz of undulose and non-undulose nature indicate derivation of sediments from a plutonic (granite) igneous source (Blatt, 1967). Along with quartz, the lithic fragments of the Datta Formation are meta-sedimentary in origin. Additionally, the inclusions of mica and garnet minerals within quartz grains are another indication of a metamorphic source. Quartz grains have spectacular mineral inclusions of mica and garnet, which indicate a metamorphic source. Young (1976) pointed out that polycrystalline quartz may cultivate from monocrystalline quartz during metamorphism under the influence of an increase in temperature and pressure. The presence of few undulatory quartz grains in the Datta Formation advocates the metamorphic source. Monocrystalline quartz shows straight to undoluse extinction, which suggests its igneous origin. Polycrystalline quartz mostly has equidimensional grains and have straight boundaries which suggest the derivation from high grade metamorphic rocks. Furthermore, the undulatory extinction of quartz suggests that the source rocks are metamorphic and have been subjected to a great deal of pressure. The quartz present in the thin section indicates granitic, schistose, and gneissic origin. This sandstone unit contains a high concentration of feldspars suggests derivation from crystalline rocks (Folk, 1980; Krainer and Spötl, 1989). Further, the minerals such as tourmaline, zircon and rutile also support involvement from the acidic igneous source (Gallala et al., 2009). The accessory mineral assemblage suggests a bimodal source of sediments; for example, epidote, garnet and staurolite point out a metamorphic source whereas rutile and tourmaline indicate igneous source rocks (Tucker, 2001). Overall, the petrographic study gives strong evidence about the origin. The clasts contain a mixture of igneous, sedimentary, and metamorphic rocks within the Datta Formation.

4.3 Paleoclimatic Conditions

The framework mineralogy of sediments was transformed by the effect of tectonic activity, but climate also has played a vital role. The indications of climatic conditions were well preserved in the siliciclastic sediments. The compositional maturity index represented a low value as given by Q_t/F+R and Q_p/F+R ratios. These values show that the sandstones of the Datta Formation are immature in composition (Fig. 5). The samples of sandstone in the study area dominantly fall into the semi-arid category with a considerable number of samples showing arid climate while semi-humid conditions show negligible contribution as indicated by bivariant log-log plot of Q_t/F+R and Q_p/F+R of Suttner and Dutta (1986). Based on observation, it is proposed that the sandstone of the Datta Formation of the study area was deposited in the cold, dry and a little bit humid climate. Climatic conditions were

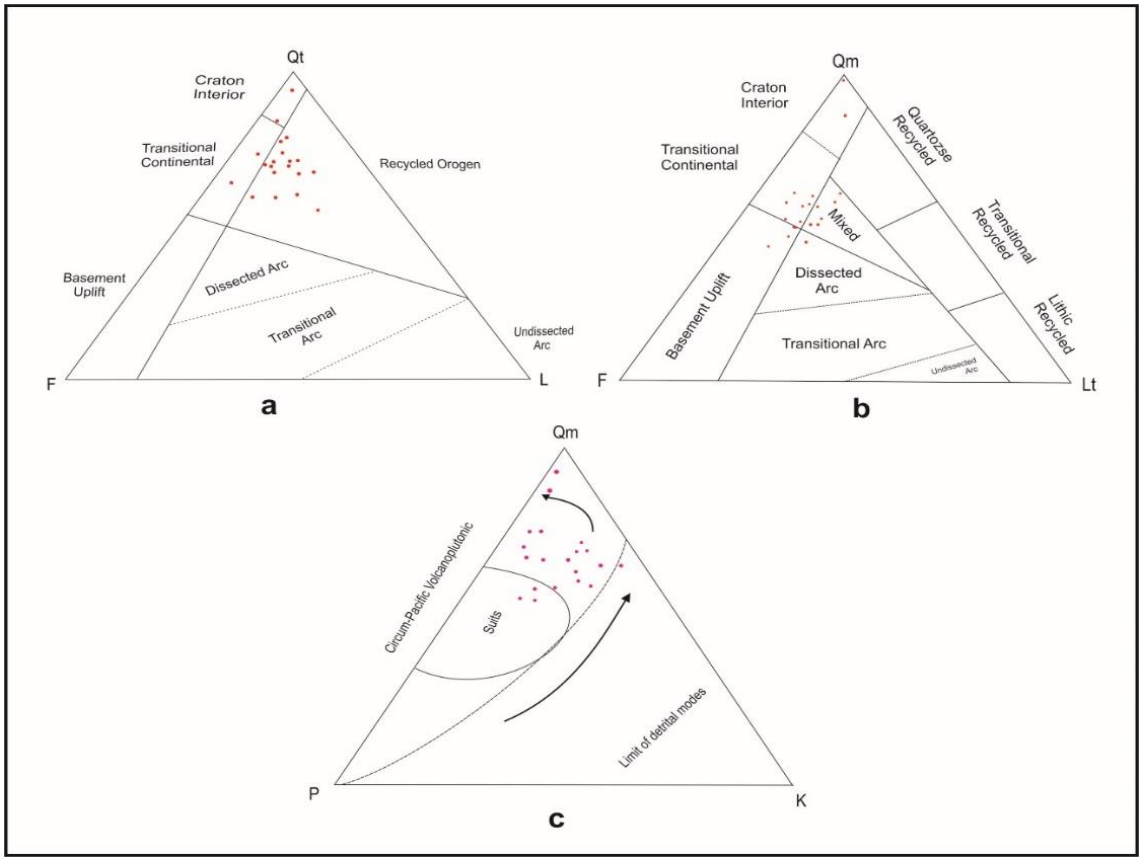

Fig. 4: Provenance field details as (a) QtFL, ternary diagram of Datta sandstone (after Dickinson, 1985), (b) QmFLt, ternary diagram of Datta sandstone (after Dickinson, 1985) and (c) QmP ternary diagram of Datta sandstone (after Dickinson, 1985) in Nammal Gorge Section.

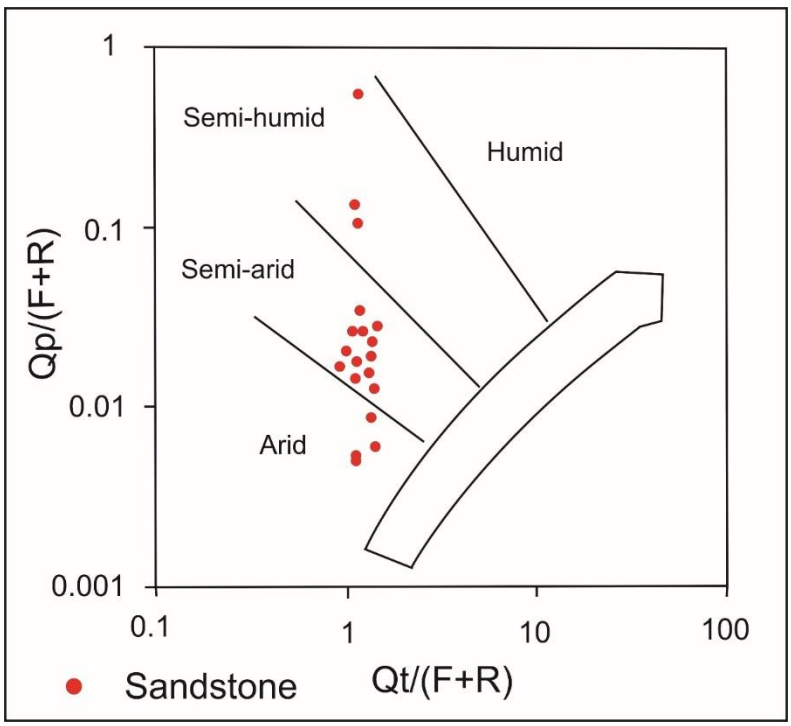

Fig. 5: Biavariant log-log plot of Qt/(F+R) and Qp/(F+R) for Datta sandstone of Nammal Gorge Section (after Suttner and Dutta, 1986).

Table 2: Recalculated detrital composition percentage of Datta sandstone in Nammal Gorge Section.

Samples	QFR			QtFL			QmFLt			QmPK			Qp/(F+R)	Qt/(F+R)
	Q	F	R	Qt	F	L	Qm	F	Lt	Qm	P	K		
DtF .05	81.42	04.28	14.30	94.42	02.28	03.30	86.04	06.97	06.97	92.05	05.89	02.06	- 0.1	2.6
DtF .07	94.59	02.17	03.24	94.59	02.17	03.24	98.72	01.51	0.57	75.00	20.00	05.00	0.1	2.1
DtF.09	68.65	16.41	14.94	83.65	11.41	04.94	58.33	22.91	18.76	71.79	10.25	17.96	0.3	2.4
DtF.10	66.66	19.29	14.05	77.66	13.29	09.05	61.11	30.55	08.34	66.66	21.21	12.13	0.1	2.1
DtF.13	70.93	18.84	10.23	70.93	18.84	10.23	50.01	35.93	14.06	58.18	27.28	14.54	0.08	1.3
DtF.14	71.33	13.33	15.34	71.33	13.33	15.34	61.22	20.40	18.38	75.00	17.5	07.50	0.1	2.1
DtF 17	78.84	11.87	09.29	78.84	11.87	09.29	50.84	30.50	18.66	70.58	23.53	05.89	0.6	2.5
DtF.19	67.31	20.39	12.30	67.31	20.39	12.30	50.01	35.71	14.28	58.33	22.92	18.75	0.1	1.4
DtF.22	77.53	13.53	08.94	77.53	13.53	08.94	53.06	28.57	18.37	65.00	05.00	30.00	0.2	1.8
DtF 23	67.17	17.17	15.66	71.17	15.17	13.66	46.87	39.06	14.07	54.55	29.09	16.36	0.1	1.2
DtF 24	69.33	20.01	10.66	69.33	20.01	10.66	43.39	45.28	11.33	48.93	12.76	38.31	0.1	1.0
DtF 32	70.24	21.13	08.63	70.24	21.13	08.63	52.63	36.84	10.53	58.82	14.71	26.47	0.4	2.2
DtF 36	67.55	11.97	20.48	67.55	11.97	20.48	56.89	27.58	15.53	67.34	24.48	08.18	0.06	1.6
DtF 37	60.63	21.01	18.36	69.63	16.01	14.36	51.78	33.92	14.30	60.41	16.67	22.92	0.8	1.2
DtF 42	55.07	17.39	27.54	55.07	17.39	27.54	50.94	32.07	16.99	69.23	10.25	20.52	0.09	1.5
DtF 43	73.69	20.58	05.73	73.69	20.58	05.73	44.82	36.20	18.98	55.32	31.92	12.76	0.2	1.4
DtF 44	67.03	15.48	17.49	67.03	15.48	17.49	57.14	30.61	12.25	65.12	09.30	25.58	0.09	1.6
DtF 45	69.67	16.10	14.23	69.67	16.10	14.23	60.31	26.98	12.71	69.09	12.72	18.19	0.009	1.8
DtF 47	59.30	24.41	16.29	59.30	24.41	16.29	58.06	33.87	08.07	63.15	15.78	21.07	0.03	1.6
DtF 50	60.22	19.31	20.47	60.22	19.31	20.47	57.62	28.81	13.57	66.67	15.68	17.65	0.06	1.8

restructured to the temperate range and more humid type in the overlying formation with the Indian plate moving over the equator.

5. Economic Implications

Economically Datta Formation is very important as it holds many economic minerals like coal, fire clay and silica sand. Moreover, it is a proven reservoir rock in the upper Indus Basin (Chaudhry and Ahsan, 1999; Mirani et al., 2015). In the studied outcrops, the following observations are noted which are helpful in devising a potential candidate for a reservoir rock when observed petrographically:

The Sandstones of the Datta Formation are mature due to the absence of angular grains and clay free material (Fig. 6 a-b). The grains are mostly of quartz and k-feldspar, which are more resistant to chemical weathering by the hydrocarbon fluids (Fig. 6 a-b). The grains of the Datta Formation are equigranular in size, which holds a good potential for the reservoir of petroleum (Fig. 6 a-b). The sandstone samples are not quite affected by diagenetic factors like cementation, so it is a good reservoir in the Punjab area.

In the studied outcrop, fire clay horizons are also observed. It is composed of light grey, very fine grained massive to thick bedded units, which breaks with the conchoidal fracture. The thickness of the unit varies from 1.54 to 4.58 meters. The quality of the deposits is very good and local mining is being done in this area for their usage in the refractory bricks (Fig. 6c).

Coal seams in the studied section are dark brown to dark black. The thickness of the coal seam varies from 0.2 to 0.6 meters. The very thin coal seam in the studied area does not have any economic importance, however, it is a potential source rock and needed to be evaluated in detail for its potential by using the geochemical parameters.

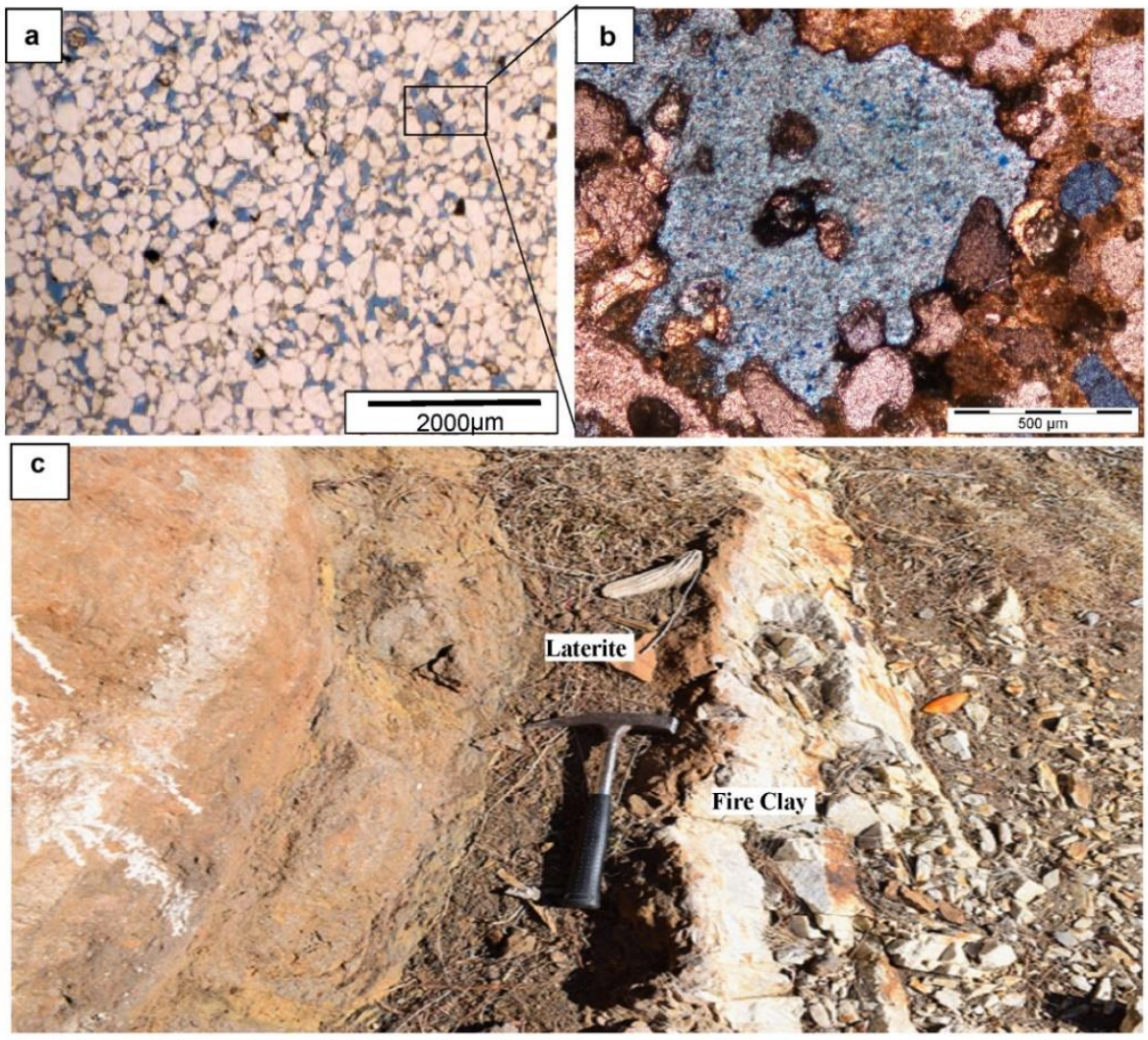

Fig. 6: The economic potential of Datta Formation (a, b). Reservoir character of the formation as shown by the blue dye injected thin section (c). Laterite and fire clay horizons are visible in the outcrop.

6. Conclusions

The following conclusions are drawn from the petrographic studies of the Datta Formation of Nammal Gorge section:

- Framework grains and the mineral composition of the Datta Formation signifies that most of the sediments were derived from the recycle region of continental provenance.
- Sediments are deposited in the high relief area with fast erosion have led to the formation of texturally and mineralogically immature sandstones such as Quartz arenite, Subarkose, sublithic arenite, lithic arkose, and feldspathic lithic arenite types.
- The analysis of obtained results specifies that the origin of the grains is from the acid igneous (granite), metamorphic and sedimentary rocks (shale, siltstone).
- The sandstone of the Datta Formation was developed in dry to cold, semi humid climatic conditions, as shown from the majority of the samples lying in the former category.
- Petrography and plots on different compositional diagrams indicate that the sandstones of the Datta Formation were fed from the inner cratonic region, however, they were recycled many times to reach the present state.
- Economically Datta Formation holds good potential due to its fire clay, silica sand and fair to good reservoir rock potential in the Upper Indus Basin.

Acknowledgements

The study was financed by the Pakistan Science Foundation research project (PSF/RES/C-PMNH/Earth(81) to the first author. The authors are also grateful to Dr. Jamil Afzal, Deputy Chief Geologist in OMV Exploration & Production Limited Islamabad Pakistan for the technical support during the completion of the project.

References

Blatt, H., 1967. Provenance determinations and recycling of sediments. Journal of Sedimentary Research, 37(4), 1031-1044.

Danilchik, W., 1961. The iron formation of the Surghar and western Salt Range, Mianwali District, West Pakistan.

Dickinson, W.R., 1970. Interpreting detrital modes of graywacke and arkose. Journal of Sedimentary Research, 40(2), 695-707.

Dickinson, W.R. 1985. Interpreting provenance relations from detrital modes of sandstones; In: Provenance of Arenites (Ed.), G Zuffa (Dordrecht: D. Reidel Publishing Company). 333–362.

Dickinson, W.R., Suczek, C.A 1979. Plate tectonics and sandstone compositions. American Association of Petroleum Geologists, 63(12), 2164–2182.

Folk, R.L., 1980. Petrology of Sedimentary Rocks. Hemphill Publishing Company, Austin, Texas, U.S.A, 182.

Gallala, W., Gaied, M.E., Montacer, M., 2009. Detrital mode, mineralogy, and geochemistry of the Sidi Aich Formation (Early Cretaceous) in central and southwestern Tunisia: Implications provenance, tectonic setting and paleoenvironment. Journal of African Earth Sciences, 53, 159-170.

Garzanti, E., Critelli, S., Ingersoll, R.V., 1996. Paleogeography and paleotectonic evolution of the Himalayan Range as reflected by detrital modes of Tertiary sandstones and modern sands (Indus transect, India and Pakistan) Geological Society of America Bulletin, 108, 631-642.

Gee E.R., 1945. The age of the Saline Series of the Punjab and Kohat. Proceedings of the National Academy of Science India, 14, 269-310.

Ghazi, S., 2009. Sedimentology and stratigraphic evolution of the Early Permian Warchha Sandstone, Salt Range, Pakistan. Ph.D. thesis., University of the Leeds, England, 234-276.

Ingersoll, R.V., Bullard, T.F., Ford, R.L., Grimm, J.P., Pickle, J.D., Sares, S.W., 1984. The effect of grain size on detrital modes: a test of the Gazzi-Dickinson point-counting method. Journal of Sedimentary Research, 54(1), 103-116.

Kadri I.B., 1995. Petroleum geology of Pakistan. Pakistan Petroleum Limited, Karachi.

Kazmi, H.A., Abbasi, I.A., 2008. Stratigraphy and Historical Geology of Pakistan, Geological Survey of Pakistan, 380-385.

Kazmi A.H., Jan M.Q., 1997. Geology and tectonics of Pakistan. Graphic, Karachi, 225–231.

Krainer, K., Spötl, C., 1989. Detrital and authigenic feldspars in Permian and early Triassic sandstones, Eastern Alps (Austria). Sedimentary geology, 62(1), 59-77.

Longiaru, S., 1987. Visual comparators for estimating the degree of sorting from plane and thin section. Journal of Sedimentary Research, 57(4), 791-794.

Mack, G.H., 1984. Exceptions to the relationship between plate tectonics and sandstone composition. Journal of Sedimentary Research, 54(1), 212-220.

Pettijohn, F.J., Potter, P.E., Siever, R., 1987. Sand and sandstone. Springer Verlag, New York. 533.

Powers, M.C., 1953. A new roundness scale for sedimentary particles. Journal of Sedimentary Research, 23(2), 117-119.

Boggs Jr. S., 1987. Principles of. Sedimentology and Stratigraphy. Fifth Edition. Published Pearson Prentice Hall, 235-250.

Suttner, L.J., Dutta, P.K., 1986. Alluvial sandstone composition and paleoclimate; I, Framework mineralogy. Journal of Sedimentary Research,

56(3), 329-345.
Tahirkhelli, R.A.K., Mattauer, M., Proust, F., Tapponnier, P., 1979. The India Eurasia Suture Zone in Northern Pakistan; Synthesis and interpretation of recent data at plate scale. In Geodynamic of Pakistan, A, and Delong, K.A. (Eds.), Geological Survey of Pakistan, Special Publication, 125-130.
Terry, R.D., Chilingar, G.V., 1955. Summary of "Concerning some additional aids in studying sedimentary formations," by MS Shvetsov. Journal of Sedimentary Research, 25(3), 229-234.
Tucker, M.E., 2001. Sedimentary petrology: an introduction to the origin of sedimentary rocks. John Wiley & Sons.
Young, S.W., 1976. Petrographic textures of detrital polycrystalline quartz as an aid to interpreting crystalline source rocks. Journal of Sedimentary Research, 46(3), 595-603.

KASHMIR JOURNAL OF GEOLOGY (KJG)
www.kjg.ajku.edu.pk

Mesozoic Structural Architecture and Petrophysical analysis of Badin South Block, Lower Indus Basin, Pakistan

Naqash Mehmood Khan[1], Muhammad Farooq[2*], Muhammad Rizwan Mughal[3], Umair Bin Nisar[4]

[1]Department of Earth Sciences, COMSATS University Islamabad (CUI), Abbottabad Campus.
[2]Institute of Geology, University of Azad Jammu and Kashmir, Muzaffarabad, Pakistan.
[3]Department of Meteorology, COMSATS University Islamabad (CUI), Islamabad 45550, Pakistan.
[4]Centre for Climate Research and Development (CCRD), COMSATS University Islamabad, Islamabad, 45550, Pakistan.

*Corresponding author:
m.farooq@ajku.edu.pk

Received: 30 March 2021
Accepted: 23 November 2021
Published Online: 27 December 2021

Abstract

The study area "Badin South Block" lies in the southern most of the Sindh Monocline, Lower Indus Basin, Pakistan. The objective of the research work is to analyze the structural architecture and hydrocarbon prospective of Mesozoic age rocks of Badin South Block. Ten 2D seismic lines and 4 wells data were used for a better understanding of the structural styles of the area and to ascertain hydrocarbon potential. The Badin South Block is located in the Lower Indus Basin and is a part of an extensional regime with normal faulting that resulted from the separation of the Indian and African plates. Four horizons were interpreted i.e., Khadro Formation, Upper Goru Formation, Lower Goru Formation and Sembar Formation. Seismic interpretation reveals the existence of horst/graben structures in the study area having listric/normal faults. The interpreted faults are oriented in NW-SE or NNW-SSE direction with high angle planer geometries having an impact on the sealing nature of each fault. The NW-SE trends of structures in the study area are similar to regional structures in the Lower Indus Basin confirming the validity of seismic interpretation. The normal high angle planer faults dip majorly in the SW direction. Additionally, the petrophysical analysis showed good reservoir quality of the Lower Goru Formation with respect to reservoir effectiveness. Additionally, the results further revealed that up-dip hydrocarbon migration is predictable in the proximity of the research area, therefore a 3D seismic survey is suggested for a better understanding of the subsurface geological structures.

Keywords: Mesozoic rocks; Structural architecture; Petrophysics; Hydrocarbon potential; Badin South Block

1. Introduction

The interpretation of seismic data is an essential measure in petroleum exploration to determine the subsurface reservoir information (Hilterman, 2001). Consistent earth models can be produced by correlating the seismic data with borehole logs data. These models are used to identify and mark the laterally consistent stratigraphic surfaces for mapping geological structures, reservoir framework and stratigraphic interpretation. The aim of quantitative petrophysical analysis of wells is to transfer the borehole logs data into predictable reservoir parameters such as volume of shale (Vsh), effective porosity (ϕe), water saturation (Sw) and hydrocarbon saturation (Sh) (Tiab and Donaldson, 2015). Correct estimates of the afore-mentioned reservoir parameters can significantly help to differentiate between hydrocarbon and non-hydrocarbon accumulated zones (Yuedong and Hongwei, 2007).

The Sindh Monocline lies in the southern most part of the Lower Indus Basin having Normal faults (Memon et al., 1999). The Sindh Monocline is surrounded by Sukkur Rift from the north, Kirther Ranges from the south-west, Runn of Kutch from the south-east and Indian Shield from the east as shown in Fig. 1 (Treloar and Izzat, 1993). Additionally, the area is considered an important hydrocarbon province due to its structural style, thus national and international petroleum exploration companies are taking a keen interest in the exploration of fossil fuel (Sheikh and Naseem., 1999). The hydrocarbon exploration in the proximity of the Karachi Arc, Lower Indus Basin have been started before the partition of Indo-Pakistan as stated by the Burmah Oil Company (BOC, 1939). The hydrocarbon production data revealed that Sindh Monocline has produced 28% oil and 13% of the country gas requirement (Energy Year Book, 2013).

Therefore, the study area is considered a prolific hydrocarbon zone. In this research work, the seismic and well log data have been used for a better understanding of the structural geometries and petroleum system of the Badin block. The main objectives include: 1) interpretation of seismic data to evaluate structural trends and structural geometries. 2) Importance of structural geometries in hydrocarbon trapping and 3) Petrophysical analysis of reservoir rock, Lower Goru Formation to evaluate the reservoir quality.

2. Tectonic Settings and Stratigraphy

The Indian Plate separated from the African Plate during the Mesozoic and started drifting towards the North. The rifting of the Indian Plate ended in Eocene with the collision of the Eurasian Plate resulting in Himalayan orogeny (Tectostrat, 1992). Drifting and collision of Indian plate results in the Formation of Indus basin of Pakistan (Bannert and Raza, 1992; Malik et al., 1988). The Indus basin of Pakistan is divided into three sub-basins named: upper Indus basin, middle Indus basin and Lower Indus Basin. These divisions are based on the structural styles associated with drifting and collision of the Indian Plate (Bannert and Raza, 1992; Kadri, 1995; Malik et al., 1988). The rifting and rotation of the Indian Plate form extensional structures in the middle and Lower Indus Basin, while collision of the front part of the Indian plate with Eurasian plate forms fold and thrust belts in the upper Indus basin (Kadri, 1995).

Badin South Block is located in Sindh Monocline, Lower Indus Basin, Pakistan. Figs. 1 and 2 show the major tectonic and stratigraphic elements of the Lower Indus Basin. The extensional tectonics of the Indian Plate in the Lower Indus Basin results in the formation of normal faults (*listric model*) with horst and graben structures, cutting the entire Mesozoic stratigraphic interval. These major faults have played an important role regarding the hydrocarbon trapping mechanism and ultimately lead toward exploration and formulation of production in the Lower Indus Basin (Abbasi et al., 2015). The Mesozoic age rocks are considered an important hydrocarbon province (Alam et al., 2002). The generalized stratigraphy shows that formations from early Jurassic (Chiltan limestone) to recent (Siwaliks) are present in the Sindh Monocline (Abbasi et al., 2015). Sindh Monocline is considered an important hydrocarbon province due to its structural style thus, national and international petroleum exploration companies are taking a keen interest in the exploration of fossil fuels (Munir et al., 2014).

3. Petroleum Play System

The southern part of the Lower Indus Basin is a prolific hydrocarbon zone as hydrocarbon is extracted from Cretaceous sands, Paleocene limestone and lower Eocene limestone, and these hydrocarbons are drawn out from Mesozoic faulted blocks system (Kadri, 1995). Pakistan has over 9 billion barrels of petroleum oil and 105 trillion cubic feet in shale oil and natural gas reserves. The daily production of oil is 70,000 barrels and 24 TCF of gas in 2016 (Energy Year Book, 2013).

The Sembar Formation of early Cretaceous age is a proven source rock in the Lower Indus basin which has thermal maturity with type-III kerogen. Moreover, the shale members of the Lower Goru Formation also act as a source rock. The rock units of the Cretaceous and Eocene ages are the main reservoir rocks in Lower Indus Basin. The sands of the Lower Grou Formation are extensively deposited and are proven reservoir rocks. The Pab Sandstone, Dungan Limestone is major gas-producing formations in the Lower Indus Basin (Abbasi et al., 2015). The cap rocks are impervious and non-permeable and act as a barrier in the migration pathways of hydrocarbon. The shale interval in the Lower Goru Formation and

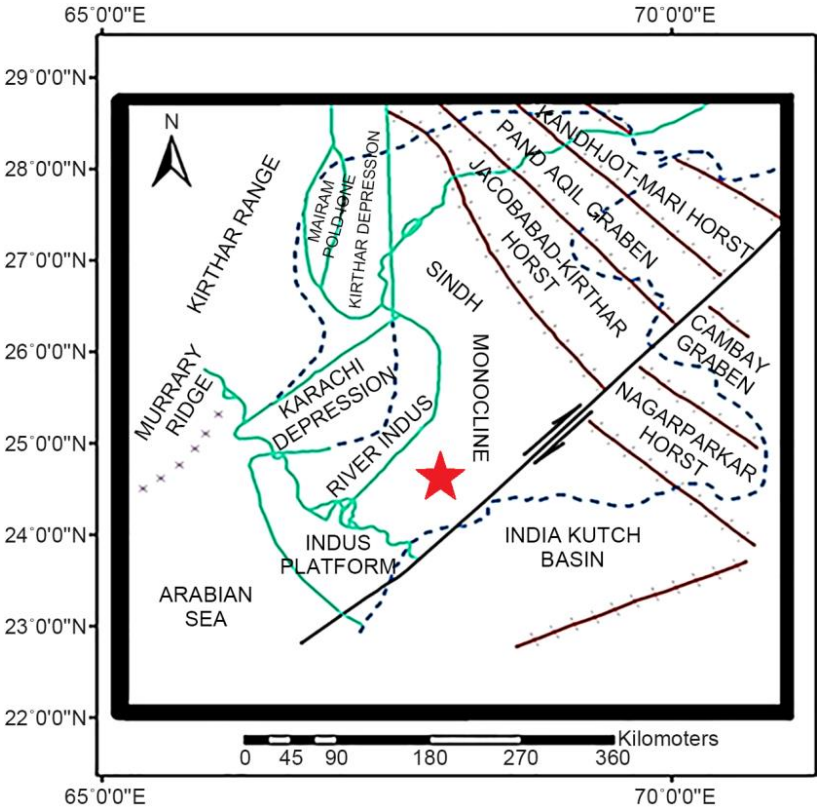

Fig. 1: Tectonic map of Lower Indus Basin with adjoining areas, red star illustrates the "Badin South Block".

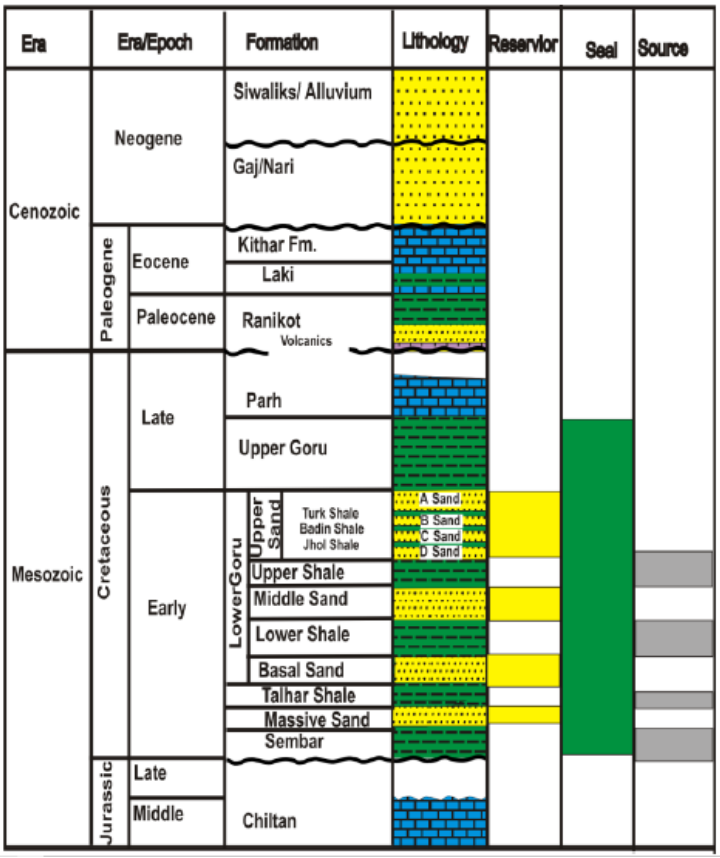

Fig. 2: Generalized stratigraphy of Southern Sindh Monocline (Abbasi, 2015).

Upper Goru Formation are proven cap rocks. A thickness of a few meters of cap rock is important because it stops migration (Abbasi et al., 2015).

The Normal faults (Listric Model) with Horst and Graben structures of Mesozoic age are important with respect to hydrocarbon production in the study area, as these Mesozoic structures are associated with rifting phase of the Indian Plate (Munir et al., 2014).

4. The Seismic and Well Log Data Set

Ten 2D seismic lines were utilized for geological modeling and data of four wells were used for the petrophysical analysis of reservoir rock in Badin south block. The seismic line contains the dip lines, strike lines and oblique Lines. The dip & oblique lines help in the structural interpretation of the study area. Four exploratory wells were drilled on these seismic lines. The base map of the study area is given in Fig. 3.

The detail of seismic lines is as follow:

1. Dip lines are: GPK85-958, GPK85-960, GPK86-1200 and GPK86-1202.
2. Strike Lines are: GPK85-935 and GPK92-1685.
3. Oblique Lines are: GPK92-1680, GPK92-1682, GPK92-1686, and GPK94-1804.

The seismic data interpretation implies its aspects in geological terms. The geological and geophysical data collectively helps in the construction of integrated depiction, which is consistent and most reliable. The workflow for the current study is shown in Fig. 4.

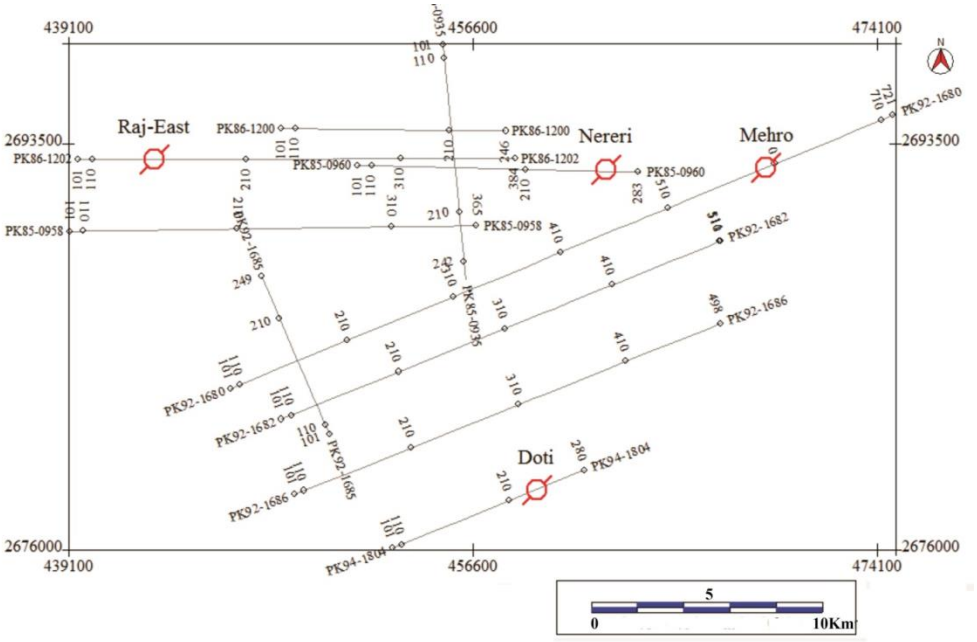

Fig. 3: Base map of study area and location of seismic lines and wells.

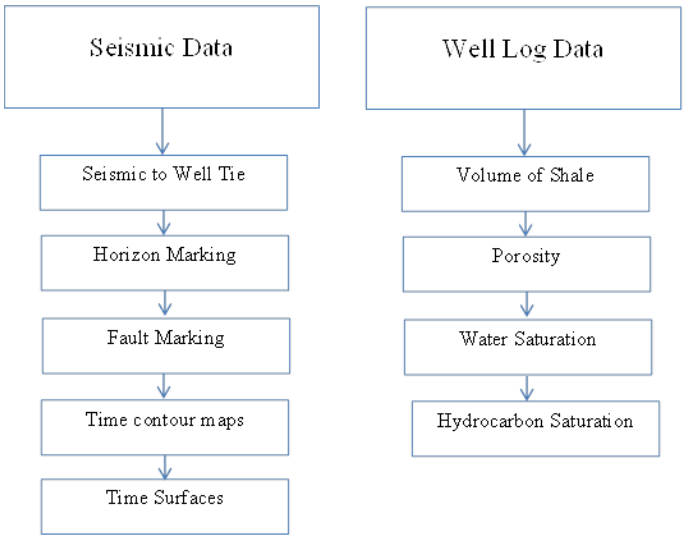

Fig. 4: Flow chart for methodology.

5. Results and Discussion

In seismic reflection interpretation, the positions of geological interfaces were calculated from which seismic waves were transmitted back to the ground surface by reflection. The irregularities from seismic reflected data were removed which gives varying geological conditions and transformed data into regular time records which gives acceptable subsurface geological models. The removal of conflicting information from seismic data is important to get the true subsurface image especially the target horizon. The structural and stratigraphic variations are revealed from the seismic survey. The structural and stratigraphic variations are marked by the mean of Acoustic impedance. Acoustic impedance is the velocity and density of the stratigraphic unit.

The provided seismic sections were 3 seconds (TWT). Each reflector was chosen on the basis of time and analysed in terms of velocity and depth. A total of four horizons named as Khadro Formation, Upper Goru Formation, Lower Goru Formation and Sembar Formation were picked up on all seismic lines (Fig. 3). The Doti well lies on the dip line GPK94-1804.

Badin South Block lies far from the collision zone; thus, the seismic sections reveal tectonic stability since the early Jurassic. The movement of the Indian Plate in the late Cretaceous causes structural evolution (Normal Faulting) of the Lower Indus Basin which is clearly seen on seismic sections where the post-Eocene strata are either not affected or very less deformed. Information about the description and deposition of rock units is available in the literature (Kadri, 1995).

Interpretation of seismic sections reveals NW-SE oriented high angle listric normal faults in the rocks of Cretaceous age. The interpreted faults originate from Sembar Formation cut the Lower Goru and Upper Goru Formation and ends in the rock units of Paleocene age (Fig. 5). All these formations are of Cretaceous age. The older Jurassic strata appear to be unaffected by the faults. It is possible if they sole-out in a Cretaceous Sembar shale detachment, like ramp-flat-ramp geometry of an extensional system (Jadoon and Khawaja, 1997). The listric models and Horst/Graben structures formed due to NW-SE oriented normal faults (Figs. 5 and 6). The time contour maps as well as the 3D structure analysis of the marked formations named as Sembar Formation; Lower Goru Formation; Upper Goru Formation support the structural geometries developed as a result of extensional regime in the area (Figs. 7 and 8).

For the petroleum system of an area, footwall blocks and horst/graben structures are important. For the generation of hydrocarbon, these structural geometries are of primary importance. The downthrown block due to normal faulting and grabens are primarily kitchen area. A high-temperature gradient gives the optimal temperature for the hydrocarbon maturation. Overburden in access as a result of subsidence delivers adequate pressure necessary for hydrocarbon production. As a result of extensional stresses, the tilted fault blocks identical to a listric model, aid the petroleum system by providing a migratory pathway for hydrocarbons.

5.1 Structural Style in Mesozoic Rock

The proven source rock, reservoir rock and seal rock named as Sembar Formation, Lower Goru Formation and Upper Goru Formation respectively

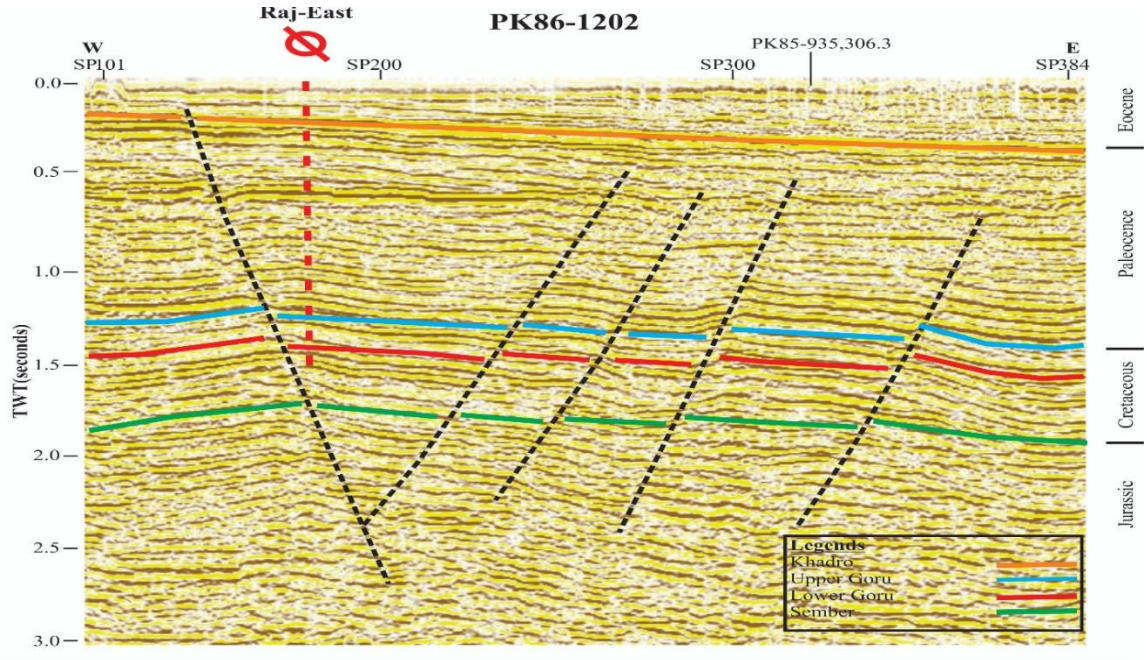

Fig. 5: Interpreted seismic line pk86-1202 shows normal fault geometries.

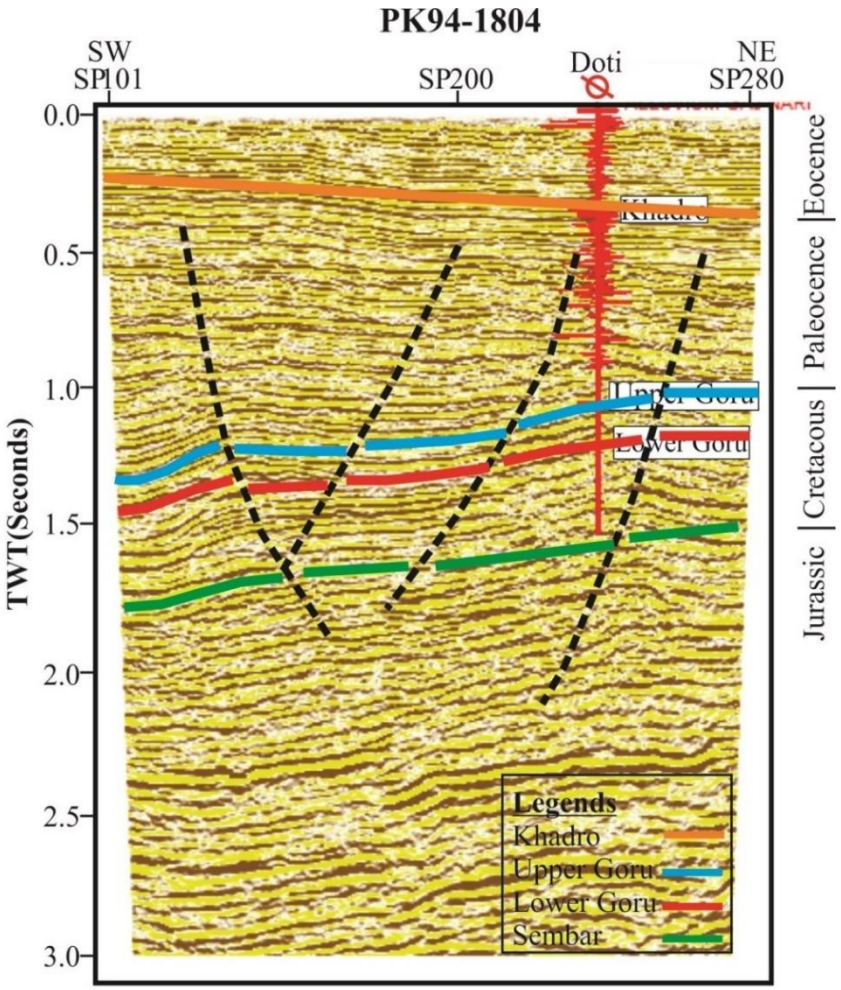

Fig. 6: Interpreted seismic line pk94-1804 exhibiting normal fault geometries in Mesozoic age.

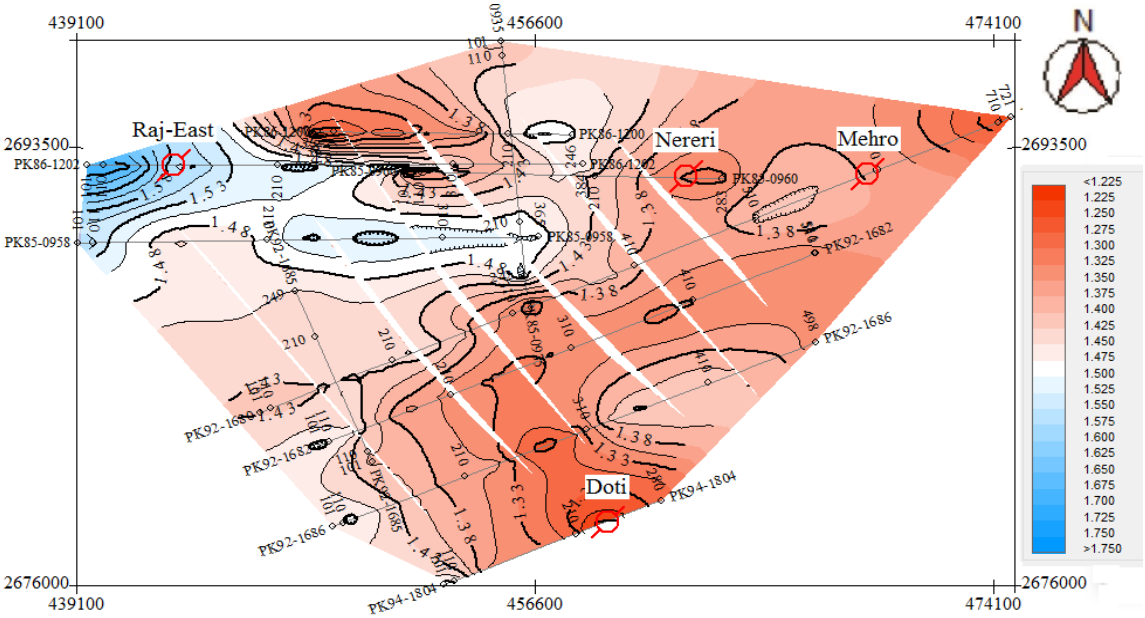

Fig. 7: Time contour map of Lower Goru Formation with NW-SE oriented faults.

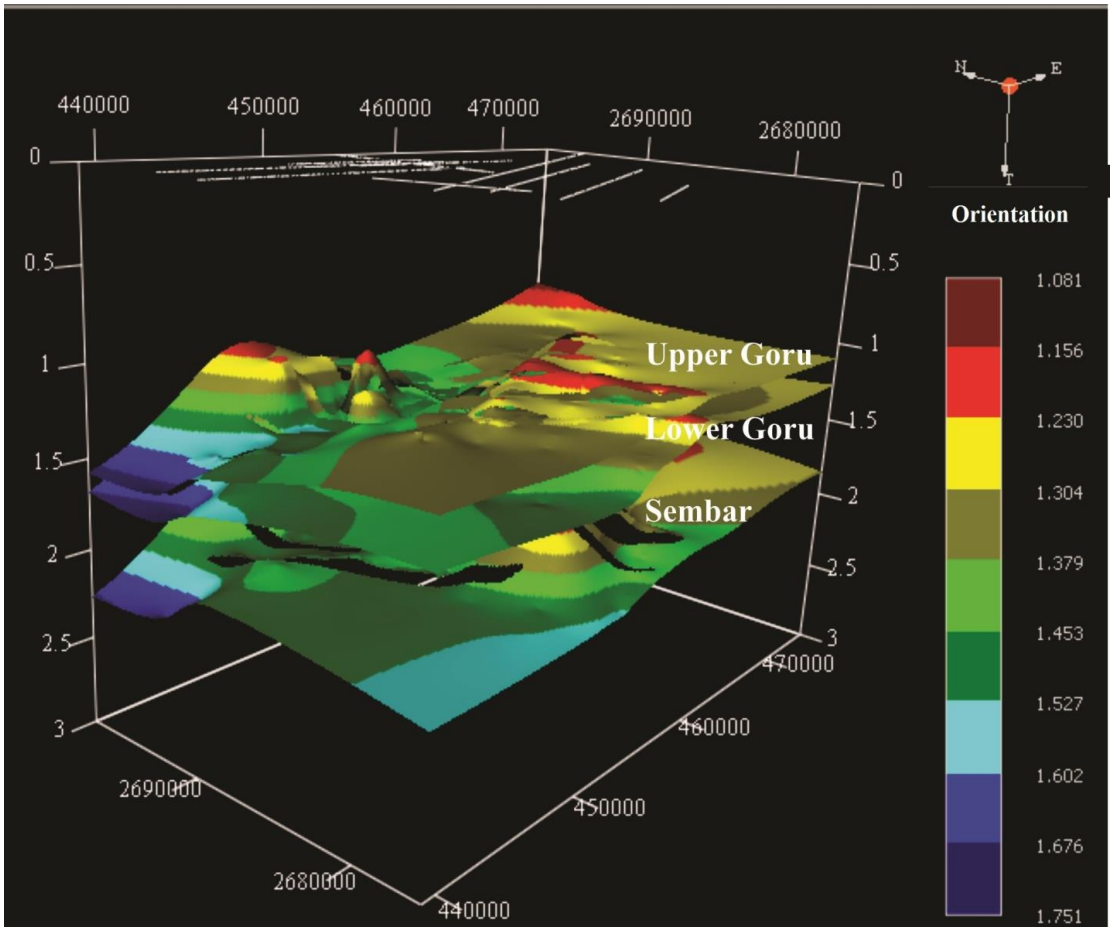

Fig. 8: 3D surface model Mesozoic age formations in the "Badin South Block".

exist in the Mesozoic age in Lower Indus Basin. The brittle deformation results in the Formation of normal faults due to the extensional regime.

The structural variance extracted along the top Sembar Formation (early Cretaceous), Lower Goru Formation (middle Cretaceous) and Upper Goru Formation (late Cretaceous) exhibit the normal faults trending in the NW-SE direction. These faults are of several kilometres in length, and they make an integral part of every faulted margin in the study area. These faults generally are vertical to sub-vertical on the seismic section. Concluding the above discussion explains the dominant extensive NW-SE trending faults developed due to extensional tectonics from the anticlockwise rotation of 20° of Indian Plate with 15cm/year an average speed of drifting (Powell, 1979).

5.2 Well Log Observations

Well log data allows to calculate the hydrocarbon potential of the area. The Lower Goru Formation is a reservoir zone, and its physical properties are determined. For sands of the prospective reservoir, namely lower Goru sands, average porosity, shale volume, hydrocarbon saturation, and water saturation were computed using well data.

The petrophysical details of well data utilized in the research work are given in Table 1. The volume of shale, porosities show that the reservoir rock is suitable for hydrocarbon accumulation and production (Fig. 9). The calculation of water saturation shows that all wells are abandoned & water-saturated.

6. Conclusions

1. Seismic interpretation of the Badin region indicates the existence of normal faults. These interpreted normal faults restricted to the Mesozoic age. The identified listric normal fault system oriented in NW-SE direction with SW dip.
2. The 3D structural analysis reveals gently dipping strata towards the west. As a result, hydrocarbon up-dip migration is predictable in the proximity of the research area.
3. The average porosity in the Lower Goru Formation is 14%, average shale volume is 11% and effective porosity is 11%. The petrophysical analysis concluded that the Lower Goru Formation is a good reservoir rock.
4. It is recommended that for the better understanding of subsurface geological structures and locating hydrocarbon prospective areas, the

Table 1: Petrophysical results of Lower Goru Formation.

Well Name	Vsh%	Sonic Porosity%	Density Porosity%	Total Porosity%	Effective Porosity%
Doti	6-8	15-17	11-13	12-14	11-13
Mehro	10-12	22-24	13-15	15-16	13-15
Nereri	6-8	18-20	13-15	15-16	13-15
Raj-East	20-25	15-17	7-9	10-12	8-10

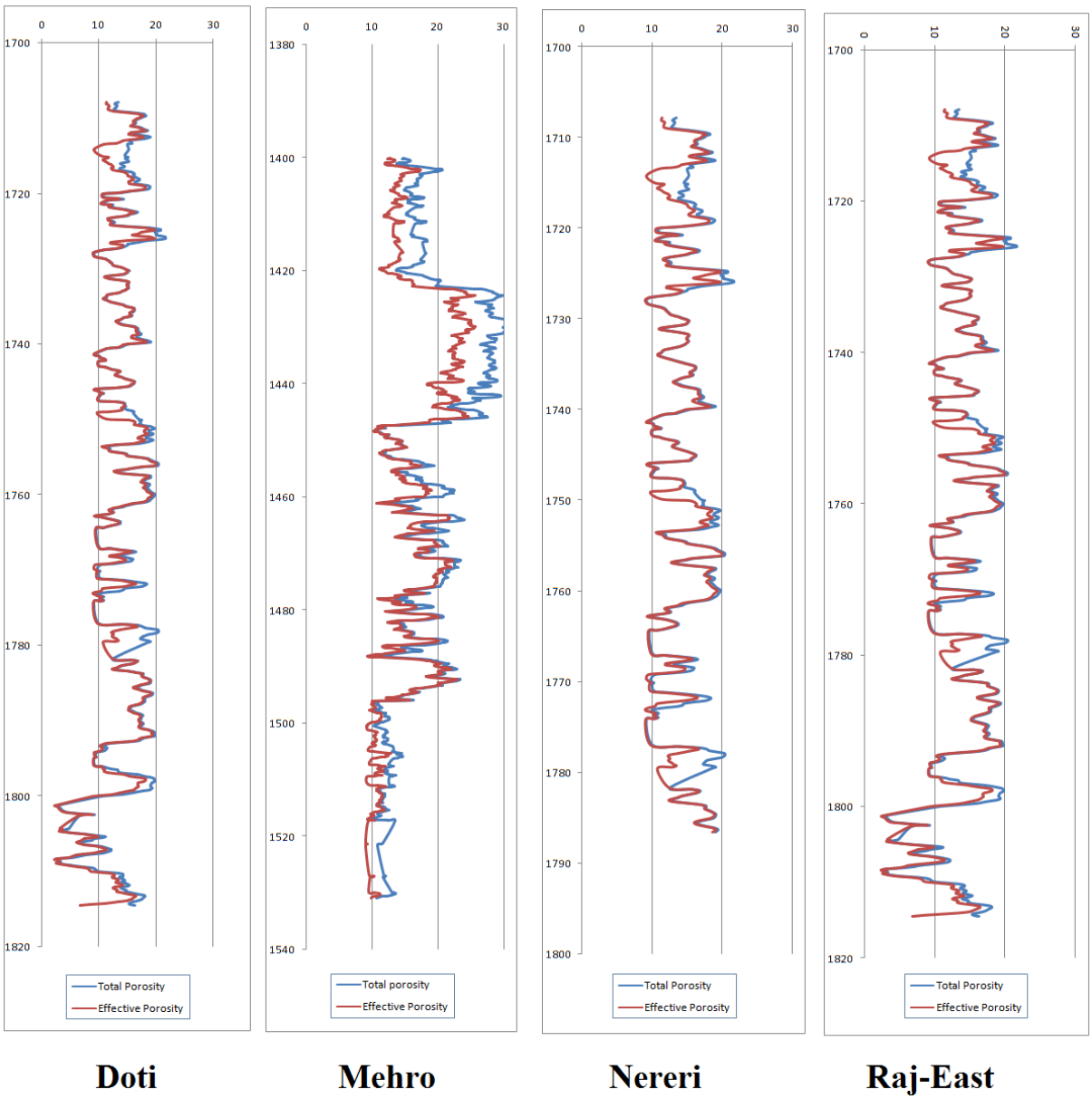

Fig. 9: Calculated porosities of wells utilized in research work.

3D seismic interpretation should be performed on a larger scale as executed in this study.

Acknowledgement

Special recognition from authors to Landmark Resources (LMKR), Pakistan with prior permission from the Directorate General of Petroleum Concession (DGPC) for providing seismic reflection data and well data of the Lower Indus Basin for this project.

References

Abbasi, S.A., Solangi, S.H., Ali, A., 2015. Seismic Data Interpretation: A Case Study of Southern Sindh Monocline, Lower Indus Basin, Pakistan. Mehran University Research Journal. 34(2), 107-115.

Ahmed, W., Azeem, A., Abid, M.F., Rasheed, A., Aziz, K., 2013. Mesozoic Structural Architecture of the Middle Indus Basin, Pakistan- Controls and Implications. PAPG/SPE Annual Technical Conference, Islamabad, Pakistan, 1-13.

Alam, M.S.M., Wasimuddin, M., Ahmad S.S.M., 2002. Zaur Structure, A Complex Trap in a Poor Seismic Data Area, BP Pakistan Exploration & Production Inc. AAPG Search and Discovery Article #90149©2012. PAPG/SPE Annual Technical Conference, 2-4 November 2002, Islamabad, Pakistan. 1-3.

Bannert, D., Raza, H.A., 1992. The Segmentation of Indo-Pakistan Plate. Pakistan Journal of Hydrocarbon Research, 4(2), 5-32.

Energy Year Book, 2012-2013. Hydrocarbon Development of Pakistan, Government of Pakistan.

Jadoon, I.A.K., Khawaja, A.A., 1997. Model Geometries of Extensional Faults: Implication on Structure of the Lower Indus Basin. Pakistan Journal of Hydrocarbon Research, 9, 35-47.

Hilterman F.J., 2001. Seismic amplitude interpretation. Society of Exploration Geophysicists and European Association of Geoscientists and Engineers.

Kadri, I.B., 1995. Petroleum Geology of Pakistan. 93-108.

Malick, Z.A., Kamal, M., Malik, A., Bodenhausen, J.W., 1988. Petroleum Potential and Prospects in Pakistan. Proceedings of the Petroleum for the Future Symposium held in Islamabad, Pakistan, 71-99.

Memon, A.D., Siddiqui, I., Memon, A.A., 1999. The Role of Cretaceous Rifts on the Occurance of Oil in Sindh Monocline. Pakistan, SPE-PAPG Annual Technical Conference Proceedings.

Munir, A., Asim, S., Bablani, S.A., Asif, A.A., 2014. Seismic Data Interpretation and Fault Mapping in Badin Area, Sindh, Pakistan. Sindh University Research Journal, 46, 133-142.

Powell, C.McA., 1979. A speculative tectonic history of Pakistan and surroundings: some constraints from the Indian Ocean. In: Farah, A. & K.A. DeJong, eds., Geodynamics of Pakistan. Geological Survey of Pakistan, Quetta, 5-24.

Sheikh, S.A. Naseem, S., 1999. Sedimentary Environment and Hydrocarbon Potential of Cretaceous Rocks of Indus Basin, Pakistan. Pakistan Journal of Hydrocarbon Research, Islamabad, 11, 1-14.

Tiab, D., Donaldson, E.C., 2015. Petrophysics: theory and practice of measuring reservoir rock and fluid transport properties. Gulf professional publishing.

Tectostrat, 1992. Trans-Indus and Salt Range Study Report.

Treloar, P.J., Izzat, C.N., 1993. Tectonics of the Himalayan collision between the Indian plate and the Afghan block: a synthesis, In: Treloar, P.J. and M.P. Searle, eds., Himalayan Tectonics. Geological Society of London. Special Publication, 74, 69-87.

Yuedong, Q., Hongwei, A., 2007. Study of petrophysical parameter sensitivity from well log data. Applied Geophysics, 4, 282-7.

KASHMIR JOURNAL OF GEOLOGY (KJG)
www.kjg.ajku.edu.pk

Diagenesis using scanning electron microscopy of carbonates of Kirthar Formation, Lower Indus Basin, Sindh, Pakistan

Muhammad Kashif Samoon[1*], Parveen Akhtar Usmani[1], Imdad Ali Brohi[1], Rafique Ahmed Lashari[1]

[1]Centre for Pure and Applied Geology, University of Sindh, Jamshoro, Pakistan.

*Corresponding author:
kashif.samoon@usindh.edu.pk

Received: 20 April 2021
Accepted: 28 October 2021
Published Online: 27 December 2021

Abstract

Diagenesis of the carbonate rocks has revealed different aspects of the sedimentology of the Kirthar Formation which is one of the significant rock units of the Lower Indus Basin. The formation is extensively distributed through the area that is the upper part of the Southern Indus Basin, and it is broadly dispersed in the Sindh Province. It comprises limestones, in places associated with shale and minor marl beds. The limestone is light grey, cream-coloured or chalky white, weathers in grey, brown or cream colours. One of the most extensively used tools in the area of earth sciences, which includes anything from materials to environmental research, is the scanning electron microscope. The investigation shows that after deposition, carbonates of the Kirthar Formation have been exposed to a range of diagenetic processes that brought about changes in porosity, mineralogy, chemistry, and texture. Unlike other carbonate minerals, the ones studied here are less prone to dissolution, recrystallization, and replacement. The present investigation of diagenesis is done with the assistance of scanning electron microscopy which has uncovered the understanding of various diagenetic processes, for example, cementation, dissolution, neomorphism and so on within the carbonates of the Kirthar Formation. Furthermore, the activities of the organisms on carbonates have also brought diagenetic changes to the textures through biogenic processes. Sediments have been reworked by leaving signs of microbes in certain locations.

Keywords: Diagenesis, Kirthar Formation, Scanning Electron Microscopy

1. Introduction

The purpose of this research is to use a scanning electron microscope to investigate the diagenetic characteristics of carbonates of the Kirthar Formation.

1.1 Kirthar Formation

The name "Khirthar" was suggested by Blanford (1876). He utilized the term Khirthar got from the "Khirthar range" to portray Eocene layers between his "Ranikot Group" and the "Nari" in western Sindh. Later, Noetling (1903) isolated the lower part with the "Laki Series" and held the term "Khirthar" from the upper part. The Khirthar Formation of the present study is comparable to the "Khirthar" of Noetling (1903) and the "Spintangi Limestone" of Oldham (1890).

The Canadian Report has characterized the rock unit as the "Brahui Limestone" (Hunting Survey Corporation, 1961) that is separated into two members one is Kirthar which is the lower part and possesses fossils of Eocene, and the other is Gorag, which is the upper part and bears Oligocene fossils. Both the individuals are characterized on the fossil content premise. Kirthar Formation comprises limestones, associated with shale and some marl. The limestone is light grey, cream-coloured or chalky-white, weathers in grey, brown or cream colours. The formation is thick-bedded to massive, occasionally nodular and incidentally contains algal and coralline features. The shale bed is calcareous, olive, orangish, yellow, dim, delicate and gritty.

The Formation is solely cliffy with monstrously composed of limestone. It is generally spread all through the area for example upper side of the "Lower Indus Basin". The unit is generally distributed in all of Sindh for example Pab Range, Khirthar Range, west of Laki Range, Thano Bula Khan, Kot Digi (District Khairpur) and Rohri. Its lower stratigraphic contact is conformed with Tiyon Formation and the upper contact of the formation is generally unconformable with the overlying Nari Formation. Nonetheless, as per Hunting Survey Corporation (1961), it has conformable contact with the Nari Formation nearby around Gaj River. The two of its lower (stratigraphic) and upper limits are proved time intrusive. As per Hunting Survey Corporation (1961), the type section/locality of the Kirthar Formation is the Gaj River Section: (Lat. 26º 56' 10" N and Long. 67º 09' 06" E).

1.2 Scanning Electron Microscopy

The benefits of the SEM as an imaging apparatus such as high known spatial resolution, the enormous profundity of the field, and easy specimens preparation make it a significant tool in different parts of geology. Concerning the study of sedimentology, especially diagenesis in carbonate rocks, three-dimensional pictures of individual sediments and between developments might be gotten. Information on texture and also porosity can likewise be created. Other than the availability and strength proportion of various types of mineral particles can likewise be searched out in the provisions of their chemically opt investigation or the more explicitly Electron Microprobe Analysis with the assistance of an extra accessory connection called Energy Dispersive X-Ray Spectrometer (EDS) whenever appended. Electron microprobe examination is in this manner done simply with the creation of EDS. The chemical testing of minerals, as well as rocks, has evolved as a daily practice by utilizing Electron Probe Microanalysis (EPMA) (Reed and Romanenko, 1995).

1.3 Diagenesis

After the deposition, carbonates particles are exposed to an assortment of diagenetic activities that achieve changes in porosity, mineralogy, and chemistry. The carbonate origin minerals are by and large more powerless to disintegration, recrystallization, and substitution than do most silicate origin minerals. The diagenetic processes assume a vital part in numerous physical, and chemical changes as well in the carbonates. Indeed, even at moderate burial depths as shallow as possible 100m, compaction might diminish the depositionally original thickness of carbonate sediment grains by as much as one-half, going with the porosity decrease of 0 to 60 percent of original pore volumes (Shinn and Robbin, 1983).

2. Materials and Methods

In total, three areas were picked for this important study. The necessary fieldwork was completed for the proper collection of samples and measurements of desired sections. Other than the other geological and also physiographic qualities were likewise taken into the note. Fresh specimens were gathered for investigation. The sample collection and field information was carefully organized as lithologic logs. Corel draw and Xara computer software packages were used to foster an obvious pictorial tale of various sedimentary skylines of the Kirthar Formation. Following is the depiction of lithological logs of the areas:

1- Gadularo Section:

Lat. 25º 25/ 20// N
Long. 67º 48/ 45// E

The region of this particular section is located around 75 km southwest of the city Hyderabad, 5

km northwest of town Thano Bola Khan, Gadularo is structurally a doubly plunging anticline as displayed in (Fig. 1A). Here the Nari Formation unconformably lies in the Kirthar Formation, whereas the underlying Tiyon Formation is totally missing. The area involves numerous limestone horizons that are thickly-bedded, compact and hard with high fossil content (Fig. 2A).

2- Kambho Jabal Section:

Lat. 25º 33/ 96// N
Long. 67º 47/ 714// E

The area is situated around 15 km close to Bachani town, which is situated in taluka Thano Bola Khan. Structurally Kambho Jabal is an enormous north-south moving anticline (Fig. 1B). Both the lower and upper stratigraphic contacts are clearly observable with Tiyon and Nari Formations individually. There available are different limestone rock units inside the formation, which are primarily hard, compact and enormous in nature. It is profoundly fossiliferous comprising bigger foraminifer shells, bivalves, echinoids, and gastropods fossils (Fig. 2B).

3- Watawaro Rojh Jabal:

Lat. 25º 10/ 20// N
Long. 67º 40/ 05// E

The section lies about 20 km southwest of Thano Bula Khan as shown in (Fig. 1C). Upper and lower contacts of the Kirthar Formation are present in the area. The limestone of the Kirthar Formation mostly is massive and thick and nodular in places and contains fossils of bivalves, echinoids, worm burrows and gastropods (Fig. 2C)

2.1 SEM Analysis

Representative and chosen specimens which were efficiently gathered from allotted units were examined under the Scanning Electron Microscope (SEM) Laboratory, available at the "Center for Pure and Applied Geology, University of Sindh, Jamshoro".

The method was instated with the cutting of chips of rock samples followed by the cleaning of similar chips with fine grit on the clean glass surface. The cleaned and flat chips were then put on a sample stub of SEM, utilizing a conductive twofold-sided carbon conductive tape. Then at that point, it was inserted in the chamber of the "JEOL JSM-6490 LV" Scanning Electron Microscope which is additionally outfitted with an additional and significant extra part of "Bruker EDS".

All appropriate functional controls of SEM were set to acquire the fine focusing resolution at high and wanted magnifications of the samples. Photomicrographs of the chosen positions were captured for study and interpretation. Then after the investigation was trailed by the elemental accusation of the samples, both qualitative and also quantitative. For that EDS was initiated. In the wake of arriving at an optimal magnification of x90, the samples were then chemically analyzed. The elemental composition was determined in the form of different spectra heights for qualitative review and simultaneously the test investigation was accomplished in tabular form for the quantitative study.

3. Results

Different diagenetic processes within the limestone microfacies of the Kirthar Formation in the present study have been interpreted and discussed. Each process has been elaborated in the light of Scanning Electron Microscopy results. The systematic description is given below:

3.1 Biogenic Alteration

The paleo-activities of the fossil organisms on the carbonate residues may likewise bring diagenetic changes to the surface texture. Living beings in such depositional conditions adjust residue by boring, burrowing, and sediments ingesting exercises, similarly to the siliciclastics conditions. These activities may destroy primary sedimentary structures (Demicco and Hardie, 1994) in carbonate sediments and leave behind spotted sheet material and different sorts of organic traces. In this work, the greater part of the hints of the fossils found inside the realms of limestone microfacies, have a place with foraminifer microfossils (Fig. 3).

3.2 Cementation

Out of the most significant cycles of limestone, diagenesis is the process of cementation. The bonding agent in limestone facies used to be calcite or the lesser steady aragonite. Cement assumes a vital part in limestones and is viewed as the dynamic reason for the quality and level of the auxiliary porosity and porousness (Fig. 4). The habit of the limestone rocks i.e., compact or loose is likewise fundamentally an element of kind of bonding cement. In the facies of the Kirthar Formation, the prevailing cement is calcite.

3.3 Dissolution

Next to cementation, dissolution is likewise accepted as a significant diagenetic process. The presence of pore spaces and the optional permeability favours the invasion of fluids inside and in this manner cause the action of dissolution. Aragonite is promptly broken down by liquids than

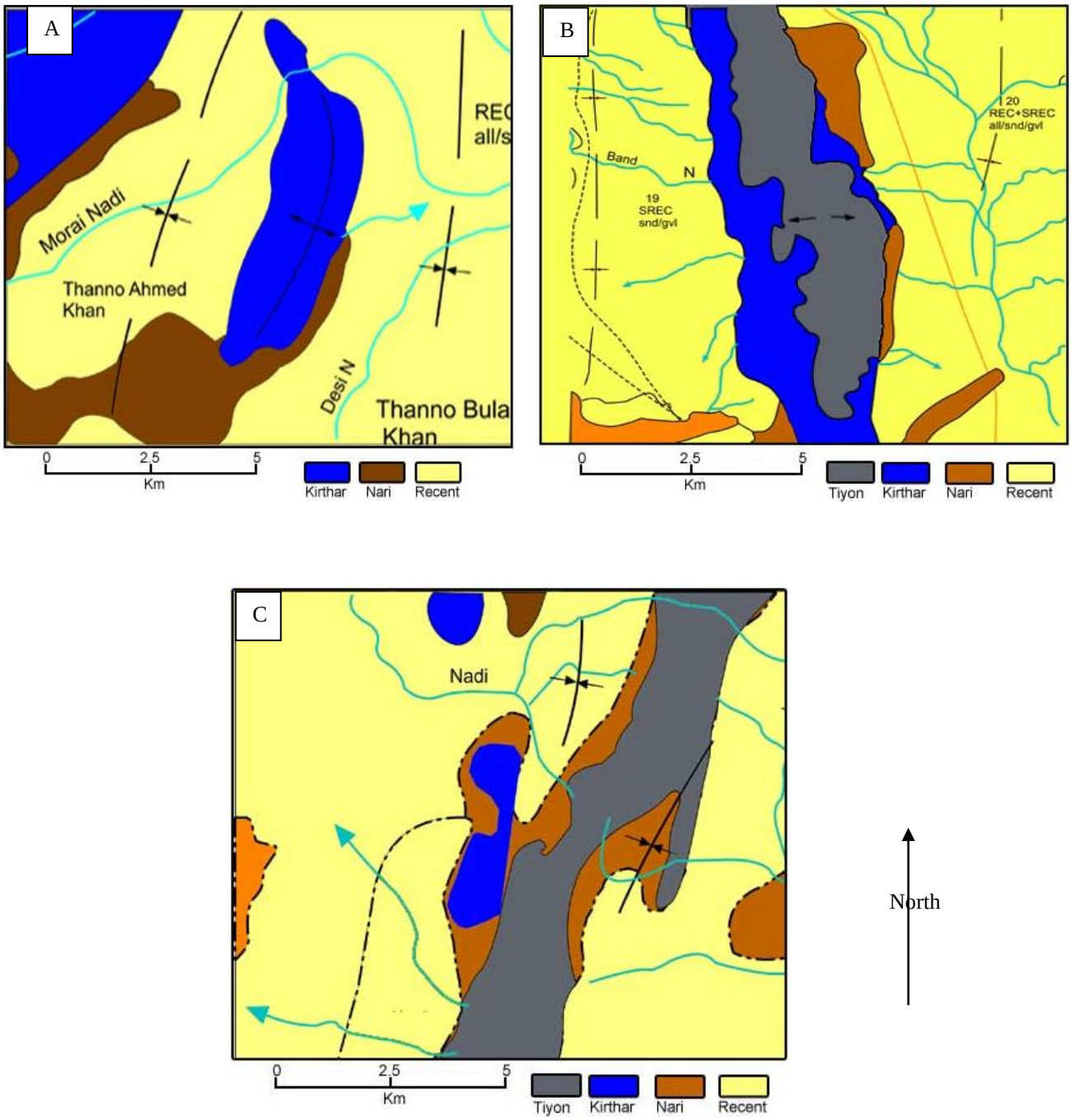

Fig. 1: Geological map shows (A) Gadularo Anticline, (B) Kambho Jabal and (C) Watawaro Rojh Jabal, along with Formations in different colours.

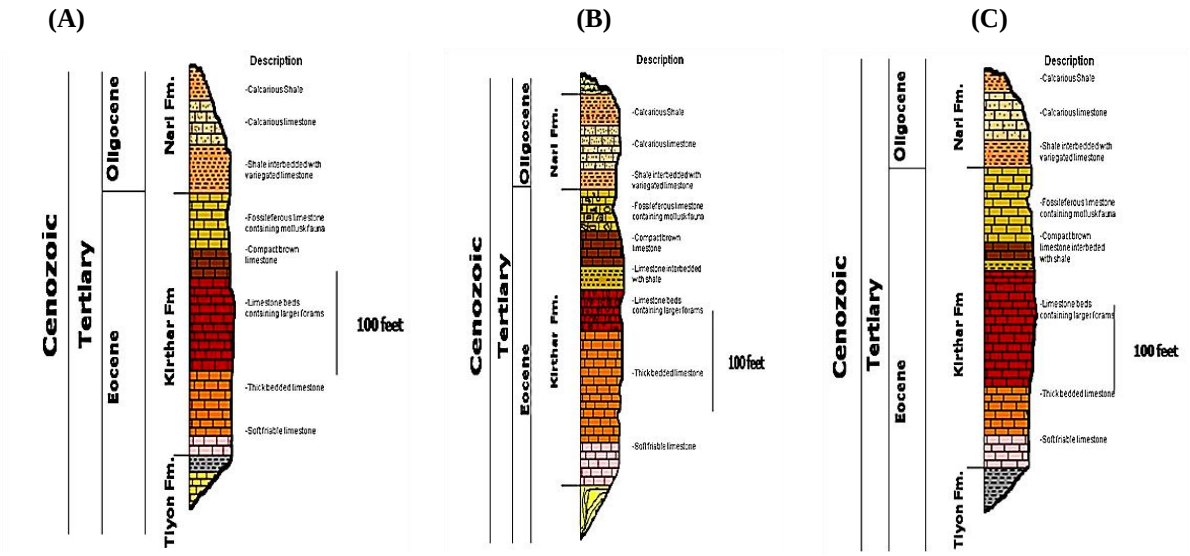

Fig. 2: Shows lithologic logs of (A) Gadularo Anticline, (B) Kambho Jabal and (C) Watawaro Rojh Jabal.

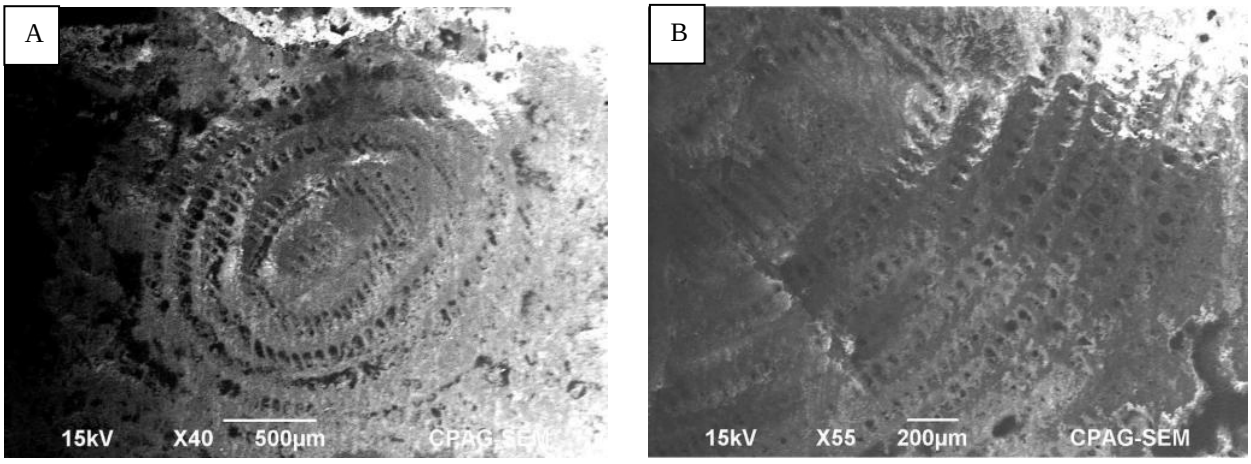

Fig. 3: Electron photomicrographs of traces of foraminifera microfossils (A, B).

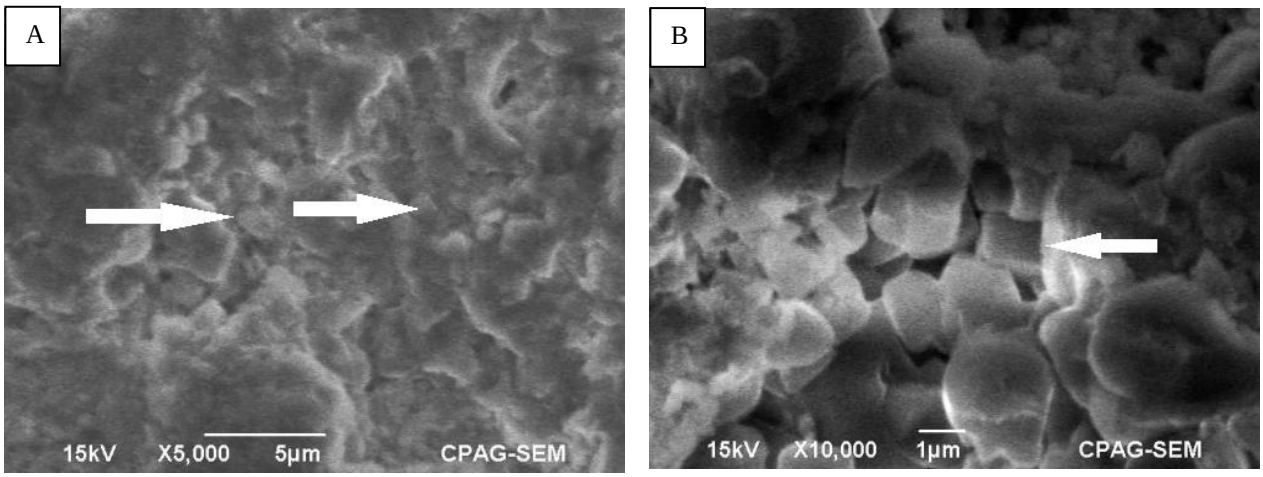

Fig. 4: An Electron photomicrograph shows the cement (A, B, arrows).

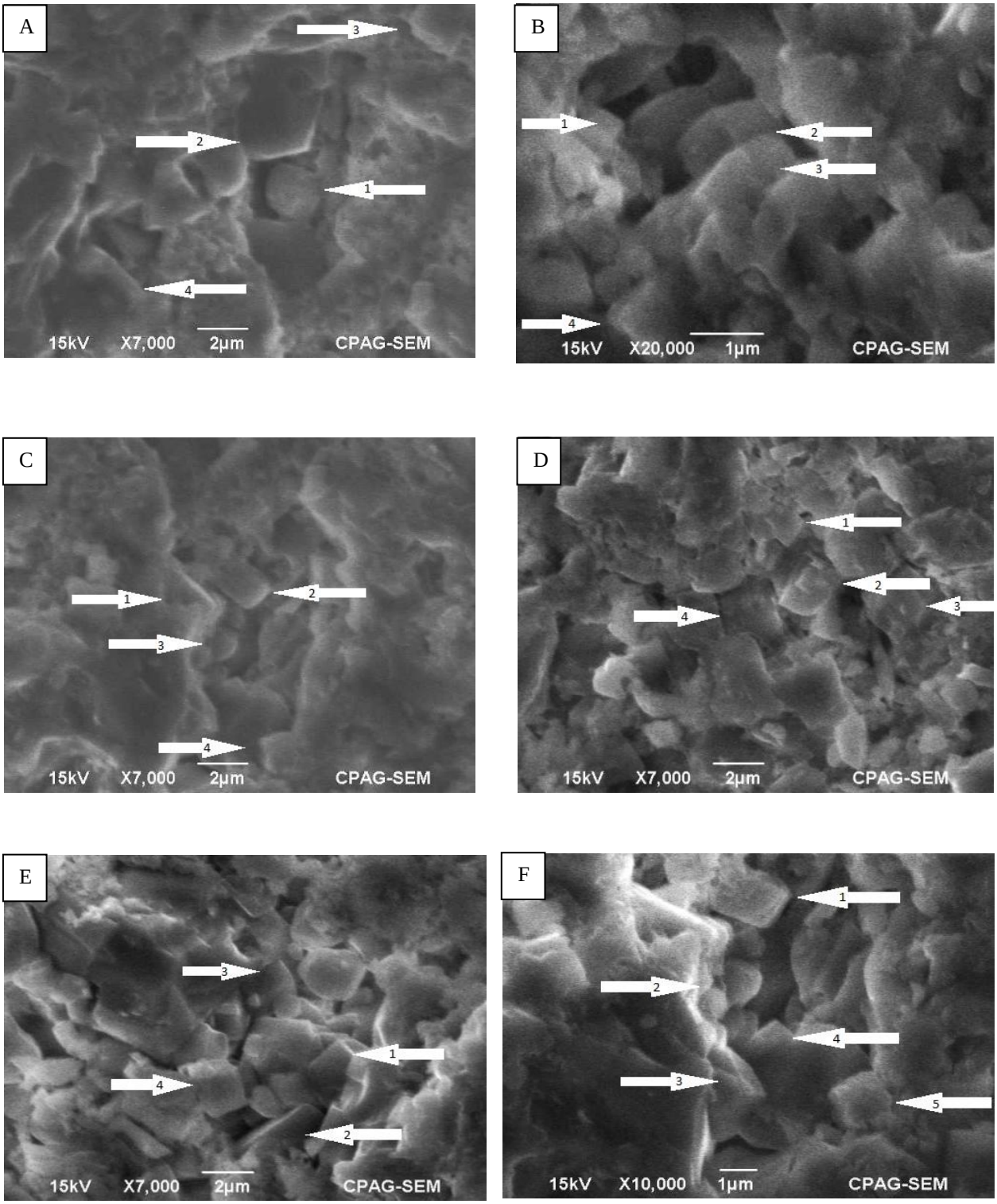

Fig. 5: An Electron photomicrograph shows the dissolution of calcite cubes (A, B, Arrows), Neomorphism (C, D, Arrows), compaction (E, F Arrows).

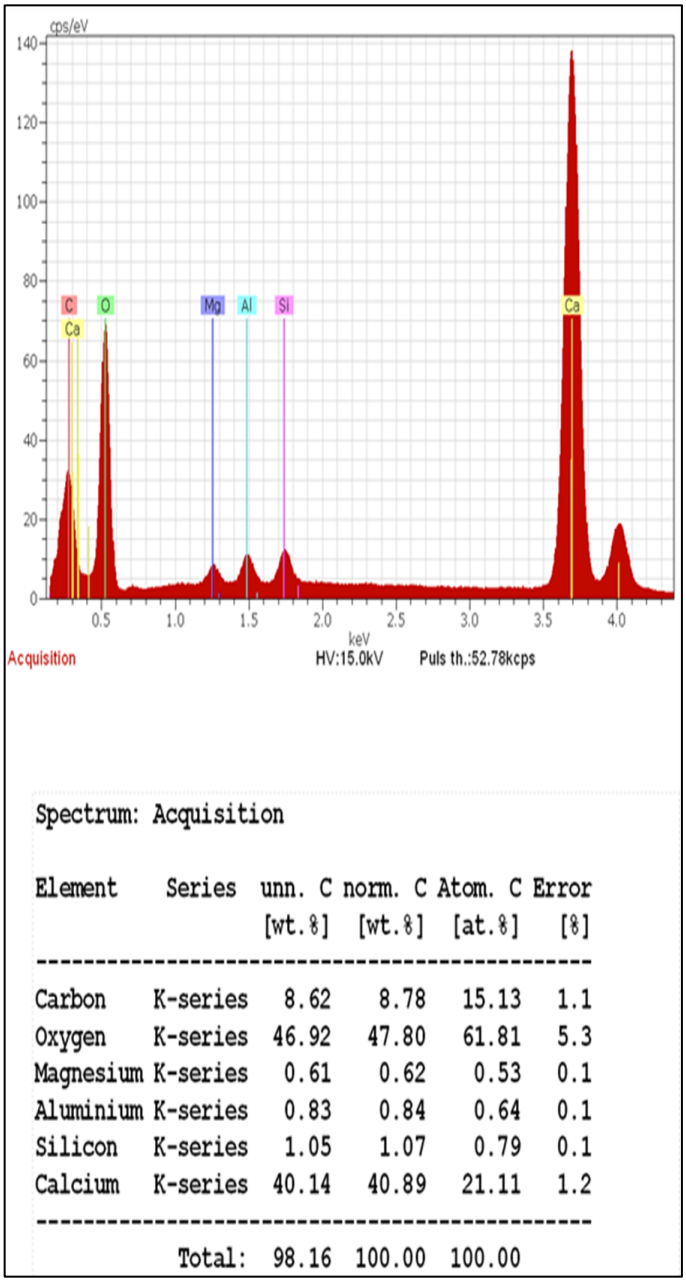

Spectrum: Acquisition

Element	Series	unn. C [wt.%]	norm. C [wt.%]	Atom. C [at.%]	Error [%]
Carbon	K-series	8.62	8.78	15.13	1.1
Oxygen	K-series	46.92	47.80	61.81	5.3
Magnesium	K-series	0.61	0.62	0.53	0.1
Aluminium	K-series	0.83	0.84	0.64	0.1
Silicon	K-series	1.05	1.07	0.79	0.1
Calcium	K-series	40.14	40.89	21.11	1.2
	Total:	98.16	100.00	100.00	

Fig. 6: An EDX Spectrum and Acquisition table of limestone specimen shows the presence of Aluminum, Magnesium and Silicon in the limestone of the Kirthar Formation.

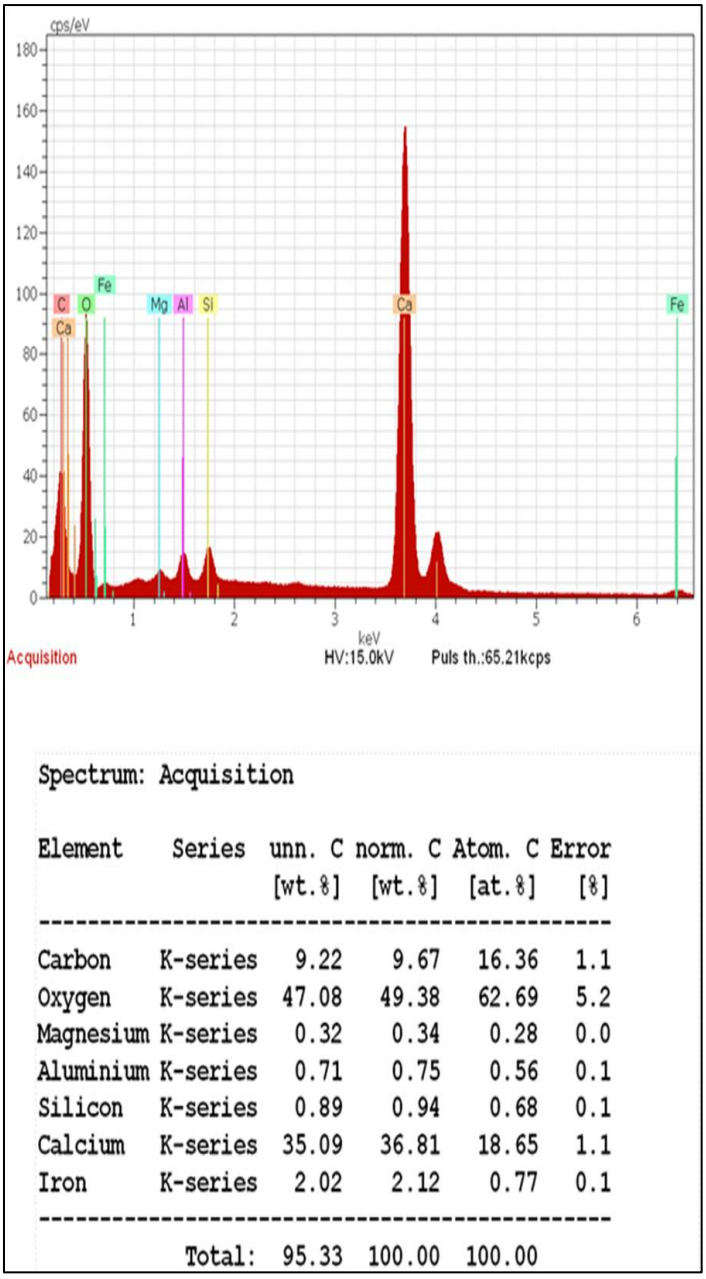

Spectrum: Acquisition

Element	Series	unn. C [wt.%]	norm. C [wt.%]	Atom. C [at.%]	Error [%]
Carbon	K-series	9.22	9.67	16.36	1.1
Oxygen	K-series	47.08	49.38	62.69	5.2
Magnesium	K-series	0.32	0.34	0.28	0.0
Aluminium	K-series	0.71	0.75	0.56	0.1
Silicon	K-series	0.89	0.94	0.68	0.1
Calcium	K-series	35.09	36.81	18.65	1.1
Iron	K-series	2.02	2.12	0.77	0.1
	Total:	95.33	100.00	100.00	

Fig. 7: An EDX Spectrum and Acquisition table of limestone specimens shows the presence of silicon and magnesium along with other elements.

the calcite relies on the forcefulness of the liquids which, if intense, can likewise disintegrate the calcite grains. (Fig. 5 A, B) shows the process of dissolution of calcite microcrystals in the Kirthar Formation.

3.4 Neomorphism

The change of one mineral into another is a common process in many carbonate hierarchies. “Neomorphism” is a term utilized by Folk (1965) to cover the joined cycles of reversal (e.g., change of aragonite to calcite) and also recrystallization. The way that the less stable aragonite is an unsteady mineral when contrasted with calcite makes the genuinely positive ground be changed into a steadier chemical compound i.e., calcite. So many such inversion and recrystallization clues are found in present examinations (Fig. 5 C, D). As infers to the course of neomorphism, it may be seen that the entire surface and texture of limestone is obliterated, and recrystallization is occurring.

3.5 Compaction

The well-known peculiarity of carbonate rocks is the tight packing of the grains which resulted into so many physical and chemical alterations. The course of compaction is straightforwardly corresponding to the depth of burial, the more the depth, the higher the compaction. The most impacted property of the limestone is porosity with the rising overburden pressure of sediments, which in most cases, remarkably decreases the original pore spaces. In the scanning electron microscopy of the chosen samples, the depth was seen which shows the reduction in pore spaces and dissolution of calcite crystals (Fig. 5 E, F). At profound burials of the carbonates, chemical compaction may likewise occur bringing about precipitation and dissolution of some non-carbonate origin minerals such as the clay minerals. This phenomenon is clearly observed in the EDS analysis of a couple of samples (Fig. 6).

3.6 Replacement

The process of replacement is common in carbonates and, more specifically, limestone rocks, as it is in most siliciclastic rocks. It is the process by which one mineral dissolve and another mineral precipitates at the same time. Dolomitization of some $CaCO_3$ sediments is one type of replacement. Likewise, numerous different types of noncarbonate minerals replace carbonate minerals during diagenesis, including microcrystalline grains of quartz. The process of replacement is very well seen in the current investigation. The EDS analysis was carried out for the determination of the presence of other minerals. The existence of silicon and magnesium alongside different other elements are indications of the replacement processes (Fig. 7).

4. Conclusion

Practically every single diagenetic process has been seen in the current investigation. Scanning Electron Microscopy with an assistance of an EDS has uncovered the micro-level features of carbonates of the Kirthar Formation. The paleo-temperature conditions during the deposition of the Kirthar Formation used to be in the warm to medium range, nevertheless, cool water also prevailed in certain cases. The diagenetic processes such as cementation and compaction caused by overburden and rising pressure and temperature have resulted in tight packing of the limestone component of the Kirthar Formation, resulting in mineral dissolution and alteration in places. Therefore, the deduced environment of deposition of the Kirthar Formation in view of diagenetic processes is the shallow shelf and categorically the Epeiric Shelf Environment.

References

Blanford, W.T., 1876. On the geology of Sindh. Records of the Geological Survey of India, 9,8-22.

Demicco, R.V., Hardie, L.A., 1994. Sedimentary structures and early diagenetic features of shallow marine carbonate deposits: SEPM Atlas Series No. 1, Society for Sedimentary Geology, Tulsa, Okla, 265.

Folk, R.L., 1965. Some aspects of recrystallization in ancient limestones. In Pray, L.C., Murray, R.C., (Eds.), Dolomitization and limestone diagenesis. Society of Economic Paleontologists and Mineralogists Special Publication, 13,1448.

Hunting Survey Corporation (HSC)., 1961. Reconnaissance geology of part of West Pakistan (Colombo plan cooperative project). Canada Govt. Toronto, 550.

Neotling, F., 1905. Vorlaufige Mitteilung uber die Entwickelung und die Gleidrung der Tertiar fornation in westhehen Sibd (Indien). Ibid. Jahrb., 6, 129-137.

Oldham, R.D., 1890. Report on the geology and economic resources of the country adjoining the Sindh-Pishin Railway between Sharigh and Spintangi, and of the country between it and Khattan. Ibid., Rec., 23, 3, 93-109.

Reed, S. J. B., Romanenko, I. M., 1995. Electron probe microanalysis. In: Marfunin, A.S., (Eds.), Advanced Mineralogy, Methods and Instrumentations: Results and Recent Developments: Springer-Verlag, Berlin, 2,240-246.

Shinn, E.A., Robbin, D.M., 1983. Mechanical and chemical compaction in fine-grained shallow-water limestones. Journal of Sedimentary Research, 53(2), 595-618.

KASHMIR JOURNAL OF GEOLOGY (KJG)
www.kjg.ajku.edu.pk

Facies Architecture and Sequence Stratigraphy of Tredian Formation in Zaluch Gorge, Western Salt Range, Pakistan

Syed Kamran Ali[1]*, Khuram Iqbal[1], Tariq Mehmood[2], Muhammad Hussain Saleem Qadri[1], Arslan Qayyum[1]

[1]Institute of Geology University of Azad Jammu and Kashmir, Muzaffarabad, Pakistan.
[2]Oil and Gas Development Cooperation Limited (OGDCL), Islamabad, Pakistan.

*Corresponding author:
kamran.ali@ajku.edu.pk

Received: 18 May 2021
Accepted: 14 October 2021
Published Online: 27 December 2021

Abstract

The Triassic sequence is well exposed in Zaluch Gorge, Western Salt Range. The present work focused on detailed facies architecture and depositional setting of Tredian Formation by using outcrop data of Zaluch Gorge, Western Salt Range. Tredian Formation is composed of coarse grained sandy facies of the Middle Triassic age. The thickness of the formation is 36 meters in the Zaluch Gorge. Four lithofacies have been identified by using outcrop data which are the cross-bedded sandstone facie (TF_1), the Greywacke facie (TF_2), the massive sandstone facie (TF_3) and medium grained sandstone with carbonate cement (TF_4) facie. For the petrographic study, 12 samples of sandstone of the Tredian Formation were collected. Three microfacies were identified during the petrography of the Tredian Formation which are sub-arkose, quartz wacke and quartz arenite. Cementing materials are silica, hematite and calcite. Hematite cement is rich at bottom of the formation and the concentration of calcite cement is high at the top. On outcrop mainly coarsening upward sequence is marked with minor local finning upward sequence. Maximum flooding surface, system tracts and facies cycles have been marked on the outcrop data. Facie analysis shows that the lower part of the Tredian Formation was deposited in a delta lobe setting marking shallow upward cycles. In the middle part, thick sandstone was deposited in a fluvial setting dominated by coarsening upward cycle. In the final stage minor fluctuation in the sea level associated carbonate deposition. Thus, the Tredian Formation is of non-marine origin and depicts some good reservoir characteristics.

Keywords: Greywacke facie, Quartz arenite, High Stand System Tract (HST), Fluvio-deltaic; Tredian Formation; Salt Range

1. Introduction

The study area comprises of Zaluch Gorge, Potwar Sub-Basin which is located 30 km northeast of the Mianwali city Punjab province. According to the tectonic division of the Himalayas, this area lies within Sub-Himalaya (Fig. 1).

The tectonics of the Potwar sub-basin show the complex structures of the world. In Eocene time, the collision between Indian and Eurasian Plates is the cause of these complex tectonics. Precambrian to Recent rocks are exposed in Salt Range (which is the southern boundary of Potwar basin), along Salt Range Thrust (SRT). Before the collision of the Indian Plate and Eurasian Plate, the organic matter (OM) maturation was not sufficiently buried and many Precambrian to Paleocene rocks were thermally immature (Khan et al., 1986).

2. Material and Methodology

Tredian Formation was detailed observed in Zaluch Nala and samples were taken for lithofacies and microfacies analysis. For lithofacies analysis, the data was obtained from the outcrop of Zaluch Gorge, which included section measurement to observe variations in lithology and mark different lithofacies. About 20 fresh and representative rock samples were taken from well-exposed rock units in the Zaluch Gorge for microfacies analysis. Thin sections are prepared for some selected samples for the determination of microfacies. Sequence stratigraphy is an analysis of sedimentation trends and facies relation between erosional or non-depositional surface or lateral correlative conformance within a chronostratigraphic system (Van Wagoner et al., 1990; Posamentier and Allen, 1990). Different system tracts and stratigraphic surfaces are marked in the study area. In this study lithofacies, microfacies and sequence stratigraphic data will be used to critically evaluate the suggested depositional settings.

3. Regional Geology

Pakistan is situated at the junction of the Indian, Arabian and Eurasian plates. The northern and northwestern Pakistan (east of the Chaman fault) consist of the Upper Indus Basin (Kohat-Potwar basin) Hazara basin, Kalachitta Range, Kirthar and Sulaiman Ranges and these represent fore-land fold-and-thrust belts. These ranges developed in Eocene time due to the collision of the Indian Plate and Asian Plate. The study area lies in the Upper Indus Basin and from the northern side, it is bounded by Main Boundary Thrust (Coward and Buttler, 1985) while Salt Range Thrust is present at the south (Fig. 2). On the eastern side, Jhelum Fault is present while the Kalabagh fault is bounded the basin from the western side (Kazmi and Rana, 1982).

The geology of the Upper Indus Basin ranges from Pre-Cambrian to Recent rock sequences (Fatmi, 1977). The oldest rock unit is Salt Range Formation with lithology salt, marl and gypsum. The Cambrian sequence consists of the Jhelum Group (Baker et al., 1988). After Cambrian, deposition ceases till Permian. Tobra Formation of Permian marks disconformity. Tobra Formation is overlying by the Nilawahan Group. This group is conformably overlain by the Zaloch Group of Late Permian (Baker et al., 1988). Permian rocks are well developed in Western Salt Range. Mesozoic rocks are separated from the Permian sequence based on paraconformity. Triassic rock sequence consists of Mianwali Formation, Tredian Formation and Kingriali Formation. The Jurassic sequence includes Datta Formation, Shinawri Formation and Samana Suk Limestone. Mesozoic rocks are well developed in Western Salt Range.

The earlier name of the Tredian Formation was Kingriali Sandstone which is named by Gee (1945), but later the formation is renamed as Tredian Formation. It is a clastic-continental unit that succeeds the Mianwali Formation. The formation contains some microfossils of the plant (Balme, 1970). The formation consists of two members (Fatmi, 1977); the Landa Member (lower) on which Kummal (1966) worked while the other is Khatkiara Member (upper) which was worked by Danilchik and Shah (1967). Iqbal (2002) undertook detailed research work focusing on the fine resolution palynology of the middle Triassic Tredian Formation. This formation conformably overlies Mianwali Formation and is also conformably overlain by the Kingriali Formation (Shah, 1977 and 2009). In the Saiyiduwali section, the thickness of the Tredian Formation is 46 m (Alam, 2008). Iqbal et al., (2014) worked on Mianwali and Tredian Formations and suggested a progradational deltaic system in the low-latitude Western Salt Range. Khan et al., (2016) worked on the dating and depositional setting of the Tredian Formation.

4. Stratigraphic Succession in the Study Area

Study area located in the Zaluch Gorge, Western Salt Range in which rocks from Salt Range Formation (Precambrian) to Datta Formation (Jurassic) are present. Tobra Formation marks the base of the Permian sequence. Warchha Sandstone lies over the Tobra Formation. Dandot Formation is missing in Zaluch Gorge. Warchha Sandstone grades upward into Zaluch Group which includes Amb Formation, Wargal Limestone and Chhidru Formation. The rocks of the Permo-Triassic (PT) boundary are marine and have a conformable relationship but paraconformity is present based on different fauna species. After Permian, the Triassic sequence starts consisting of Mianwali Formation followed by Tredian Formation and Kingriali Formation. Datta Formation of Jurassic age, mainly sandstone rests conformably on Kingriali Formation. Stratigraphic succession of the Zaluch Gorge is shown in Table 1.

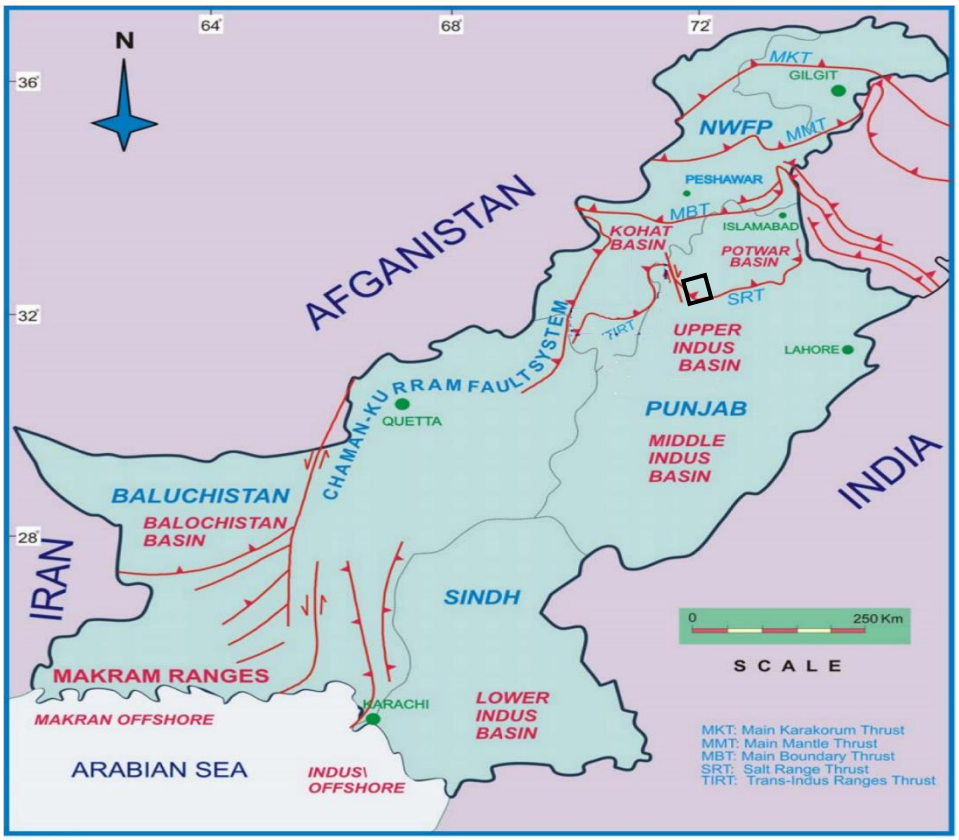

Fig. 1: Tectonic map of Pakistan. The rectangle shows the location of the study area (Kazmi and Rana, 1982).

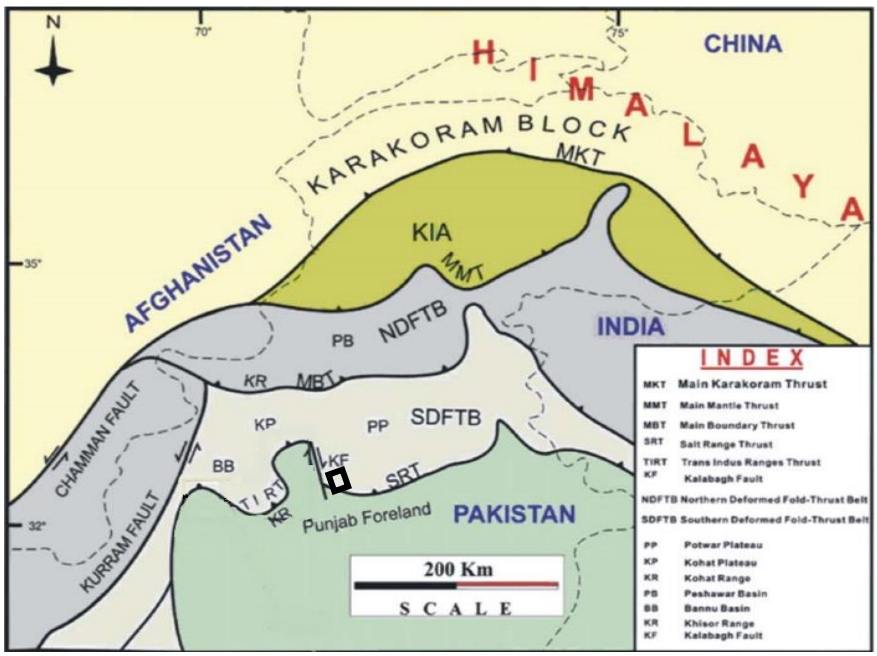

Fig. 2: Tectonic map of North Pakistan (modified after Pegler and Das, 1998). The rectangle shows the location of the study area.

5. Results and Analyses

5.1 Lithofacies of Tredian Formation

This formation comprises clastic rocks divided into two members. The lower sandstone and shale unit is the Landa member. The upper one is white sandstone Khatkiara member, which is massive, thickly bedded and gradually transfer into the overlying Kingriali Formation. The thickness of the Tredian Formation is 36 meters (Fig. 3). In the study area, the section is fully exposed with lower contact with the Mianwali Formation and the upper contact with Kingriali Formation (Photo 1 and 2). The upper contact is gradational with the Kingriali Formation while the lower contact is sharp with the Mianwali Formation. Four lithofacies of the Tredian Formation were identified in the study area (Photo 3; Fig. 3) which are as follows:

i) The cross-bedded sandstone facie (TF_1)
ii) The Greywacke facie (TF_2)
iii) The massive sandstone facie (TF_3)
iv) Medium grained sandstone with carbonate cement (TF_4).

5.1.1 The Cross bedded sandstone facie (TF_1)

This facie is dominantly consisting of cross-bedded, brownish sandstone. The presence of cross-bedding in this facie shows a common feature of the fluvial environment. The sandstone of this facie is fine to medium grain. The thickness of (TF_1) facie in the study area is 5 meters (Fig. 3).

5.1.2 Clayey-sand facie (TF_2)

This facie is dominantly consisting of whitish fine-grained clay and sand. The thickness of this facie is 8 meters in the study area (Fig. 3). This facie is composed of fine-grained material. Clay percentage is high. Clayey Sand facie is less compacted as compared to the cross-bedded sandstone facie.

5.1.3 Massive sandstone facie (TF_3)

This facie is dominantly composed of pinkish whitish massive sandstone. The thickness of this facie is 19 meters in the study area (Fig. 3). Four rock samples (ZT_6, ZT_7, ZT_8 and ZT_9) were taken for petrographic study. This facie is consists of sandstone (medium to coarse grained). It is massive sandstone and shows a fluvial environment.

5.1.4 Sandstone with carbonate cement (TF_4)

This facie is composed of sandstone with carbonate cement. The thickness of this facie is 4 meters in the study area (Fig. 3). This facie is composed of medium grained, bedded sandstone. It has carbonate cement in composition which indicates an environment in between deltaic to transitional.

5.2 Microfacies of Tredian Formation

For the petrographic study, twelve thin sections are prepared from the measured section and studied under the microscope. Visual modal mineralogical data and the percentage of quartz, feldspar and rock fragments are presented in Tables 2 and 3 respectively. The data are plotted on QFL sandstone classification diagrams by Petijohn et al., (1987) (Figs. 4 and 5). Mineralogically sandstone of this formation is composed of quartz, rock fragments, feldspar, muscovite, zircon and tourmaline.

5.2.1 Sub arkoses facies (TF_1)

Three rock samples (ZT_1, ZT_2 and ZT_3) are recognized as sub-arkose according to sandstone classification based on the quartz, feldspar, and rock fragment (Fig. 4). This microfacie extends up to 5m with coarsening upward sequence in this zone. The lithology of this zone is dominantly sandstone. Sandstone mainly consists of quartz 90-92%, feldspar 6-8% and rock fragments 2-3%. Cementing material is hematite. Angular to sub-angular grains represent that TF_1 facie is immature (Plate 1-1 and 1-2). Accessory minerals like tourmaline, chlorite and greenish-pinkish muscovite have been observed in this facie.

5.2.2 Quartz wacke facies (TF_2)

This microfacie is 8m thick and the grain size is fine. In this facies clay is 10% and a high amount of matrix is present. ZT_4 and ZT_5 are recognized as quartz wacke micro facie. Sub-hedral crystals of quartz are observed in thin sections. Accessory minerals like epidote and muscovite are observed (Plate 1-3 and 1-4). This facie is mainly consisting of quartz 47-51%, feldspar 1-2%, rock fragments 1-2%, matrix 30%, clay 10% and cement 8%. Quartz grains are subangular and fractured.

5.2.3 Quartz arenite facies (TF_3)

Four rock samples (ZT_6, ZT_7, ZT_8 and ZT_9) are recognized as quartz arenite according to the sandstone classification based on the percentage of quartz, feldspar, and rock fragments. These samples belong to massive sandstone lithofacies. This facie is 19 meters thick. The grain size of quartz mineral is almost the same and grain to grain contact shows that sandstone is mature and lack cementing material. In this facie percentage of quartz is high, which is 94-96%. Quartz is well sorted and angular to subangular. Other minerals are feldspar 3-4% and rock fragments 1-3%. Accessory minerals like tourmaline, muscovite, perthite, microcline and epidote has been observed in this microfacie (Plate 1-5 and 1-6).

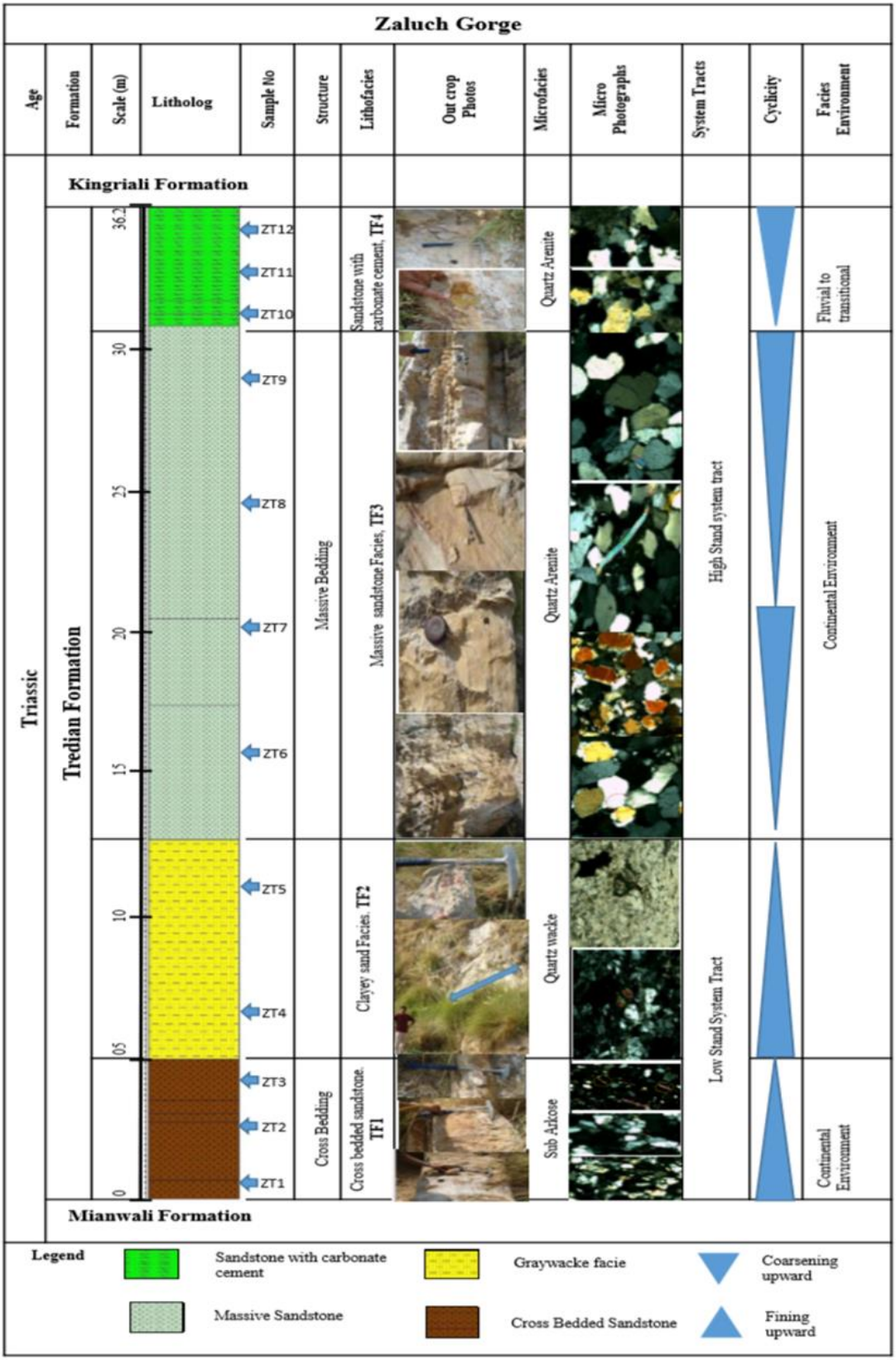

Fig. 3: Composite stratigraphic log of Tredian Formation in Zaluch Gorge showing lithofacies, microfacies, sequence stratigraphy and facies environments.

Table 1: Stratigraphic succession of the Zaluch Gorge, Western Salt Range.

FORMATION	LITHOLOGY	AGE
Datta Formation	Sandstone, Siltstone, Glass sand, Fire clay	Jurassic
Kingriali Formation	Dolomite, Limestone, Marl, Shale	Triassic
Tredian Formation	Sandstone, Shale	Middle Triassic
Mianwali Formation	Sandstone, Shale (Heterogeneous lithology)	Lower Triassic
Unconformity		
Chhidru Formation	Limestone, Sandstone	Late Permian
Wargal Limestone	Limestone, Dolomite	Late Permian
Amb Formation	Shale, Limestone	Middle Permian
Unconformity		
Sardhai Formation	Shale	Early Permian
Warchha Sandstone	Sandstone	Early Permian
Tobra Formation	Conglomerates having Tillitic, fresh water and complex facies	Early Permian
Unconformity		
Salt Range Formation	Salt, Marl, Gypsum	Precambrian

Table 2: Model mineralogical composition of sandstone of Tredian Formation, Zaluch Gorge (visual estimation).

Sample No.	Qtz.	Feld	R.F	Mus	Cement		Accessories
					Hem	Cal	
ZT_{12}	84	4	2	1	2	8	-
ZT_{11}	82	3	3	1	2	10	-
ZT_{10}	81	5	3	1	5	7	Epidote, Tourmaline
ZT_9	88	4	2	2	2	-	-
ZT_8	91	3	3	2	1	-	-
ZT_7	86	3	1	1	11	-	Epidote, Tourmaline
ZT_6	87	4	1	1	9	-	Epidote
ZT_5	51	1	1	1	2	1	Zircon
ZT_4	47	1	1	1	3	5	Epidote
ZT_3	50	2	3	4	38	-	Chlorite, Tourmaline
ZT_2	64	5	2	2	5	22	Zircon
ZT_1	79	7	2	2	9	-	Chlorite, Tourmaline

Table 3: QFL percentage and classification of sandstone (Petijohn et al., 1987) of Tredian Formation, Zaluch Gorge.

Sr. No.	Sample	Quartz	Feldspar	Rock fragments	Rock Type
12	ZT_{12}	93	5	2	Quartz arenite
11	ZT_{11}	93	4	3	Quartz arenite
10	ZT_{10}	91	5	4	Quartz arenite
9	ZT_9	94	4	2	Quartz arenite
8	ZT_8	94	3	3	Quartz arenite
7	ZT_7	96	3	1	Quartz arenite
6	ZT_6	94	4	2	Quartz arenite
5	ZT_5	96	2	2	Quartz wacke
4	ZT_4	96	2	2	Quartz wacke
3	ZT_3	92	6	2	Subarkose
2	ZT_2	91	6	3	Subarkose
1	ZT_1	90	8	2	Subarkose

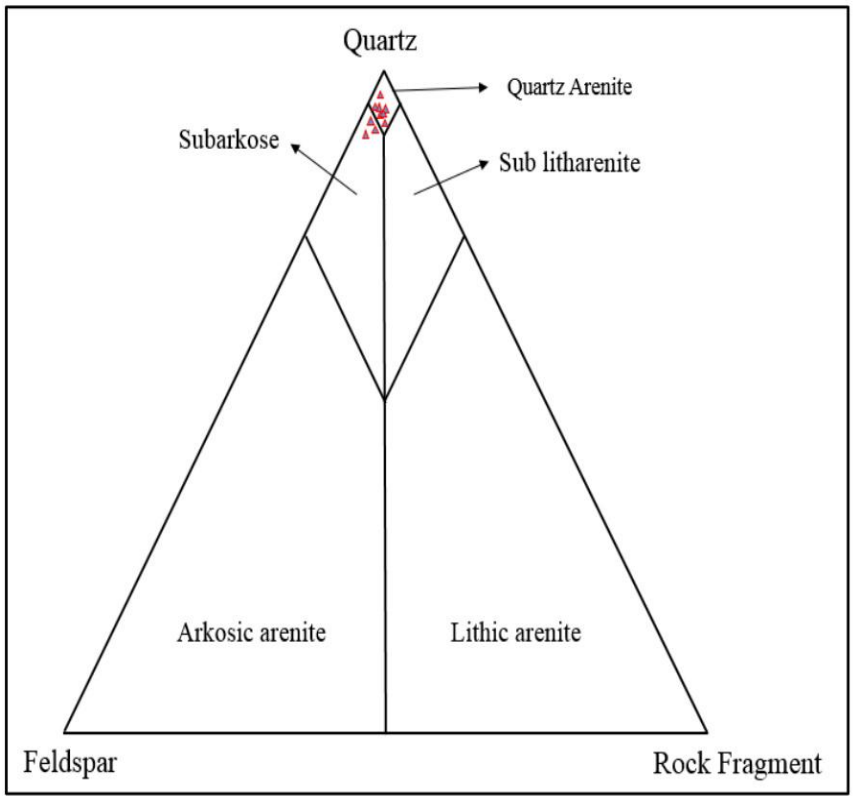

Fig. 4: QFL diagram shows the classification of sandstone (Petijohn et al., 1987) of Tredian Formation.

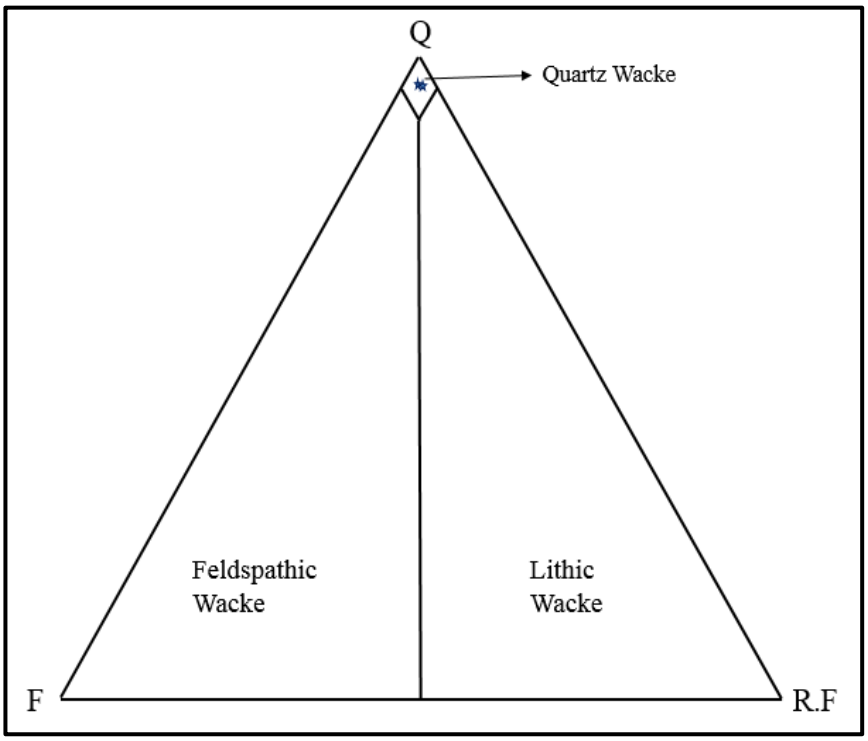

Fig. 5: QFL diagram shows the classification of sandstone (Petijohn et al., 1987) of Tredian Formation. (Q= Quartz, F= Feldspar and R.F= Rock fragment)

5.2.4 Quartz arenite facie (TF_4)

Three rock samples (ZT_{10}, ZT_{11} and ZT_{12}) are recognized as quartz arenite according to sandstone classification based on quartz, feldspar, and rock fragments (Fig. 3). The thickness of this facie is 4 meters in the study area. The grain size of quartz mineral is almost the same. Cementing material of this facie is carbonate cement (Plate 1-7 and 1-8). This microfacies has a high quartz percentage, which is 81-84%. The grains are well-sorted and angular to subangular. The percentage of feldspar and rock fragment ranges from 4-5% and 2-4% respectively. Calcite is a cementing material of this facie. The amount of calcite ranges from 7-10%.

5.3 Sequence Stratigraphy

Sequence Stratigraphy is a classic study of sedimentary basins which fills by genetic packages and these packages have erosional surfaces/unconformities and their correlative surfaces. The present work is focused on the sequence stratigraphy of the Tredian Formation in Zaluch Gorge. The overall Triassic period is marked by progradational strata. Paraconformity is marked on the base of the Mianwali Formation. Deposition of the Mianwali Formation is marked by different cycles of retrogradation and progradation. Sequence Boundary is marked in the field between Tredian Formation and Mianwali Formation. Contact between Tredian Formation and Mianwali Formation is shown in Photo 1.

On the basis of sequence stratigraphy, different cycles are marked in the field which are mainly coarsening up and rarely fining up sequence (Photo 4). TF_1 and TF_2 lithofacies are marked by sandstone and sandstone with clay respectively, which show slightly transgression. While TF_3 and TF_4 are marked by regression. The overall trend of the Tredian Formation is coarsening upward, and two systems tracts have been marked (Fig. 3) which are as follows.

5.3.1 Low stand System Tract (LST)

The LST comprises strata that deposited on the Falling Stage System Tract (FSST) after the fall of sea-level during regression and corresponding up-dip subaerial unconformity. Stacking pattern comprises fore stepping, thick aggrading clinoforms and top set of fluvial, coastal/deltaic deposits.

5.3.2 High stand System Tracts (HST)

The HST comprises the progradational strata that form when accumulation rates of sediment exceed the rate of increase in accommodation in the late stages of fall of sea level, causing a shoreline regression. At the base, the maximum flooding surface (MFS) is present and top marked by a composite surface. HST directly lies on MFS. HST is bounded by an unconformity and its correlative surface (Posamentier & Allen, 1990). Prograding and aggrading clinoforms stacking pattern comprise thin down dip, bounded by a top set of fluvial, coastal/deltaic deposits.

6. Discussion and Conclusions

6.1 Depositional Environment of Tredian Formation

The Triassic sequence of the Salt Range is composed of well-developed siliciclastic and carbonate units. Mianwali Formation is composed of clastic and carbonate units and represents the deep sea to the deltaic environment and overall coarsening upward cycles. Contact between Mianwali Formation and Tredian Formation marks the change in the environment of deposition which is marked by the clastic deposition of the Tredian TF_1 facie and the complete missing of aquatic fossils in this formation. Lithofacies and microfacies show that the initial facie (TF_1) of the Tredian Formation was accumulated in channel bar and delta front setting with the influence of some effect of shore-beach. These mark shallow upward cycles. In the middle part, thick sandstone was deposited in delta plain or fluvial setting dominated by fluvial influence representing the coarsening upward cycle. In the final stage, minor fluctuation in the sea level gives a chance to associate carbonate deposition. Thus the whole sequence represents a siliciclastic unit with carbonate deposition in the progradational delta settings (Fig. 6a).

Sequence Stratigraphy of Tredian Formation shows mainly coarsening upward cycles and some finning upward cycles which indicate prograde depositional settings. Contact between Tredian Formation and Kingriali Formation is gradational. Carbonates of the Kingriali Formation also form a prograde deposition system. The depositional model of the Tredian Formation in Zaluch Gorge is shown in Fig 6a and 6b.

6.2 Conclusion

The Tredian Formation is dominantly composed of sandstone unit. Different lithofacies has been marked on the outcrop. TF_1 facies is composed of fine grain sandstone, TF_2 facies is composed of fine grained sandstone with clays, which represent fining upward sequence. TF_3 facies is composed of massive sandstone of light grey colour. TF_4 facies is composed of sandstone with carbonate cement. Three microfacies were identified in the sandstone of the Tredian Formation. These microfacies include sub-arkose, quartz wacke and quartz arenite. The sandstone of the Tredian Formation is rich in quartz and grains are euhedral to subhedral. Sandstone is mature and lacks lithic fragments. The small amount

Photo 1: Photograph shows the lower contact of Tredian Formation with Mianwali Formation in Zaluch Gorge, Western Salt Range.

Photo 2: Photograph shows the upper contact of Tredian Formation with Kingriali Formation in Zaluch Gorge, Western Salt Range.

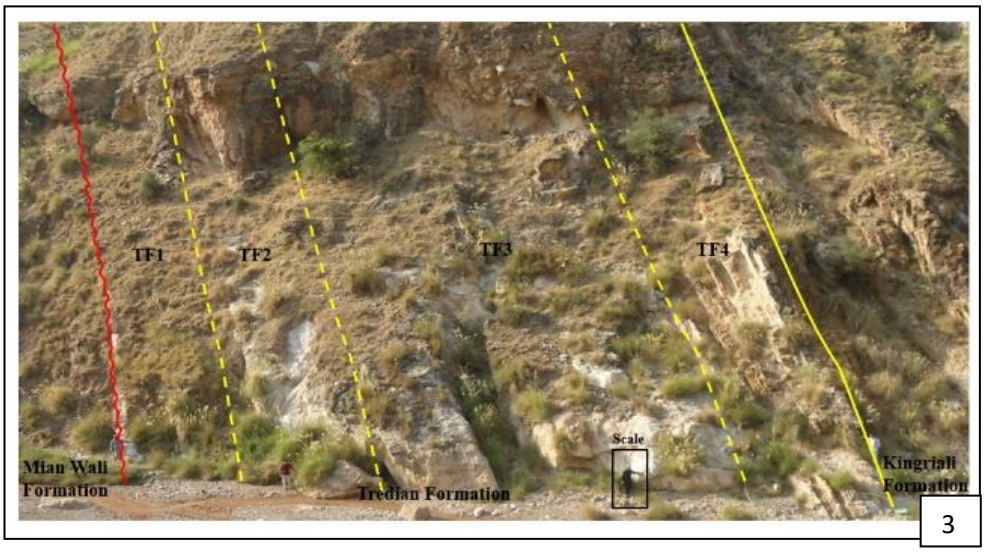

Photo 3: Photograph shows different facies of Tredian Formation in Zaluch Gorge.

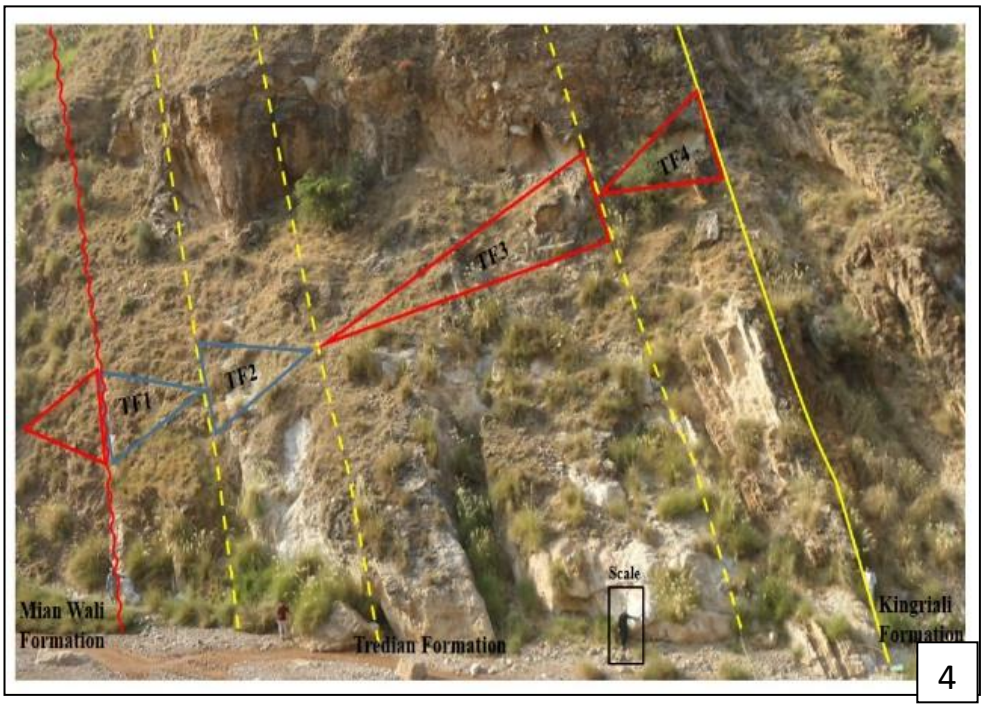

Photo 4: Photograph shows the stratigraphic cycles of Tredian Formation in Zaluch Gorge.

PLATE 1

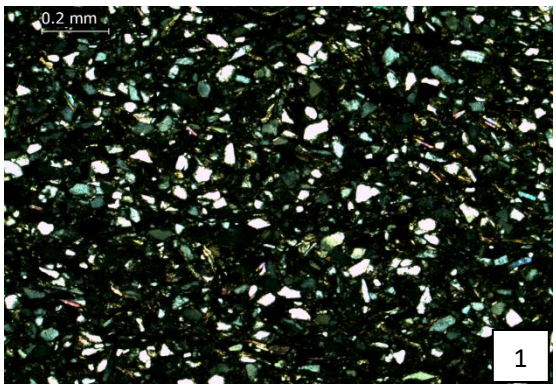

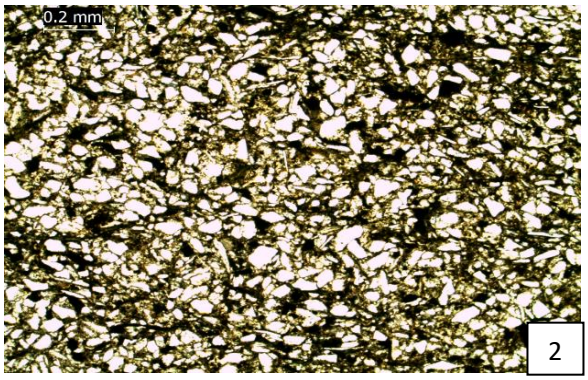

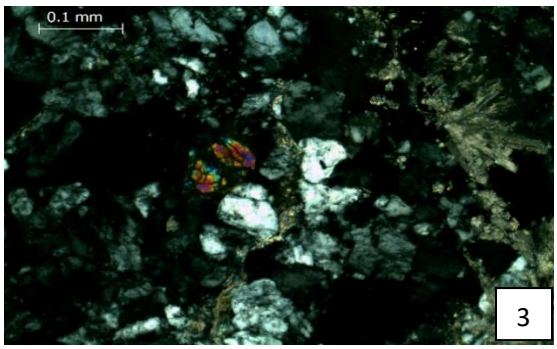

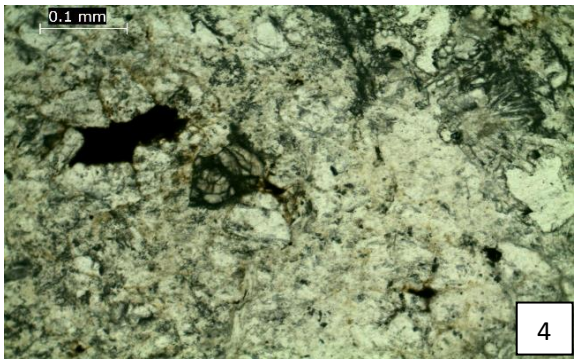

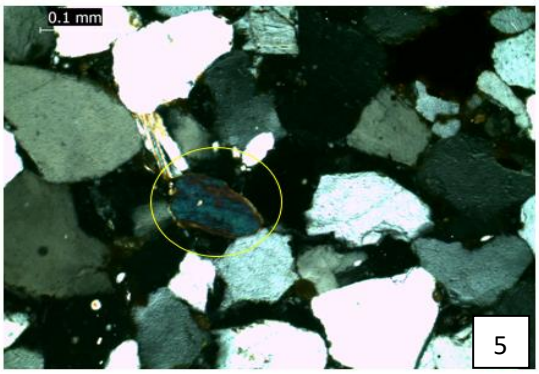

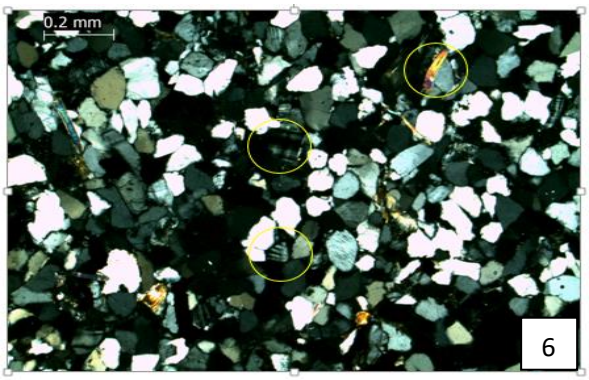

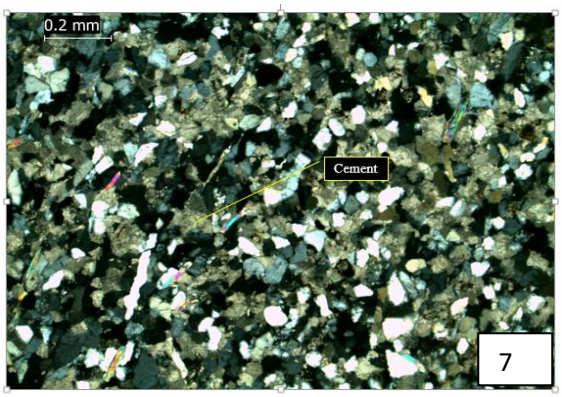

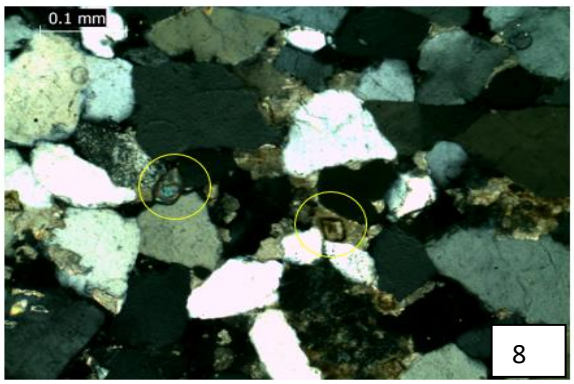

PLATE 1

1. Microphotograph of Subarkose facie (TF_1) of sandstone (ZT_3) of Tredian Formation showing quartz grains in hematite cement (Cross Nicol; 4x).
2. Microphotograph of Subarkose facie (TF_1) of sandstone (ZT_3) of Tredian Formation showing angular quartz in hematite cement (PPL; 4x).
3. Microphotograph of Quartz wacke facie (TF_2) of sandstone (ZT_4) of Tredian Formation showing epidote (Cross Nicol; 10x).
4. Microphotograph of Quartz wacke facie (TF_2) of sandstone (ZT_4) of Tredian Formation showing epidote (PPL; 10x).
5. Microphotograph of Quartz arenite Facie (TF_3) of sandstone (ZT_6) of Tredian Formation showing encircled tourmaline (Cross Nicol; 10x).
6. Microphotograph of Quartz arenite Facie (TF_3) of sandstone (ZT_8) of Tredian Formation showing muscovite, perthite and microcline (Cross Nicol; 4x).
7. Microphotograph of Quartz arenite Facie (TF_3) of sandstone (ZT_{11}) of Tredian Formation showing carbonate cement (Cross Nicol; 4x).
8. Microphotograph of Quartz arenite Facie (TF_3) of sandstone (ZT_6) of Tredian Formation showing zircon and carbonate cement (Cross Nicol; 10x).

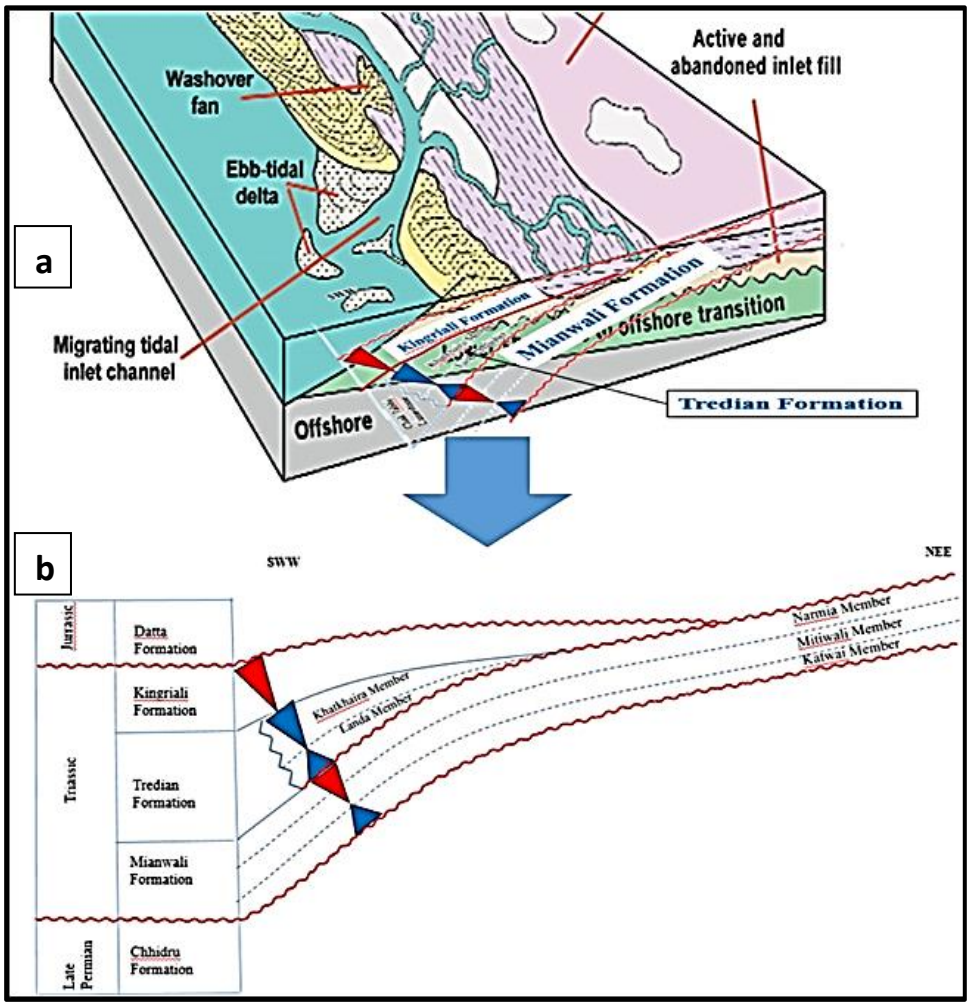

Fig 6: Depositional model for Tredian Formation. (a) Systematic depositional modal showing Fluvial, Transitional and marine environments. (b) Sequence Stratigraphic modal showing deposition of Triassic rocks in Zaluch Gorge.

of feldspar is also examined in thin sections, however, no fossils have been reported. It is noticed that deposition of sandstone of Tredian Formation took place in a fluvial environment, as multiple cycles of coarsening upwards are identified along with minor finning upward. Coarsening upward cycles mark the regression. Sequence stratigraphic study shows that the Tredian Formation overall shows coarsening upward cycles. Sequence boundary (SB), Transgressive surface (TS), Maximum flooding surface (MFS), Highstand system tract (HST) and Low stand system tract (LST) are identified. Tredian Formation is of non-marine origin and depicts some good reservoir characteristics.

Acknowledgement

We are thankful to Director, Institute of Geology, UAJ&K, Muzaffarabad for their help and friendly attitude during our research work which is always a source of inspiration for us.

References

Alam, I., Sajjad, A., Athar, A., Irfan, M., 2005. Fold-thrust styles in the Marwat-Khisor Ranges, NWFP, Pakistan. Pakistan Association of Petroleum Geoscientists, ATC Conference proceedings, 80-93.

Alam, I., 2008. Stratigraphic and Structural Framework of the Marwat-Khisor Ranges, NWFP, Pakistan. Ph.D. thesis, National Centre of Excellence in Geology, University of Peshawar, Pakistan, 1-142.

Baker, D.M., Lille, R.J., Yeats, R.S., Johnson, G.D., Yousaf M., Zaman, A.S.H., 1988. Development of the Himalayan frontal thrust zone: Salt Range, Pakistan. Geology, 16(1), 3-7.

Balme, B.E., 1970. Palynology of Permian and Triassic strata in the Salt Range and Surghar Range, West Pakistan. In: Stratigraphic Boundary Problems: Permian and Triassic of West Pakistan, Kummel, B., Teichert, C. (Ed.) Geology Department, University of Kansas, Special Publication, 4, 305-454.

Coward, M.P., Butler, R.W.H., 1985. Thrust tectonics and the deep structure of the Pakistan Himalaya. Geology, 13, 247-265.

Danilchik, W., Shah, S.M.I., 1967. Stratigraphic nomenclature of formations in TransIndus Mountains Mianwali District, West Pakistan. US. Geological Survey Project Report, 33-45.

Fatmi, A.N., 1977. Mesozoic. In: Shah, S.M.I., (Ed.), Stratigraphy of Pakistan. Memoir of the Geological Survey of Pakistan, 12, 29-56.

Gee E.R., 1945. The age of the Saline Series of the Punjab and Kohat. Proceedings of the National Academy of Science India, 14, 269-310.

Iqbal, F., 2002. Palynology of the Middle Triassic (Nammal Gorge), Western Salt Range, Pakistan. Unpublished Ph.D. thesis, University of Punjab, Pakistan, 199.

Iqbal, S., Jan, I.U., Hanif, M., 2014. The Mianwali and Tredian Formations: An Example of the Triassic Progradational Deltaic System in the Low-Latitude Western Salt Range, Pakistan. Arabian Journal for Science and Engineering, 39(7), 5489-5507.

Kazmi, A.H., Rana, R.A., 1982. Tectonic map of Pakistan: Quetta. Geological Survey of Pakistan, scale, 1:2,000,000.

Khan, M. A., Ahmed, R., Raza, H. A., Kemal, A., 1986. Geology of petroleum in Kohat-Potwar depression, Pakistan. American Association of Petroleum Geologists Bulletin, 70(4), 396-414.

Khan, S., Ahmad, W., Ahmad, S., Khan, J.K., 2016. Dating and depositional environment of the Tredian Formation, western Salt Range, Pakistan. Journal of Himalayan Earth Sciences, 49(2), 14-25.

Kummel, B., 1966. The Lower Triassic formation of the Salt Range and Trans Indus Ranges, West Pakistan. Bulletin of the Museum of Comparative Zoology at Harvard College, 134(19), 361-429.

Pegler, D., Das, S., 1998. An enhanced image of the Pamir-Hindu Kush seismic zone from relocated earthquake hypocenters. Geophysical Journal International, v.134, p.573-595.

Pettijohn, F.J., Potter, P.E., Siever, R., 1987. Sand and sandstone. Springer Verlag, New York. 533.

Posamentier H.W. Allen, G.P., 1990. Siliciclastic sequence stratigraphy: concepts and applications. SEPM Concepts in Sedimentology and Paleontology, 7, 1-209.

Shah, S.M.I., 1977. Stratigraphy of Pakistan. Memoir of the Geological Survey of Pakistan, 12, 138.

Shah, S.M.I., 2009. Stratigraphy of Pakistan. Memoir of the Geological Survey of Pakistan, 22, 381.

Van Wagoner, J.C., Mitchum, R.M., Campion, K.M., Rahmanian, V.D., 1990. Siliciclastic sequence stratigraphy in well logs, cores, and outcrops: Tulsa, Oklahoma. American Association of Petroleum Geologists, Methods in Exploration Series 7, 1-55 Verlag, 518.

KASHMIR JOURNAL OF GEOLOGY (KJG)
www.kjg.ajku.edu.pk

Structural and Stratigraphic Investigations along major faults in Poonch division of Azad Jammu and Kashmir

Aamir Asghar[1*], Muhammad Adil[1], Faheem ullah[2], Muhammad Afaq Hussain[3], Shaid Khan[1], Muhammad Ibrar[1]

[1] Institute of Earth Sciences, University of Poonch Rawalakot AJK, Pakistan.
[2]Institute of Mountain Hazards and Environment Chengdu Sichuan P.R. China.
[3]China University of Geosciences Wuhan P.R. China.

*Corresponding Author:
aamirasghar@upr.edu.pk

Received: 31 March 2021
Accepted: 08 September 2021
Published Online: 27 December 2021

Abstract

This study was carried out to investigate prominent geological structures including faults and folds in Dhirkot, Rangla, Arja, Thorar, and Mang areas of Poonch division Azad Kashmir. The area lies along the eastern limb of Hazara Kashmir Syntaxis (HKS) which is the part of the Sub-Himalayas of Pakistan. This deformation is the result of Indian and Eurasian plates collision in the Eocene time. The surface and subsurface rock units are also marked and mapped during detailed field surveys and lab work. The well-exposed rocks are sedimentary in nature, included Murree Formation, Kamlial Formation, and Recent Alluvium. In this study, the researchers marked and scaled some major deformational structures; these structures include local and regional scaled folds and faults. Structural analysis shows that the folds are open and gentle in nature. The major faults of the area are Riasi Thrust (RT) and Dhirkot Fault (DF). Satellite imageries and remote sensing data are used to construct hydrological drainage networks and watershed models to examine linear offsets and topographical changes along with hanging and footwall blocks. The transpressional movement is found along Riasi Thrust (RT) and Dhirkot Fault (DF). The area consists of high slopes with a number of active geological hazards under substantial compressional stresses and large-scaled structural deformations.

Keywords: surficial and sub-surficial, Hazara Kashmir Syntaxis, geological hazards, structural deformations

1. Introduction

Regionally, the study area lies in the Sub-Himalayas and is bounded by Bagh Basement Fault (BBF) from the northeast, Jhelum Fault (JF) from the west and Salt Range Thrust (SRT) from the south. This area is part of the Kashmir Basin and lies between the coordinates 73 30.161 E, 34 10.136 N; 73 44.586 E, 34 10.122 N and 73 30.068 E, 33 43.145 N; 73 44.582 E, 33 43.141 N on the Survey of Pakistan toposheets no. 43F/12, 43 G/9 and 43 G/10 (Fig. 1).

Previously various authors (e.g., Middlemiss, 1896; Wadia, 1931; Latif, 1960; Marks and Ali, 1961; Calkins and Ali, 1969; Baig and Lawerence, 1987)

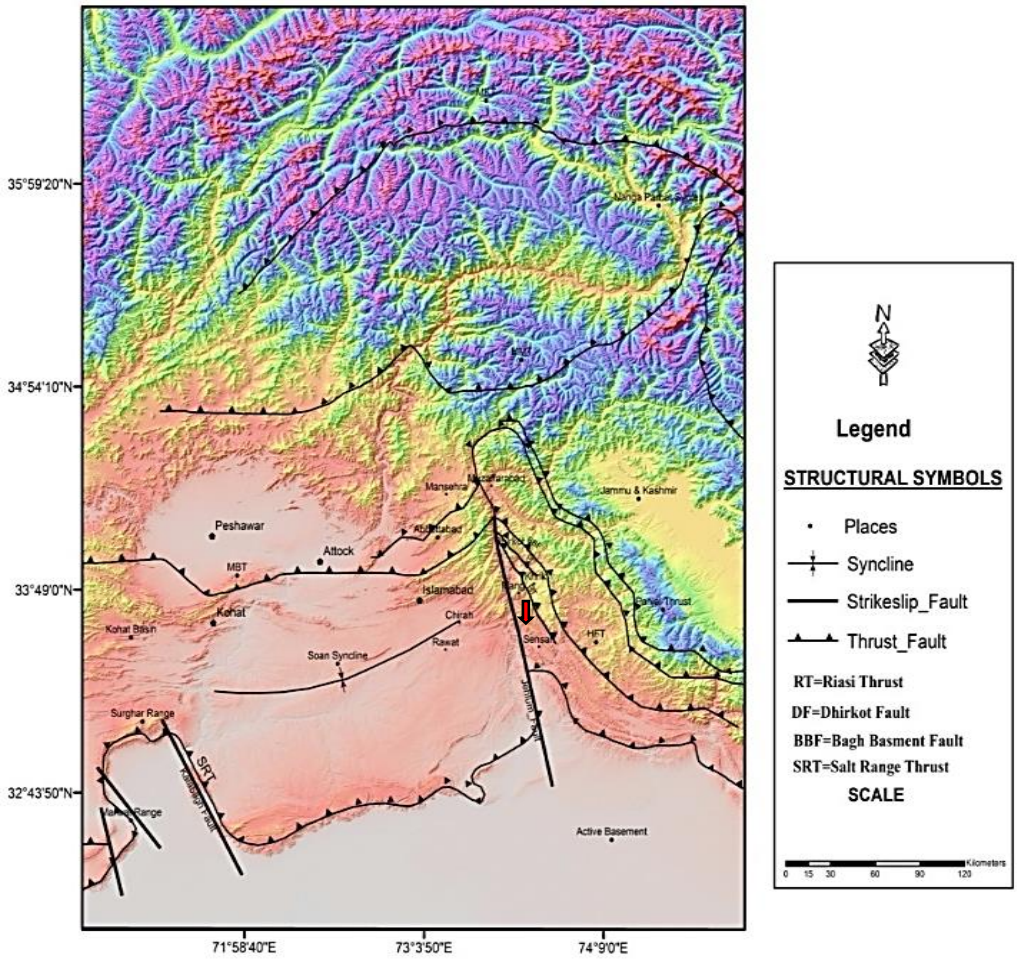

Fig. 1: Regional tectonic map of the Northwest Himalayas of Pakistan. (Wadia, 1931; Calkins et al., 1965; Baig and Lawrence, 1987; Greco, 1991; Baig, 2006; Yeats et al., 2006). Modified after Asghar et al., (2017). The arrow shows the location of the study area.

worked on the regional nature of the rocks and had established the regional stratigraphy but local scale detailed investigation is still needed. The Geological Survey of Pakistan mapped the area at a scale of 1:50,000. Munir and Baig (2006) studied the microfacies of Neogene rocks. The targeted area has a population of estimated 1 million peoples living sparsely on the mountains and densely in cities developed in narrow to vast valleys of the Poonch division. Tectonically the area is folded and faulted (Baig and Lawerence, 1987), and giant faulted structures are capable to produce massive earthquakes. In the past the area has not been investigated by using remote sensing techniques, the local scaled geological structures are also not marked and their relative movement is unknown. This study is planned for a detailed investigation of stratigraphic and structural elements by using remote sensing tools to find out the surficial movement of sliding blocks. The objectives of this study are to investigate surficial lithological units, major faults and folds; to construct the geological map with detailed subsurface structural cross-sections on a 1:50,000 scale; to explicate lineaments by preparing different remote sensing maps including hydrological drainage models and watersheds to understand the offsetting and topographical changes along major faults.

2. Methods and Techniques

Initially, detailed fieldwork of fifteen days was organized and carried out in the area. Traverses were

made along streams, roads and across the regional strikes of exposed geological structures. The basic field tools which were used during fieldwork comprised of Geological Hammers, Chisels, Brunton Compass, Global Positioning System (GPS), etc. The top and bottom of the stratigraphic units were identified with the help of primary sedimentary structures while fossils and lithological characters have been used to distinguish the surficial rocks units. Geological cross-sections of the sub-surface are prepared by using the Kink method which is widely used for large folds of sedimentary rocks composed of a series of sharp bends and it has good prediction in many cases tested by drilling (Suppe, 1985). Sub-surface folds can be interpreted by using Kink geometries (Mitra, 2003). Stereographic projections are constructed to draw the structural data of major folds. The field obtained lithological and structural data including (rock samples, bedding attitudes, data related to orientation of faults and folds) are analyzed in the laboratory. The fossils are also collected to confirm the age and environment of rock units. Remote sensing tools and Geographic Information System (GIS) is used to draw the different types of maps for detailed analysis of geomorphological features associated with faulting. These analyzed remote sensing maps with different geological parameters are used to highlight the structural settings of active faults.

3. Regional Geology

The well-exposed rock formations are ranging from Miocene to the Recent age. This includes Murree and Kamlial formations with overlying patches of Recent Alluvium. The targeted area lies in the vicinity of the eastern limb of Hazara Kashmir Syntaxis (HKS). According to Wadia (1931), these syntaxial flexures are the result of the compressional folding of the Indian shield. Stratigraphically, the area lies in Kashmir Basin and the oldest rocks of Precambrian to recent rock formations are well-exposed in this basin (Shah, 2009). In the research area, Miocene to Recent rocks are exposed (Table 1). These rocks are sedimentary in nature and mostly comprised of Himalayan molasse deposits (Fig. 2). The detailed description of these rock units is as under:

3.1 Murree Formation

Wynne (1874), named it Mari Group whereas the term Murree Beds is used by Lydekker (1876), while Pilgrim (1910), called it Murree Series which is now known as Murree Formation. This recent name came from its type locality of Murree Hills. Murree Formation is widely found in Ghora Gali, Murree Cantonment. It is well-exposed in different places of the study area such as Khohal, Chamiati, Dhirkot, Makhiala, Arja, Bangoi, Jandala, Thala, Titrot, Thorar, Gui Nala and Azad Pattan. Sandstone, shales, clays and intraformational conglomerates are the main constituents of this formation. In the study area, Murree Formation displays cyclic behaviour (Fig. 3).

The texture of sandstone ranges from fine to medium-grained while its colour changes from red to purple-red. Greenish grey sandstone is very common in this area whereas ripple marks and cross beddings are the most common primary sedimentary features of this formation. It overlies the Kuldana Formation and has upper gradational contact with Kamlial Formation. Its age is the Early Miocene.

3.2 Kamlial Formation

Pinfold (1918) used Kamlial beds for it but later on the Stratigraphic Committee of Pakistan named it as Kamlial Formation and it is equivalent to the Kamlial Stage (Pascoe, 1963). It is well exposed in different places of the study areas such as Rangla Gali, Gingoli, Sultanabad and Mang (Fig. 4). The sandstone in Kamlial Formation is purple-grey and greenish-grey, which is medium to coarse-grained and comprised of interbeds of shales and intraformational conglomerate. The Kamlial Formation depicts spheroidal weathering (Fig. 5). Petrified wood fossil and leaf prints have been observed in the Kamlial Formation (Fig. 6). The Kamlial Formation with Murree Formation contact at the lower end is a gradational contact. The Kamlial Formation ranges from the Middle to Late Miocene age.

3.3 Quaternary Alluvium

The Late Tertiary sedimentation of mainly fluvial nature continued into the Quaternary Period. The quaternary deposits are the surficial deposits which included modern alluvial fans, river and lake deposits (McDougall, 1988). The Quaternary alluvium is comprised of unconsolidated deposits of sand, gravel, pebble, cobble and boulder. Terraces along the stream and nalas are composed of Quaternary deposits. Major Quaternary deposits are found in Arja Nala, Mahl River and Gui Nala.

4. Structural Settings

The successive chain of mountains surrounding Pakistan to the northeast, north and northwest were developed because of Eurasian and Indian plate collisions in the Tertiary ages. Indian Plate and the Kohistan Island Arc pileups during Eocene and as a result Himalayas are formed Molnar and Tapponier (1975). The collision of two continental plates results in the formation of compressional thrust or reverse fault system with some strike slip component which is dominant in the north whereas, the fault shows listric or pseudonormal behaviour in the hinterland areas. Hazara Kashmir syntaxis is also the result of the rapid movement of the Indian Plate. It is an antiformal

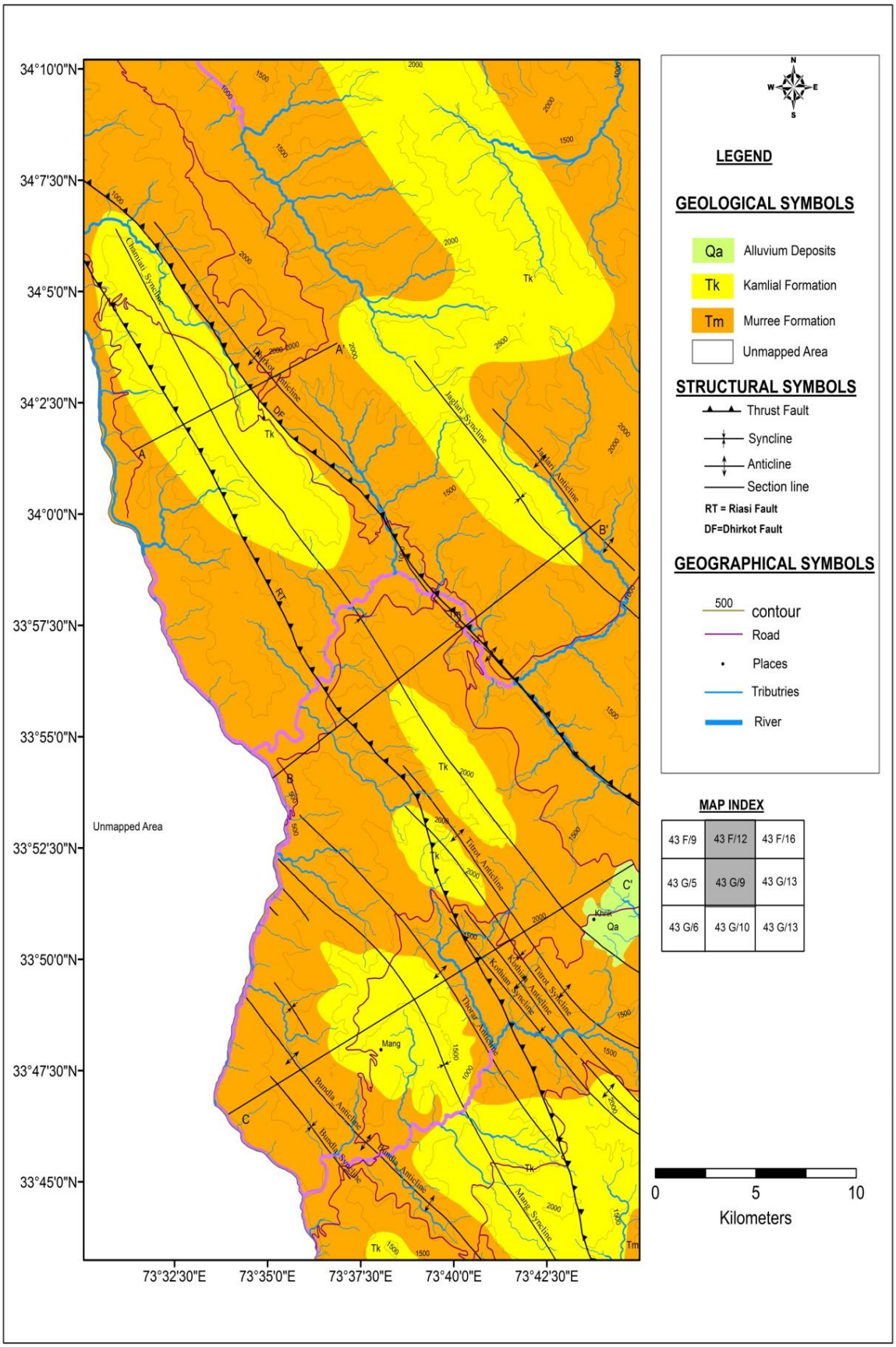

Fig. 2: Geological map with dominant lithologies in the investigated area where A-A/, B-B/ and C-C/ are the profiles lines for geological cross-sections.

Table 1: Stratigraphic sequence.

Formation	Age	Lithologies
Alluvium	Quaternary	Deposit of clay, gravel, and pebble mostly unconsolidated.
……. lies an unconformity…….…..…..		
Kamlial Formation	Middle Miocene	Variegated colour Sandstone, clays and having intraformational conglomerates.
Murree Formation	Early Miocene	Sandstone, shales, and clay with cyclic behaviour. Fine to medium-grained red and purple red coloured sandstone.

Fig 3: The alternate sandstone beds (A) clays (B) shales (C) of Murree Formation in Chamiati areas. Photo is facing southeast.
34 02.197 N and 07 34.093 E

Fig 4: Kamlial Formation in Mang area where photo facing is southeast.
33 47.347 N and 073 37.734 E

Fig 5: Spheriodal weathering in Kamlial Formation of the Mang area.
3347.894 N and 7336.932 E

Fig 6: Leaves imprints in Kamlial Formation of the Gingoli area.
33 47.347 N and 073 37.734 E

synclinal structure where Precambrian to Cenozoic rocks are imbricated and folded in this region. Punjal Thrust (PT), the Main Boundary Thrust (MBT) and the Himalayan Frontal Thrust (HFT) Baig and Lawrence (1987), or the Kashmir Boundary Thrust (KBT) Ghazanfar et al., (1990) are the major faults of the Kashmir foreland fold and thrust belt of the Sub-Himalaya. The Himalayan Frontal Thrust (HFT) runs on the east side while Jhelum Fault passes from the western side (Fig. 1). The southern part of the area is away from the collision zone hence it is tectonically stable while the central and northern part of the study area is unstable.

4.1 Major Structural Folds

Structurally the area consists of open to gentle folds and consists of major anticlines and synclines (Table 2). Folds are greatly influenced by adjoining giant structural faults as their axial planes majorly accompanied the trends of these faults i.e., northwest to southeast (Fig. 2). Geological cross-sections of the major folds and faults are shown in (Fig. 7).

4.1.1 Jaglari Anticline

Jaglari Anticline is an open fold with an interlimb angle ranging from 90.4˚ to 91.1˚ (Fig. β-1). The Jaglari Anticline is an intraformational fold formed within Murree Formation and is present on both the limbs and core of the anticline as shown in Fig. 7.

4.1.2 Jaglari Syncline

The Jaglari Syncline is formed by the combined folding of Murree and Kamlial Formation. In the core, the Kamlial Formation is present while the Murree Formation is on the limbs of Jaglari Syncline (Fig. 7). Some part of it is also consist of Murree Formation present on both the limbs and core of the syncline. It has an interlimb of 110.1˚ (Fig. β-2).

4.1.3 Dhirkot Anticline

The Dhirkot Anticline is an open to gentle intraformational fold and its interlimb angle varies from 95.2˚ to 125.1˚ (Fig. β-3). Murree Formation is present on both the limbs and core of this anticline (Fig. 7).

4.1.4 Chamiati Syncline

The Chamiati Syncline is formed by the folding of Murree and Kamlial formations. The Kamlial Formation exists in the core while the Murree Formation lies on the limbs (Fig. 7). Some part of the Chamiati Syncline lies only in the Murree Formation where it is present on both the limbs and core of the syncline (Fig. 7). The interlimb angle of Chamiati angle varies from 95.9˚ to 100.1˚ (Fig. β-4).

4.1.5 Titrot Anticline

The Titrot Anticline is an intraformational fold constructed by folding of Murree Formation where it is present on both the limbs and core of the anticline (Fig. 7). It is open to gentle fold where variation in interlimb angle is from 99˚ to 158˚ (Fig. β-5).

4.1.6 Titrot Syncline

The Titrot Syncline is an open fold with 100.3˚ to 110.1˚ interlimb angle (Fig. β-6). It is the result of folding in Murree and Kamlial Formation where Kamlial Formation is found in core and Murree Formation on the limbs. The major part of Titrot Syncline is due to the folding of the Murree Formation lies on both the limbs and core of the syncline (Fig. 7).

4.1.7 Kothian Anticline

The Kothian Anticline passes through the Kothian area (Fig. 2). This anticline is the result of folding in the Murree Formation where it is present on both the limbs and core. Its interlimb angle varies from 95˚ to 110.2˚ (Fig. β-7).

4.1.8 Kothian Syncline

The Kothian Syncline is also the result of folding in the Murree Formation where it is present on both the limbs and core of the syncline (Fig. 7). It has an interlimb angle of 95.4˚ to 145˚ and it is open to gentle fold (Fig. β-8).

4.1.9 Thorar Anticline

The Thorar Anticline passes through the Thorar area (Fig. 7) with variation in interlimb angle from 105.3˚ to 112.6˚ (Fig. β-9). This anticline is also the result of folding in the Murree Formation where it is present on the both, limbs and core of the anticline (Fig. 2).

4.1.10 Mang Syncline

The Mang Syncline is a gentle fold with the variation of 120.1˚ to 130.1˚ interlimb angle (Fig. β-10). The syncline is constructed by folding of Kamlial Formation which is present on both the limbs and core of syncline (Fig. 7).

4.1.11 Bundla Anticline

The Bundla Anticline is an open fold (Fig. β-11). The anticline is constructed by folding in Murree Formation and is present on both the limbs and core of the anticline (Fig. 7).

4.1.12 Bundla Syncline

The Bundla Syncline is an open to gentle fold which passes through the Bundla area (Fig. β-11). The Bundla Syncline is developed by the deformation in the Murree Formation which is present on both the limbs and core of the syncline (Fig. 7).

4.1.13 Intraformational Folds

In the study area, some intraformational folds also have been observed in Murree and Kamlial formations which are the result of compressional stresses in the region.

4.2 Major Structural Faults

Riasi Thrust and Dhirkot Fault are the major faults in the study area. The description of these faults (Fig. 2 and Fig. 7) is given below.

4.2.1 Riasi Thrust

The fact about Riasi Thrust being the main active fault in Kashmir with no earthquake's events in the more recent geologic record is also mentioned by Yann and Gavillot (2016). The activity along the Riasi fault incised 300m old river terrace in the southwest, has developed deep gorges through the front ranges of the Kashmir Himalaya, northwest India and it is almost 200km long stepwise fault system initiated from the Balakot-Bagh fault in Pakistan and extends up to northwestern India (Gavillot et al., 2016). This is majorly reverse thrust fault and is marked in different places like Munasa, Thorar and Gui Nala areas. The Riasi Thrust is oriented in a northwest-southeast direction and is mapped between the Murree and Kamlial formations. The Murree Formation is thrusted over the Kamlial Formation in the study area. Kamlial Formation lies in the footwall and Murree Formation found in hanging wall of the fault. In the Daar area along Gui Nala, the truncation of strata has been observed where the dips are intersecting almost at a right angle possibly due to the massive fault movement in the past times (Fig. 9). The fault indicates reverse behaviour which is confirmed during the construction of the watershed by using Advanced Spaceborne Thermal Emission and Reflection Radiometer (ASTER-30) digital elevation model (DEM) with 30m resolution freely provided by the United States Geological Survey (USGS) on the Geographical Information System (ArcGIS Desktop 10.7) by Environmental Systems Research Institute (ESRI). In the morphology of reverse faults, the hanging wall block acquires large watersheds due to continuous ride on footwall which is concluded by the preparation of watershed along Riasi Thrust (Fig. 11). This type of analysis is applied for the first time in this region to understand the constructions of watersheds and their relationship with the movement along two faulted blocks. In this study, it is clearly observed that the geometry, density, size and drainage pattern acquired by watersheds are greatly influenced and controlled by fault movement. The drainage pattern is of Tralaus type and majorly runs on the hanging wall block. Digital elevation model and satellite images depict that the Riasi Thrust is dominant and have developed prominent geomorphological features in the shape of drainage pattern, topographical changes, and mass movements etc. (Fig. 8). The detailed analysis of the stream network model and satellite images indicates that the Riasi Thrust has transpressional movement in the targeted area as stream bending shown in (Fig. 8). The presence of multiple scarps in northern and southern parts shows multiple events along Riasi Thrust. The topographical changes associated with Riasi Thrust depicted that the Mahl River contributed in the transportation of sediments to Jehlum River. Historically, Riasi Thrust hasn't reported any seismicity and is storing energy over an extended period and the release of such energy may cause an earthquake of a stronger magnitude.

4.2.2 Dhirkot Fault

The Dhirkot Fault trends in a northwest-southeast direction and displays reverse behaviour with clear geomorphological imprints of active faulting. In the study area, it passes through Dhirkot and Hari Gehl areas. This Fault is marked between Murree and Kamlial formation on Dhirkot Rangla road where Murree Formation is thrusting over the Kamlial Formation at an angle of 57˚. The Kamlial Formation lies in the footwall while Murree Formation is deformed in hanging wall faulted block. The movement of blocks has already polished slickensides which are also observed on Dhirkot Rangla road (Fig. 10). According to the morphology of reverse faults, the hanging wall block acquires large watersheds due to continuous ride on the footwall. The construction of the watershed by using Advanced Spaceborne Thermal Emission and Reflection Radiometer (ASTER-30) on Geographical Information System (ArcGIS Desktop 10.7) shows that the hanging wall block has vast and long watersheds as compared to the footwall block (Fig. 11). The edges of watershed boundary will follow the highest ridgeline of the stream channel and intersect at the bottom or lowest point where water flows out (Fig. 11). Dhirkot Fault shows lateral movement on the surface during the detailed analysis of the stream network model where the offset of major streams is present along the fault line (Fig. 8). In the morphology of reverse faults, the bending of streams along fault line occurs due to transpressional movement which is also observed during analysis. It is also observed that the common shared hanging wall of Riasi Thrust and footwall of the Dhirkot Fault have rotational anti-clockwise movement in the northwestern part of the area (Fig.

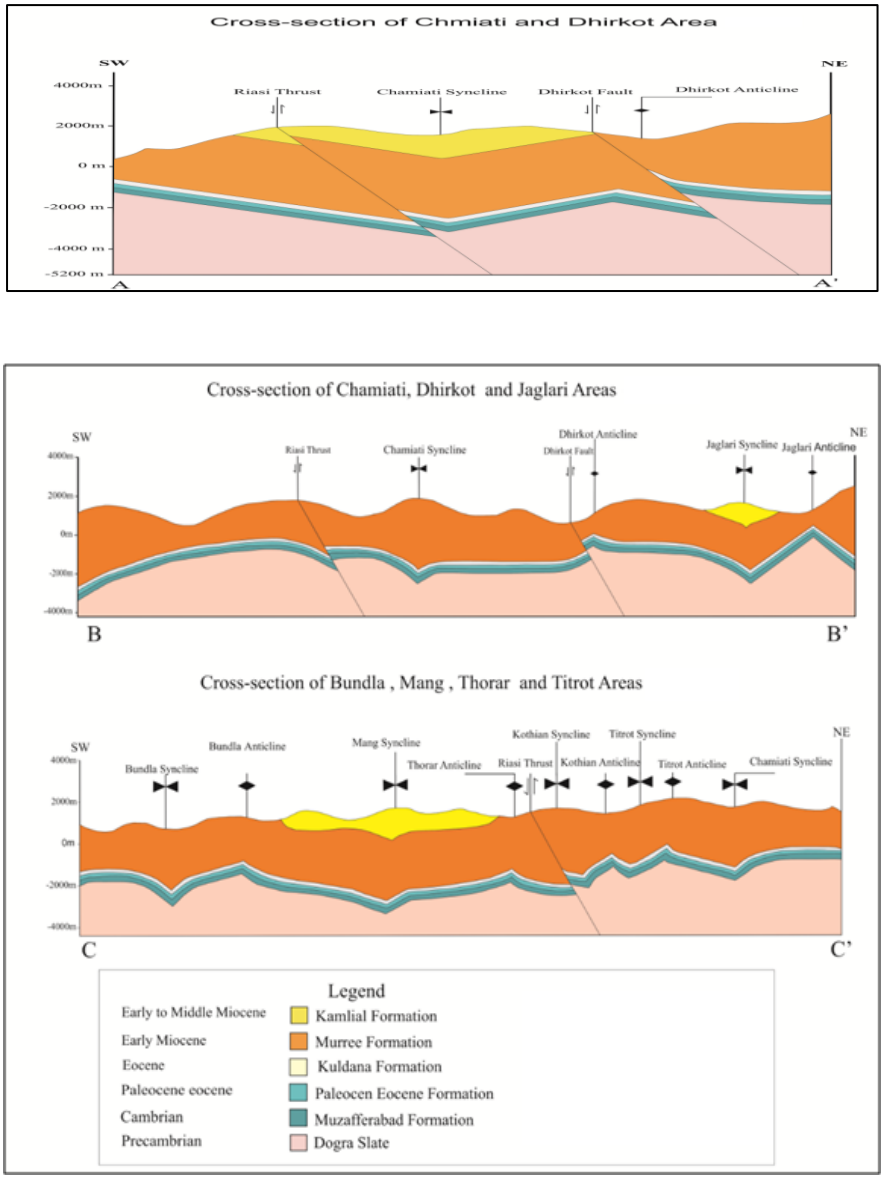

Fig. 7: Geological cross-section A-A/ shows Chamiati and Dhirkot areas where B-B/ and C-C/ are of Jaglari, Bundla, Mang, Thorar and Titrot Areas.

8). Multiple fault scarps along Dhirkot Fault are also witnessed but historical and instrumental data has not shown any known seismic event in the past.

5. Discussions and Conclusions

Tectonically the area is bounded by three major faults namely, Main Boundary Thrust which is running in the north-east, Jhelum Fault in the west and Salt Range Thrust on the southern side (Fig. 1). The research area lies in Sub-Himalayas of Kashmir along the eastern limb of Hazara Kashmir Syntaxis which is an antiformal structure that resulted in the northeast to northwest changes in thrust directions (Bossart et al., 1988). Rocks exposed in the study area are sedimentary in nature ranging in age from Miocene to Recent. These rock units include the Murree Formation, Kamlial Formation and Recent Alluvium. The area is highly deformed, sheared and fractured due to Himalayan and Hazaran Orogeny. The study area is folded and faulted. Jaglari Anticline and Syncline, Dhirkot Anticline, Chamati Syncline, Titrot Anticline and Syncline, Kothian Anticline and Syncline, Thorar Anticline, Mang Syncline, Bundla Anticline and Syncline are the major folds of the area.

Table 2: Structural data of major folds.

Fold Name	Part	Bedding Attitude of Northeastern Limb	Bedding Attitude of Southwestern Limb	Axial Plane	Fold Axis	Interlimb Angle	Fold Type
Jaglari Anticline	**NW**	N50˚W/40˚NE	N40˚W/50˚SW	N44.6˚W/85˚NE	05˚/316˚	90.4˚	Open
	SE	N46˚W/54˚NE	N50˚W/35˚SW	N47.7˚W/80.5˚SW	02˚/133˚	91.1˚	Open
Jaglari Syncline	**NW**	N40˚W/50˚SW	N50˚W/20˚NE	N43.1˚W/75˚NE	02˚/317˚	110.2˚	Open
	SE	N54˚W/30˚SW	N59˚W/40˚NE	N56.8˚W/85˚SW	01˚/303˚	110.1˚	Open
Dhirkot Anticline	**NW**	N62˚W/50˚NE	N70˚W/35˚SW	N65.4˚W/82.5˚SW	04˚/114˚	95.2˚	Open
	SE	N58˚W/25˚NE	N50˚W/30˚SW	N53.7˚W/87.5˚NE	02˚/307˚	125.1˚	Gentle
Chamiati Syncline	**NW**	N25˚W35˚SW	N40˚W/50˚NE	N33.6˚W/82.5˚SW	06˚/326˚	95.9˚	Open
	SE	N40˚W/55˚SW	N46˚W/25˚NE	N42˚W/75˚NE	01˚/319˚	100.1˚	Open
Titrot Anticline	**NW**	N43˚W/12˚NE	N50˚W/10˚SW	N46.2˚W/89˚SW	01˚/134˚	158˚	Gentle
	SE	N50˚W/36˚NE	N50˚W/45˚SW	N50˚W/85.5˚NE	00˚/310˚	99˚	Open
Titrot Syncline	**NW**	N40˚W/50˚SW	N50˚W/30˚NE	N43.9˚W/80˚NE	04˚/317˚	100.3˚	Open
	SE	N50˚W/20˚SW	N55˚W/50˚NE	N53.5˚W/75˚SW	01˚/306˚	110.1˚	Open
Kothian Anticline	**NW**	N50˚W/35˚NE	N49˚W/50˚SW	N49.4˚W/82.5˚NE	00˚/310˚	95˚	Open
	SE	N50˚W/50˚NE	N60˚W/20˚SW	N53.1˚W/75˚SW	03˚/128˚	110.2˚	Open
Kothian Syncline	**NW**	N50˚W/35˚SW	N60˚W/50˚NE	N55.7˚W/82.5˚SW	04˚/304˚	95.4˚	Open
	SE	N60˚W/20˚SW	N59˚W/15˚NE	N59.6˚W/87.5˚NE	00˚/120˚	145˚	Gentle
Thorar Anticline	**NW**	N55˚W/40˚NE	N45˚W/35˚SW	N50.3˚W/87.5˚SW	03˚/310˚	105.3˚	Open
	SE	N35˚W/45˚NE	N66˚W/25˚SW	N46.5˚W/79.7˚SW	10˚/135˚	112.6˚	Open
Mang Syncline	**NW**	N54˚W/35˚SW	N48˚W/25˚NE	N51.5˚W/85˚NE	02˚/128˚	120.1˚	Gentle
	SE	N52˚W/20˚SW	N60˚W/30˚NE	N56.8˚W/85˚SW	01˚/303˚	130.1˚	Gentle
Bundla Anticline	**NW**	N46˚W/35˚NE	N41˚W/40˚SW	N43.4˚W/87.5˚NE	01˚/317˚	105.1˚	Open
	SE	N48˚W/45˚NE	N33˚W/20˚SW	N43.1˚W/77.4˚SW	04˚/316˚	115.5˚	Open
Bundla Syncline	**NW**	N41˚W/40˚SW	N44˚W/35˚NE	N42.4˚W/87.5˚NE	01˚/318˚	105˚	Open
	SE	N45˚W/35˚SW	N30˚W/20˚NE	N40˚W/82.4˚NE	04˚/140˚	125.5˚	Gentle

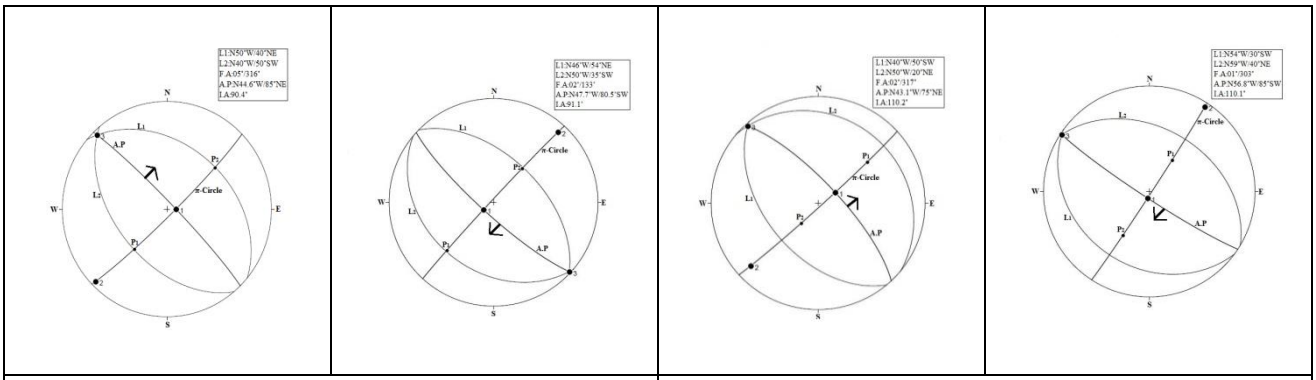

Fig. β -1: π and β diagrams of Jaglari Anticline.

Fig. β-2: π and β diagram of Jaglari Syncline.

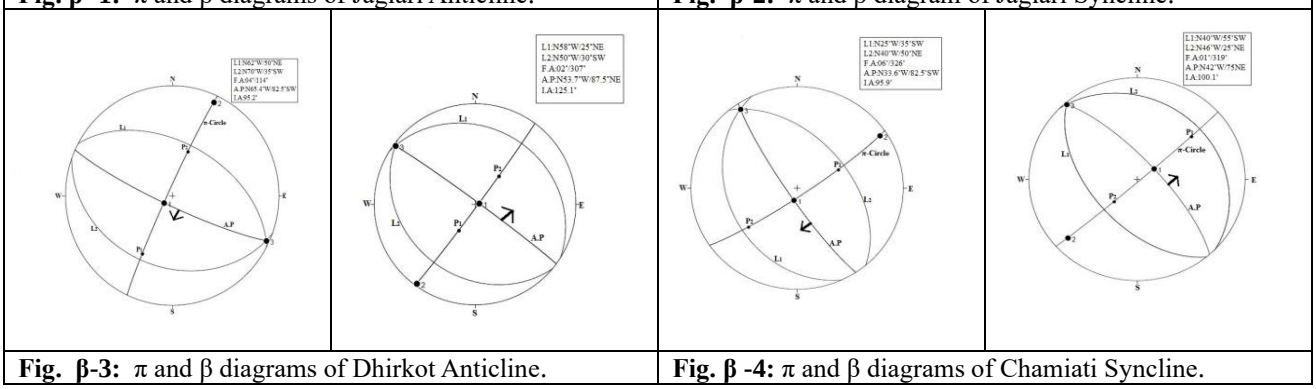

Fig. β-3: π and β diagrams of Dhirkot Anticline.

Fig. β -4: π and β diagrams of Chamiati Syncline.

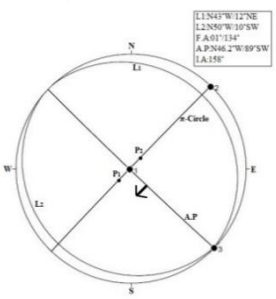

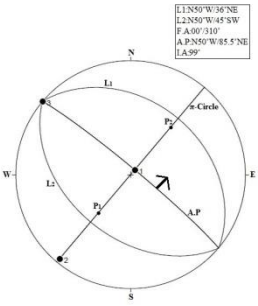

Fig. β-5: π and β diagrams of Titrot Anticline.

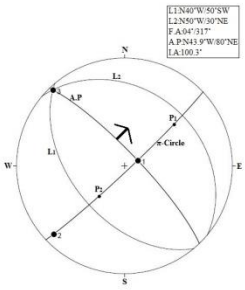

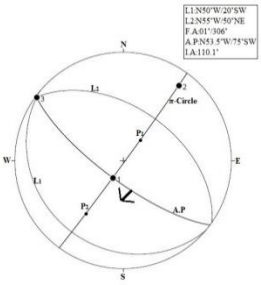

Fig. β-6: π and β diagrams of Titrot Syncline.

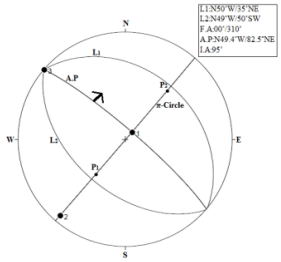

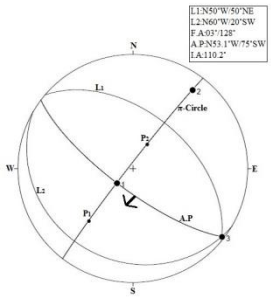

Fig. β -7: π and β diagram of Kothian Anticline.

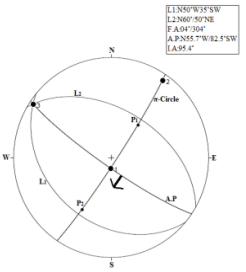

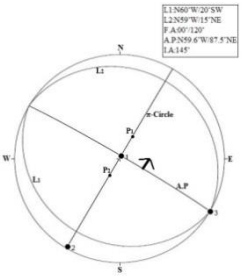

Fig. β -8: π and β diagram of Kothian Syncline.

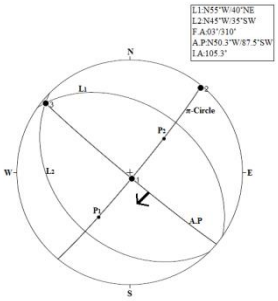

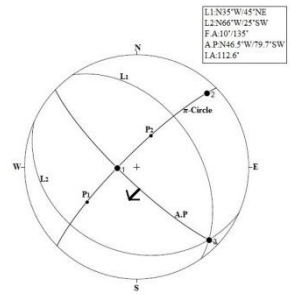

Fig. β -9: π and β diagram of Thorar Anticline.

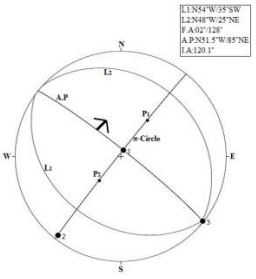

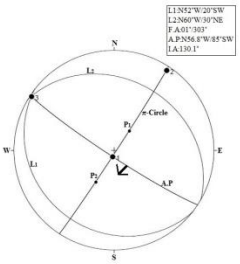

Fig. β -10: π and β diagram of Mang Syncline.

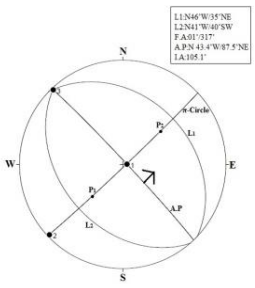

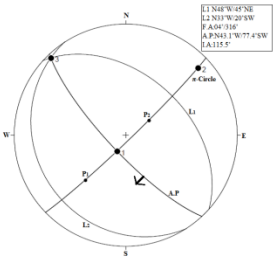

Fig. β -11: π and β diagram of Bundla Anticline.

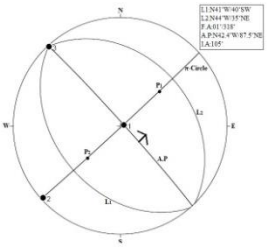

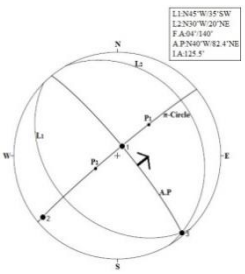

Fig. β -12: π and β diagram of Bundla Syncline.

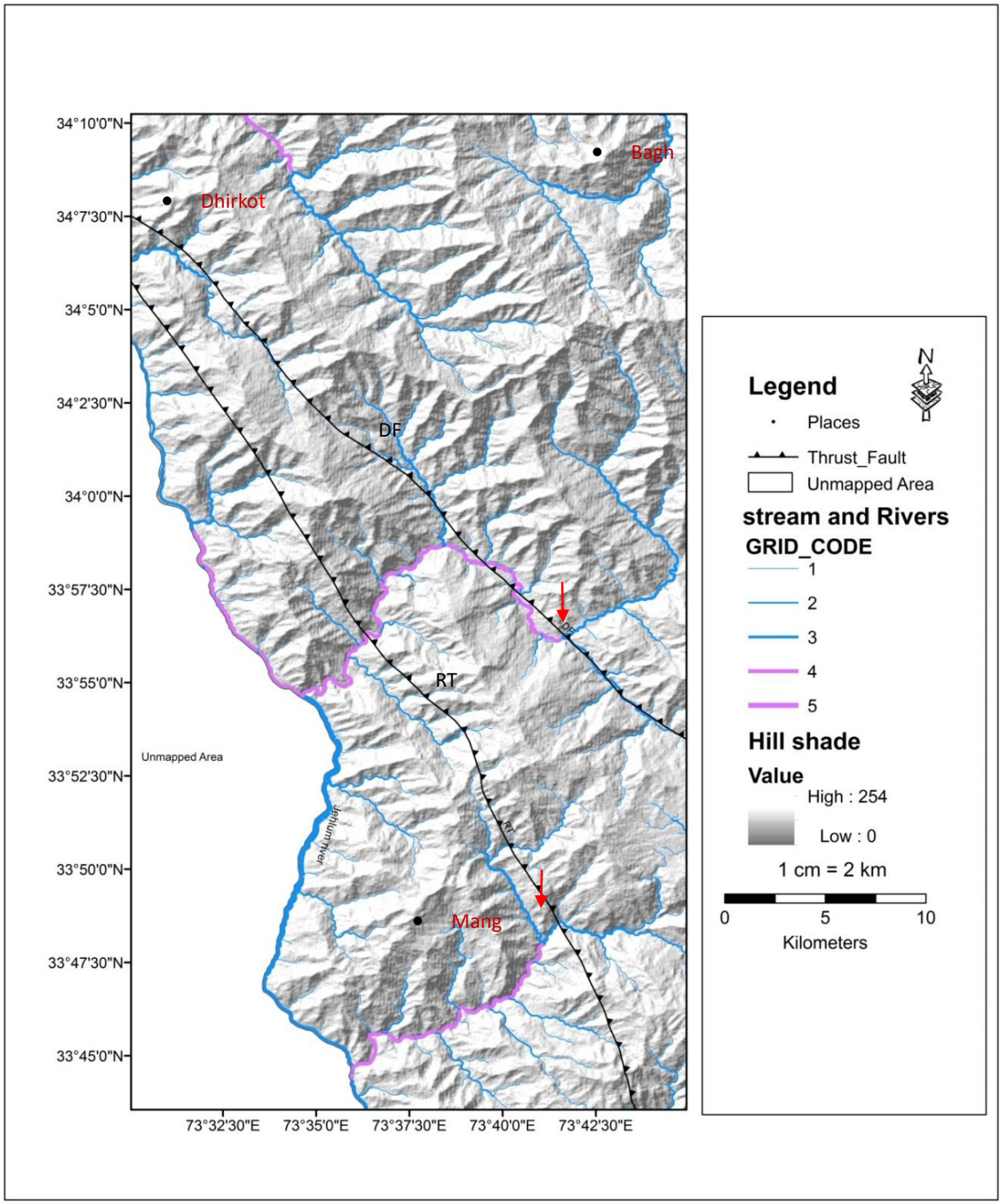

Fig. 8: Red arrows show the deflection of stream channels along Dhirkot Fault (DF) and Riasi Thrust (RT).

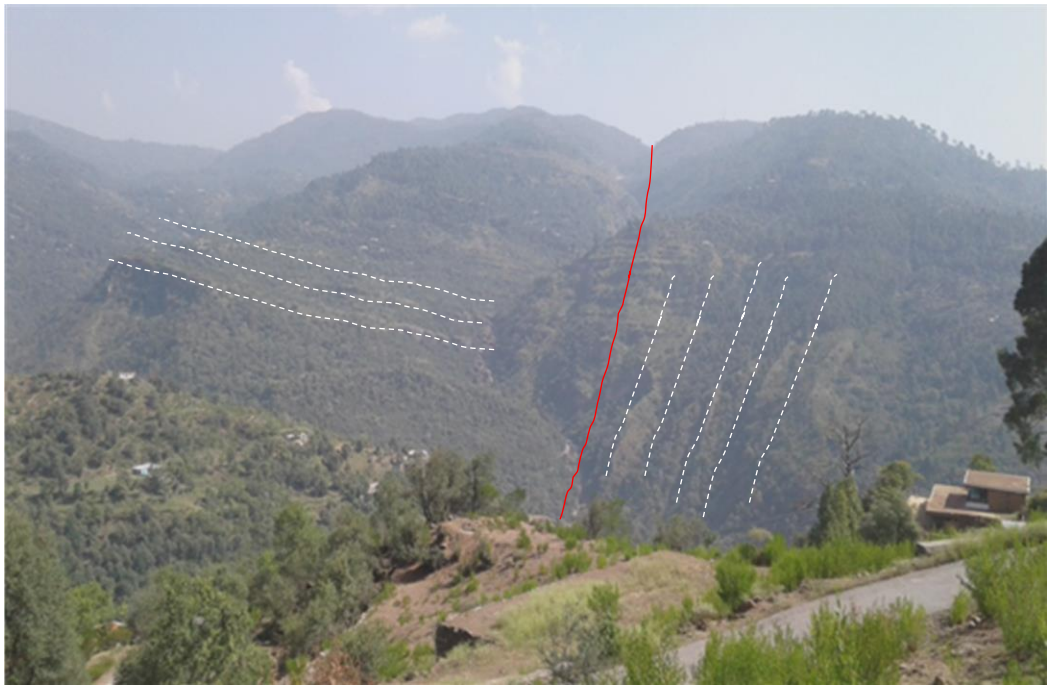

Fig. 9: The Riasi Thrust in Daar, the lines show dip direction of truncated beds. 3348.214 N 07340.889 E

Fig. 10: The Dhirkot Fault marked along Dhirkot Rangla road, where Murree Formation (A) is thrusted over Kamlial Formation (B). 3402.571 N 7334.661 E

The Jaglari Anticline is an intraformational fold shaped by the folding of the Murree Formation. The Murree Formation is extended on both limbs and core of the anticline. The Jaglari Syncline is formed by the Murree and Kamlial Formations where the Kamlial Formation is in core while the Murree Formation is on limbs. The Dhirkot Anticline is an intraformational fold constructed by folding of the Murree Formation and it is present on both the limbs and core of the anticline. The Chamiati Syncline is the result of folding in the Murree and Kamlial Formations where the Kamlial Formation is in core while Murree Formation on limbs. Some part of the Chamiati Syncline is formed by Murree Formation only. The Titrot Anticline is an intraformational fold in Murree Formation and it is present on both the limbs and core of the anticline. The Titrot Syncline is the result of folding in the Murree and Kamlial formations

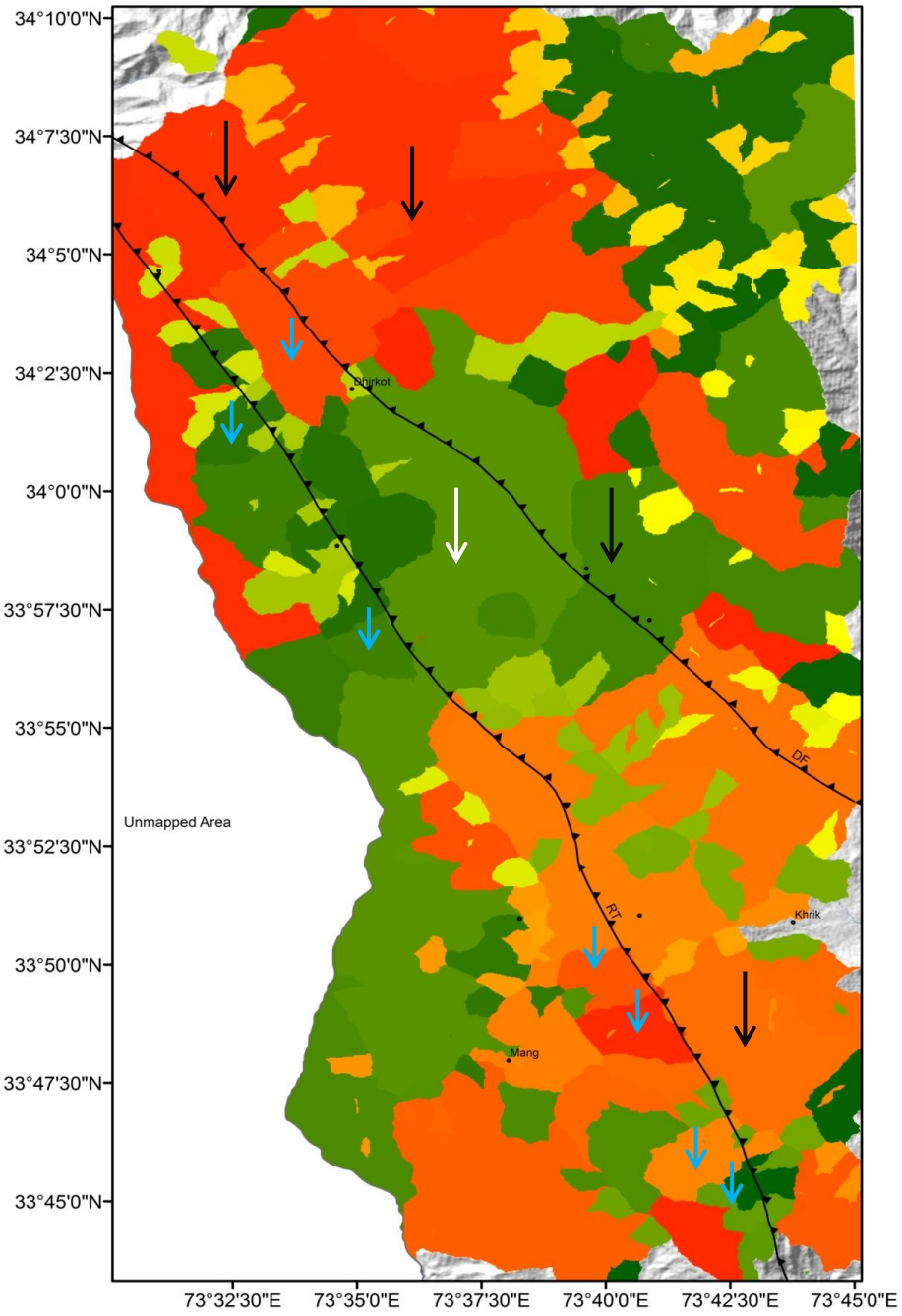

Fig. 11: Major faults i.e., Riasi Thrust (RT) and Dhirkot Fault (DF) are plotted over watershed generated by ASTER-30 DEM where blue colored arrows show watershed on footwall block while black arrows show watershed on hanging wall block while white arrows show degraded fault scarp by water channel flowing across the fault line.

where Kamlial Formation is in core while Murree Formation is on its limbs. The major part of the Titrot Syncline is in Murree Formation present on both the limbs and core of the syncline. The Kothian Anticline is formed by the folding of the Murree Formation where it is present on both the limbs and core of the anticline. The Kothian Syncline is formed by folding of the Murree Formation and it is present on both the limbs and core of the syncline. The Thorar Anticline is formed by folding of Murree Formation and is present on both the limbs and core of the anticline. The Mang Syncline is formed by the folding of Kamlial Formation only whereas Bundla Anticline is formed by folding of the Murree Formation. The Bundla Syncline is formed by the folding of the Murree Formation and it is present on both the limbs and core of the syncline.

Riasi Thrust and Dhirkot Fault are the major

faults of the area. The Riasi Thrust is marked between Murree and Kamlial formation, running in the northwest-southeast direction. In the study area, the Murree Formation is thrusted over Kamlial Formation. Kamlial Formation lies in footwall and Murree Formation in hanging wall. Dhirkot Fault is marked between Murree and Kamlial formations and is also running in the northwest-southeast direction.

The primary sedimentary structures like cross-bedding, rip ups, graded bedding and mud cracks are very clear in the area. The facing of rock units is marked based on sedimentary structures.

It is concluded that the surficial rock units, Murree and Kamlial formations are part of Himalayan Molasses and are purely sedimentary in nature. The study area is vastly deformed into regional folds and faults. The structural data depicts that the dominant folds in the area are tight, open and gentle in nature. These are either northwest or southeast verging folds and northeast or southwest plunging in nature. It is also concluded that the Riasi Thrust and Dhirkot Fault are the major reverse faults in the area. Field investigations and detailed analysis of remote sensing data demonstrated that these major faults are influenced by regional transpressional tectonics which needs further detailed work. It is also observed that these faults are accompanied by active mass movements which could generate a catastrophic event in the future.

References

Baig, M.S., Lawrence, R.D., 1987. Precambrian to Early Paleozoic orogensis in the Himalaya. Kashmir Journal of Geology, 5, 1-22.

Baig, M.S., 2006. Active Faulting and Earthquake Deformation in Hazara-Kashmir Syntaxis, Azad Kashmir, northwest Himalaya, Pakistan. In: Kausar AB, Karim T, Khan T (eds) Extended abstracts, International Conference on 8 October 2005 Earthquake in Pakistan: Its implications and hazard mitigation. Geological Survey of Pakistan, Islamabad. p. 27-28

Baig, M.S., Yeats, R.S., Pervez, S., Jadoon, I.A.K., Khan, M.R., Siddiqui, I., Monalisa., Saleem, M., Masood, B., Sohail, A., Mughal, M.S., Ahmed, M.J., Butt, W.A., Rehman, H., Abbasi, H.R., Abbasi, N., Nadeem, M., 2010. Active tectonics, October 8, 2005 earthquake deformation, active uplift, scarp morphology and seismic geohazards microzonation, Hazara Kashmir Syntaxis. Northwest Himalayas, Pakistan. Journal of Himalayan Earth Sciences, 43, 17-21.

Bilham, R., Gaur, V.K., Molnar, P., 2001. Himalayan Seismic Hazard. Science, 293, 1442-4.

Calkins, J.A., Offield, T.W., Ali, S.T. 1969. Geology and mineral resources of southern Hazara District, West Pakistan, and parts of western Azad Kashmir. United States Department of State and Government of Pakistan project report, 43, 92.

Calkins, J. A., Offield, T. W., Abdullah, S. K. M., & Ali, S. T. (1975). Geology of the Southern Himalaya in Hazara, Pakistan, and adjacent areas. Geological Survey Professional Paper, 716–C, 29.

Disaster Risk Management Plan Azad Jammu and Kashmir, November 2008. State Disaster Management Authority.

Gavillot, Y., Meigs, A., Yule, D., Heermance, R., Rittenour, T., Madugo, C., and Malik, M., 2016. Shortening rate and Holocene surface rupture on the Riasi fault system in the Kashmir Himalaya: active thrusting within the Northwest Himalayan orogenic wedge. Bulletin, 128(7-8), 1070-1094.

Greco, A., 1991. Stratigraphy, metamorphism and tectonics of the Hazara Kashmir Syntaxis area. Kashmir Journal of Geology, 8-9, 39-66.

Latif, M.A., 1970. Explanatory notes on the Geology of the southern Hazara to accompany the revised geological map. Jahrbuch Derngeol Sogischen Bundesanstalt, Wien Sonderband, 15, 5–19.

Lydekker, R., 1876. Notes on the geology of the Pir Panjal and neighbouring districts. Records of the Geological Survey of India, 9 (4), 155-162.

Marks, P., Ali, C.M., 1961. The Abbottabad Formation: a new name for Middlemiss' Infra-Trias. Geological Bulletin of the Punjab University, 2, 56.

Middlemiss, C.S., 1896. The geology of Hazara and the black Mountains. Geological Survey of India, Memoir, 26, 320.

Mitra, S., 2003. A unified kinematic model for the evolution of detachment folds. Journal of Structural Geology, 25(10), 1659-1673.

Molnar, P., Tapponnier, P., 1975. Cenozoic tectonics of Asia, effects of continental collision: Science, 189, 419-426.

Pinfold, E. S., 1918. Notes on structure and stratigraphy in the North-West Punjab. Records of the Geological Survey of India, 49, 137-160.

Pascoe, E.H., 1963. Petroleum in the Punjab and northwest Frontier Province. Memoirs of the Geological Survey of India 20, 330-489.

Pilgrim, G.E., 1910. Preliminary notes on a revised classification of the Tertiary freshwater deposits of India. Records of the Geological Survey of India, 40, 185-205.

Shah, S.M.I., 1977. Stratigraphy of Pakistan. Memoirs of the Geological Survey of Pakistan, 12, 1-138.

Suppe, J., 1985. Principles of structural geology. Prentice Hall.

Wadia, D.N., 1931. The Syntaxis of the North-west Himalaya: its rocks, tectonic and orogeny. Records of the Geological Survey of India, 65 (2), 189-220.

Wynne, A.B., 1874. Notes on the geology of neighbourhood of Mari hill station in the Punjab. Records of the Geological Survey of India, 7(2), 64-74.

KASHMIR JOURNAL OF GEOLOGY (KJG)
www.kjg.ajku.edu.pk

Biostratigraphy and Paleoecology of the Early Eocene Nammal Formation and Sakesar Limestone from eastern and western Salt Range, Upper Indus Basin, Pakistan

Rafiq Samad[1,2], Syed Ahsan Hussain Gardezi[3]*, Nawaz Ikram[1], Amir shahzad[1], Nadeem Ahmad Usmani[3,4]

[1]Institute of Geology, University of Azad Jammu and Kashmir, Muzaffarabad, Pakistan.
[2]Departement of Elementary and Secondary Education, Government of Azad Jammu and Kashmir, Muzaffarabad, Pakistan.
[3]Geological Survey of Pakistan, Azad Jammu and Kashmir Directorate, Muzaffarabad, Pakistan.
[4]Institute of Mountain Hazards and Environment, University of Chinese Academy of Sciences, Chengdu, China.

*Corresponding author:
ahsangardezi2504@gmail.com

Received: 06 May 2021
Accepted: 13 October 2021
Published Online: 27 December 2021

Abstract

Two sections from the eastern and western Salt Range were selected for the detailed study of microfossils, depositional environment and paleoecology of Eocene carbonates i.e., Nammal Formation and Sakesar Limestone. Sections were measured and more than 40 samples were collected. The systematic micropaleontology of the current study suggested that many genera of larger benthic Foraminifers such as *Nummulites*, *Alveolina*, *Assilina*, *Textularia*, *Nodosaria*, *Miliolids*, *Lockhartia* and green algae were heterogeneously distributed in targeted formations. Our results indicate shallow to the deep marine depositional environment for Nammal Formation, whereas the Sakesar Limestone represents the shallow marine depositional environment. Based on the identified benthic genera, an Early Eocene age has been assigned to both formations.

Keywords: Micro-paleontology, Depositional Environment, Nammal Formation, Sakesar Limestone, Salt Range

1. Introduction

The area under investigation is located in Pakistan's eastern and western Salt Range (SR) (Fig. 1). The SR demarcates the southern-most boundary of Sub-Himalayas in north Pakistan. It is the result of emplacement of Pre-Cambrian SR Formation over younger sediments along the SR Thrust (SRT), which itself accepted as Main Frontal Thrust (MFT) in Pakistan (DiPietro and Pogue, 2004). The name of SR originates from salt deposits embedded in marl and gypsum of the SR Formation (Shah, 2009). The SR is an east-west trending narrow trough, bounded by the Jhelum River on the eastern side, whereas the Indus River defines its western limit (Kazmi and Rana, 1982). The SR is an important element in Pakistan, known as the "World Field Museum of Geology and Paleontology", displaying a wide variety of tectonic and paleontological features (Sameeni, 2009). In addition, the SR is an easily accessible place providing an excellent opportunity to investigate the sedimentological and tectonic record along the roadside and at some deep gorges exposing the older strata. In the eastern side of SR, the older sedimentary successions are exposed in Khewra Gorge in the vicinity of Khewra, Choa Saidan Shah and Kussak Fort sites. While, beyond the Kallar Kahar town, the Nilawahan Gorge, Nammal Gorge and Chichali Gorge outcropped the younger rocks, which preserved unique planetological remains in the surrounding of Nurpur, Mianwali and Kalabagh areas, respectively (Fig. 1). Furthermore, the SR has always been attracted by different researchers around the globe to explore the stratigraphic, tectonic and paleontological history preserved in the sedimentary successions up to Recent.

The pioneer and first-ever geologist to investigate the SR was Gee (1935), who almost spent his entire professional career to produce geological maps including six toposheets (1:50,000) of SR in addition to define the ages of erstwhile "Saline Series". The large forams of Lower Tertiary in the SR were identified and demarcated by Davies and Pinfold (1937). Similarly, the Brachiopods of Permian succession in SR were studied by Waagen (1895); Kummel and Teichert (1966, 1970) and defined the biostratigraphy. Whereas, Fatmi (1973) investigated Triassic Ceratitids of the Trans-Indus Range and SR and developed a detailed stratigraphic chart of SR which was further elaborated by Shah (1977). Grant (1966) identified trilobites, while small forams of Tertiary strata were studied by Haque (1956) in the Nammal Section of SR. Ashraf and Bhati (1991) targeted the Patala and Nammal formations to explore the micro-fossils in western SR. The Paleogene Planktonic forams of SR were recognised by Afzal (1997), who further studied Patala Formation to define Planktonic-biostratigraphy of SR (Afzal and Daniels, 1991; Afzal and Butt, 2000). Paleogene-biostratigraphy in SR based on Alveolinid fossil of Eocene was defined by Sameeni and Hottinger (2003). Shahzad et al. (2017) studied the biostratigraphy of Eocene carbonate in the core of Hazara Kashmir Syntaxis.

This study mainly focuses on, the detailed micropaleontological investigation of the Early Eocene carbonate sequence of the eastern and western SR. Secondly, to correlate this foraminiferal fauna with the Early Eocene carbonate rock units exposed in the northern mountainous region of Hazara, KPK, Pakistan. For this purpose, two sections were selected for the detailed biostratigraphy study of Eocene carbonates i.e., Nammal Formation and Sakeasar Limestone. One section was situated in eastern SR i.e., from Khewra Gorge (32°40'28.77"N; 73° 0'10.34"E), whereas the other section was selected from western SR i.e., from Nammal-Gorge (32°39'53.81"N; 71°48'7.24"E) (Fig. 1).

2. Tectonic Setting and Stratigraphy of the Study Area

The SR is primarily a complex anticlinorium representing salt-related deformational elements in the form of secondary folding and faulting. The central segment of SR is wider than its eastern and western flanks, outcropping Eocambrian and Paleozoic sequences. The structural setting in its northern part of SR illustrates a series of gentle to open folds associated with thrust/ reverse faults representing thin skin deformation. On the other hand, in the southern part, the folds become tight to overturned, generally associated with E-W trending thrust and/or reverse faults which demarcate a high deformation rate in contrast to the northern part. The Eo-Cambrian evaporites were emplaced over the younger strata due to the displacement along the SRT, resulting in the formation of complex structural geometry. In the eastern part of SR, the rocks changed their regional strike from east-west to north-east due to the transpressional tectonics in addition to the salt-diapirism, which is demonstrated by Chambal-Jogi Tilla and Diljabba thrusts (Kazmi and Rana, 1982).

The rocks were severely deformed due to salt-tectonics and changed their strikes to north-south, opposing their regional trend in the vicinity of the SRT zone. This type of thin-skin deformation followed by salt tectonics is evidenced in the Kohat Basin, a westward extension of the Potwar fold and thrust belt in the Upper Indus Basin (UIB) (Ikram et al., 2020; Gardezi et al., 2021; Khalid et al., 2020).

The Pre-Cambrian to Quaternary successions were outcropped in SR and adjacent basin i.e., Potwar Plateau. These rocks are comprised of SR Formation (Eo-Cambrian evaporites), Jhelum Group (Cambrian sandstone, dolomite and shales etc.), which represent an unconformable relationship with overlying Nilawahan and Zaluch groups (carbonates and clastic sequence of Permian). Furthermore, the rocks comprising of clastic and carbonates of Triassic to Eocene were exposed throughout the SR, followed by

the molasse deposits of Rawalpindi and Siwalik groups resulting from Himalayan orogeny in Miocene to Pliocene time (Shah, 2009; Fig. 2).

The stratigraphic sequence of UIB highlights four different phases of depositional gaps: i) The Potwar Plateau in Ordovician-Carboniferous time was uplifted, which resulted in a regional unconformity; ii) Permo-Triassic (P-T) boundary; iii) Cretaceous-Tertiary (K-T) boundary, and iv) Unconformity lies between Eocene and Miocene rocks where the Oligocene sequence is missing (Gee, 1945; Shah, 2009).

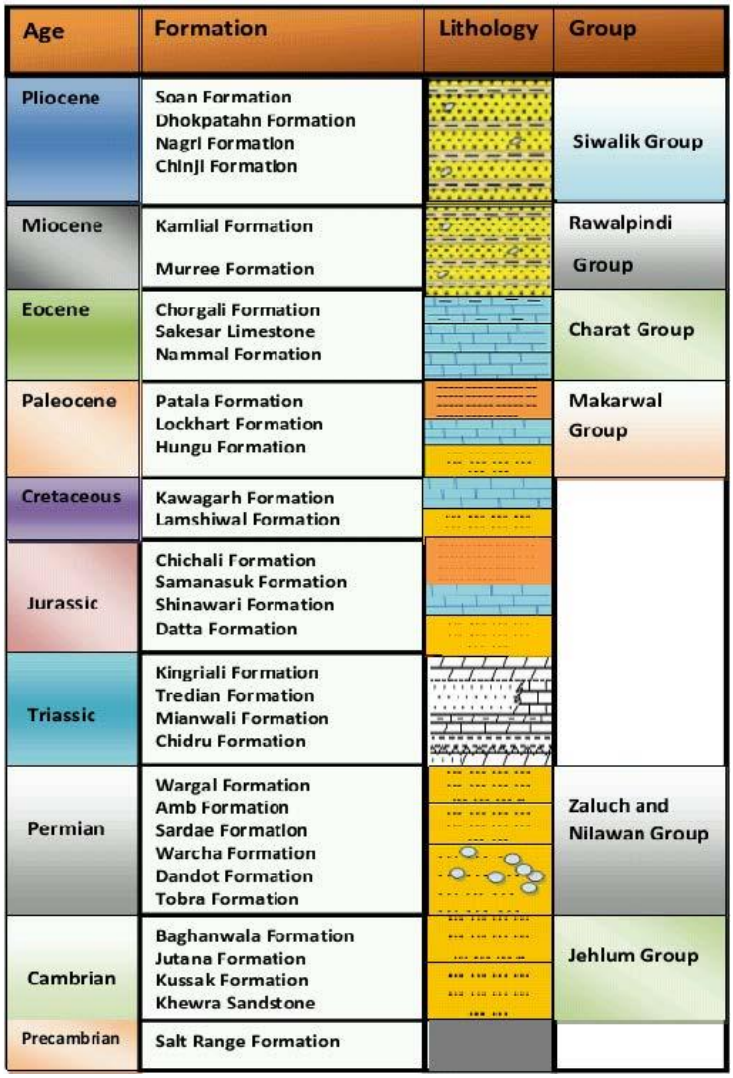

Fig. 1: Stratigraphic column of the Potwar Basin (modified after Gee, 1945).

2.1 Nammal Formation

The Nammal Formation is mainly divided into two units. In the lower unit, light grey to bluish-grey marls with a slightly medium grey, thinly to medium bedded limestone is dominant. One thin bed of fossils containing marly limestone is present at the base of the Nammal Formation and the frequency of limestone increases from bottom to top. Near the upper part of the Nammal Formation, fossils containing thick limestone beds are present. The upper part of the Nammal Formation is slightly bluish-grey cliff-forming, fossiliferous and thin-medium bedded limestone. The microfossils were abundant in the upper as well as in the lower component of the Nammal Formation.

In the Nammal Gorge area, Haque (1956) placed the base of the Nammal Formation at the limestone shelf, which separates the middle and upper units of Patala. He placed these black shales in Nammal Formation. Because of the lithological and color variations, the contact between the Patala and Nammal formations is marked by thinly bedded marly limestone, which is present in the Patala Nalah and has become very dominant in the eastward direction. It becomes very thick where the pure limestone bed of Nammal Formation rest directly above this marly limestone. This boundary is marked with the help of

faunal change. The upper contact of the formation is with Sakesar Limestone, which is sharp and confirmable. The rock units are distinguished based on nodules. The regional distribution of the Nammal Formation is the same as Patala Formation in SR, Potwar Basin, Surgur Range, and the adjoining sub-basins. The maximum thickness measured during the field of the Nammal Gorge area is 142.5 meters (Fig. 3).

The basal units of the Nammal Formation contain larger foraminifers. These forams show deeper to middle shelf environments. The overlying marly limestone unit having benthic foraminifers show deep marine outer shelf to upper slope environments. The thin bed in the formation obtains abundant larger foraminifers that may show the downward movement of the forams from the shallow part of the shelf to deep marine environments. The presence of these microfossils shows that the depositional environment of the Nammal Formation is shallow to deep marine.

2.2 Sakesar Limestone

The Sakesar Limestone is examined in the field from Khewra Gorge and Nammal Gorge sections. Limestone consists of light grey to medium grey, medium to massive bedded, irregular, nodular, cherty and cliff-forming behaviour. The Sakesar Limestone contains large numbers of black cherty nodules, larger forams, green and red algae and Mollusks. The age of the Sakesar Limestone based on these fossils is classified as Early Eocene.

The lower contact of the Sakesar Limestone in the Nammal Gorge area is sharp and confirmable with Nammal Formation whereas, Sakesar Limestone in Nammal Gorge have an unconfirmable upper contact with the Siwalik Group. The lower contact of the formation in the Khewra Gorge area is with Patala Formation, where Nammal Formation is missing. The upper contact is with Siwaliks, which is unconformable. The distribution of the Sakesar Limestone is throughout the study area. The thickness measured during the field in Khewra Gorge is 100 meters and 30.5 meters in the Nammal Gorge section (Fig. 3, 4). Planktons are absent in the Sakesar Limestone. The larger benthic forams like *Alveolina* and *Lokhartia*, green and red algae, show very shallow to inner shelf environments. The nodular behaviour of this rock unit exhibits the shallow marine environment.

3. Methodology

Sections were measured using the measuring tape, and lithologs were prepared using Sedlog. Field sketches and photographs of the formations at the sections are taken to document fossils. More than 60 rock samples were collected randomly in the field, where we found lithological variation and thin sections were prepared in the University of Peshawar, Pakistan. Streozoom microscope was used for the interpretation of microfossils in the laboratory. The microphotographs of the foraminiferal fauna were taken by LEICA DM750P microscope.

4. Results

4.1 Systematic Micropaleontology

This study deals with the biostratigraphy and systematic Paleontology of the early Eocene carbonates of eastern and western SR. To study micro-paleontology and thin-section preparation, 40 samples were selected, which were collected from the targeted sections. Following are the species identified in this study:

4.1.1 Genus: *Nummulites* (Lamarck, 1881)

4.1.1.1 *Nummulites atacicus* (Leymerie,1846)

The test is generally smooth, the last whorl is occasionally marked off, and polar pillars can also be observed on its surface including thin and whirled septal filaments. The septa showed the curved appearance in upper halves whereas appears normal along the lower halves. (Fig. 5A).

4.1.1.2 *Nummulites mamillatus* (Fichtel and Moll)

The test is apparent, with a very small border. It has a small but distinct and prominent polar pustule. The marginal cord is represented as the end of the septa as inclined, well forward (Fig. 5B).

4.1.2 Genus*: Assilina* (d' Orbigny, 1826)

4.1.2.1 *Assilina granulosa* (d' Archiac, 1847)

Flat discoidal shape along with the granulated surface are the characteristic features of this specie. Along its axial section, the sutures of this specie bears granules concentrated into a bunch at poles whereas its Meridian section represents the whorls are enveloping with radial and straight septa.

4.1.2.2 *Assilina spinosa* (Davies and Pinfold, 1937)

Assilina spinosa is differentiated from *Assilina granulose* because of form thickness, more close sets of granules and appearance of bars on the last whorls making sutures. The test of this specie is usually biconvex, rounded to sub-rounded periphery, ornamented with close-set of granules, covering the central part of the test excluding the outermost whorl. The last whorls sutures are straight and raised (Fig. 5D).

4.1.2.3 *Assilina subspinosa* (Davies and Pinfold, 1937)

Assilina subspinosa is characterized by their large and noticeable granules packed closely over the central portion of the test, whereas the outer-most whorl is comparatively smoother which shows more or less distinctive septa and marginal cord. The nature of ornamentation makes it distinct from *Assilina spinosa*

as it possesses the denser and coarser ornamentation along the poles vicinity. Its meridian section represents like spines as central granules stand out; the broad and enclosed chamber is observed in these sections, with minor of the proceeding whorl. Septa seems similar to the *Assilina spinosa,* with the chambers are generally about one to half time as high as long (Fig. 5E).

4.1.2.4 *Assilina laminosa* (Gill, 1953)

The axial section specifies a thick marginal cord and test wall. The surface of the test is fairly smooth (Fig. 4).

4.1.2.5 Assilina sp.

Assilina sp. is recorded from Sakesar Limestone from Khewra and Nammal gorges. The species are recorded from KS-2, 3 and NS-5 (Fig. 5D; Fa).

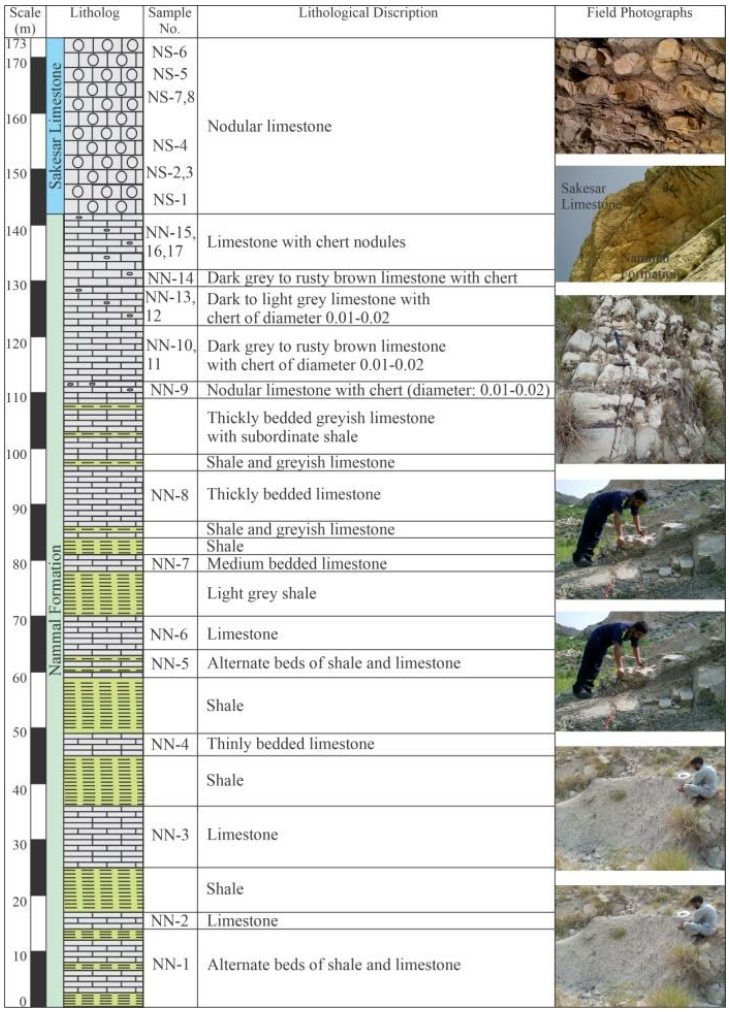

Fig. 2: Litholog of Nammal Formation and Sakesar Limestone Nammal Gorge, western SR.

4.1.3 Genus: *Lokhartia* (Davies, 1932)

4.1.3.1 Lokhartia sp.

Lokhartia sp. generally exhibits a low trochospiral shell with a rounded peripheral margin having thicker pustules on the umbilical side. The axial section possesses umbilical cavities, which are relatively large and regular. The pillars are distinct but regular, and umbilical plates are well-developed (Fig. 6B).

4.1.4 Genus: *Quinquoloculina* (d' Orbiginy, 1926)

4.1.4.1 Quinqueloculina sp.

The specimen exhibits sections from numerous slides. The test represents changing pattern of chamber development. It possesses three to four chambers, with smooth surface. Wall is calcareous in nature and imperforate (Fig. 6C).

4.1.5 Genus: *Spiroloculina* (d' Orbiginy, 1926)

4.1.5.1 Spiroloculina sp.

The test is well compressed, almost twice the width of the test. A few chambers are present cylindrical, compressed, nearly of uniform shape. The thickness and the width are almost the same. The surface is smooth and depressed sutures are present. Aperture is terminal in shape and with a circular neck. The calcareous walls are imperforate (Fig. 6D).

4.1.6 Genus: *Textularia* (Defrance, 1824)

4.1.6.1 *Textularia mississippiensis* (Cushman, 1922)

The test is elongate compressed, broad, widest at the apertural end, thickest in the middle, somewhat rhomb shaped in the cross-section; the periphery is acute, corinate somewhat irregular, chambers distinct, low and broad suture distinct somewhat limbate/ raised meeting in the middle part of the test forming a zigzag ridge, initial and is tapering. The test is finally agglutinated of very minute calcareous particles, and sand grains are smoothly finished with much cement (Fig. 6E).

4.1.7 Genus: *Nodosaria* (Lamarck, 1804)

4.1.7.1 Nodosaria sp.

The test is elongated, and the chambers are also elongated. Three to five chambers are indicated in the specimen. In one of the sections, the specimen's chambers are distorted, separated by deep constrictions.

4.1.8 Genus: *Alveolina* (Leymerie, 1846)

4.1.8.1 Alveolina globula

The specimen is generally spherical to sub-elliptical, spirally coiled. Well-developed whorls are present. Initially, spacing between the chambers is larger than the spacing of the final chamber, which is closely developed.

4.1.8.2 *Alveolina pasticillata* (Schwager, 1883)

This species is recorded from the Sakesar Limestone of the Khewra Gorge area. The stratigraphic range of this species is from Upper Paleocene to the Early Eocene age. This species is recorded from the KS-4 thin section slide (Fig. 7E).

4.1.8.3 *Aleoline conredi* (Sameeni, 1997)

This species is recorded from the Sakesar Limestone of the Khewra Gorge area. Porcelaneous, medium size ovoid shells. In the axial section, the magalospheric form shows a pointed poles chamber-let rounded in cross-section (Fig. 7C).

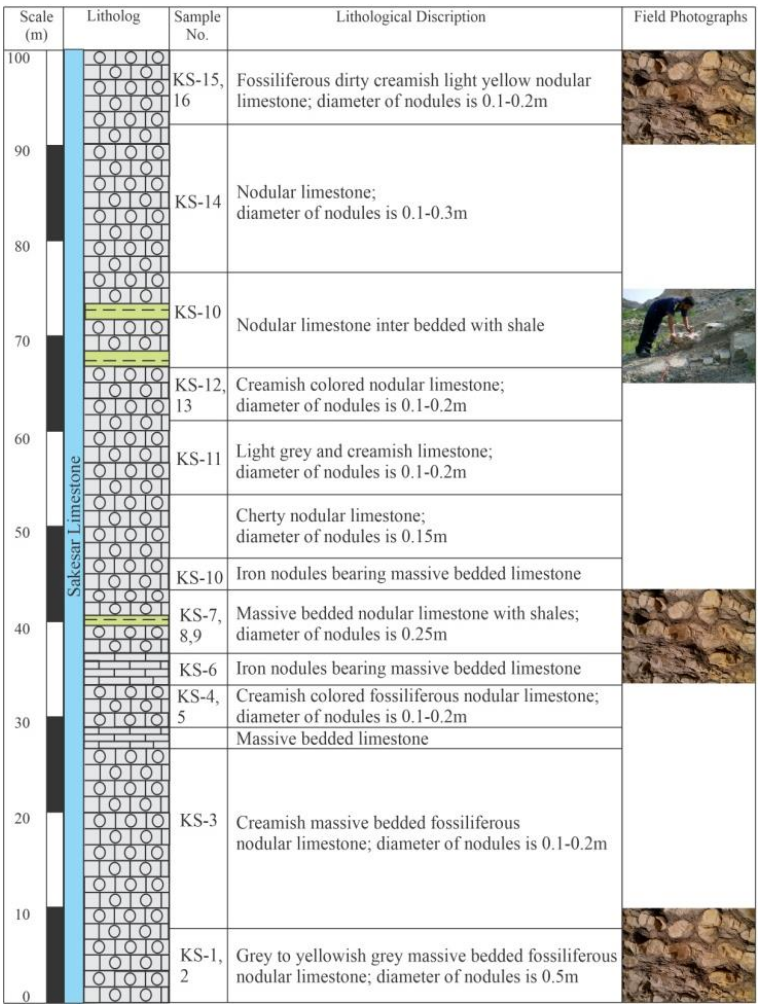

Fig. 3: Litholog of Sakesar Limestone Khewra Gorge, eastern SR.

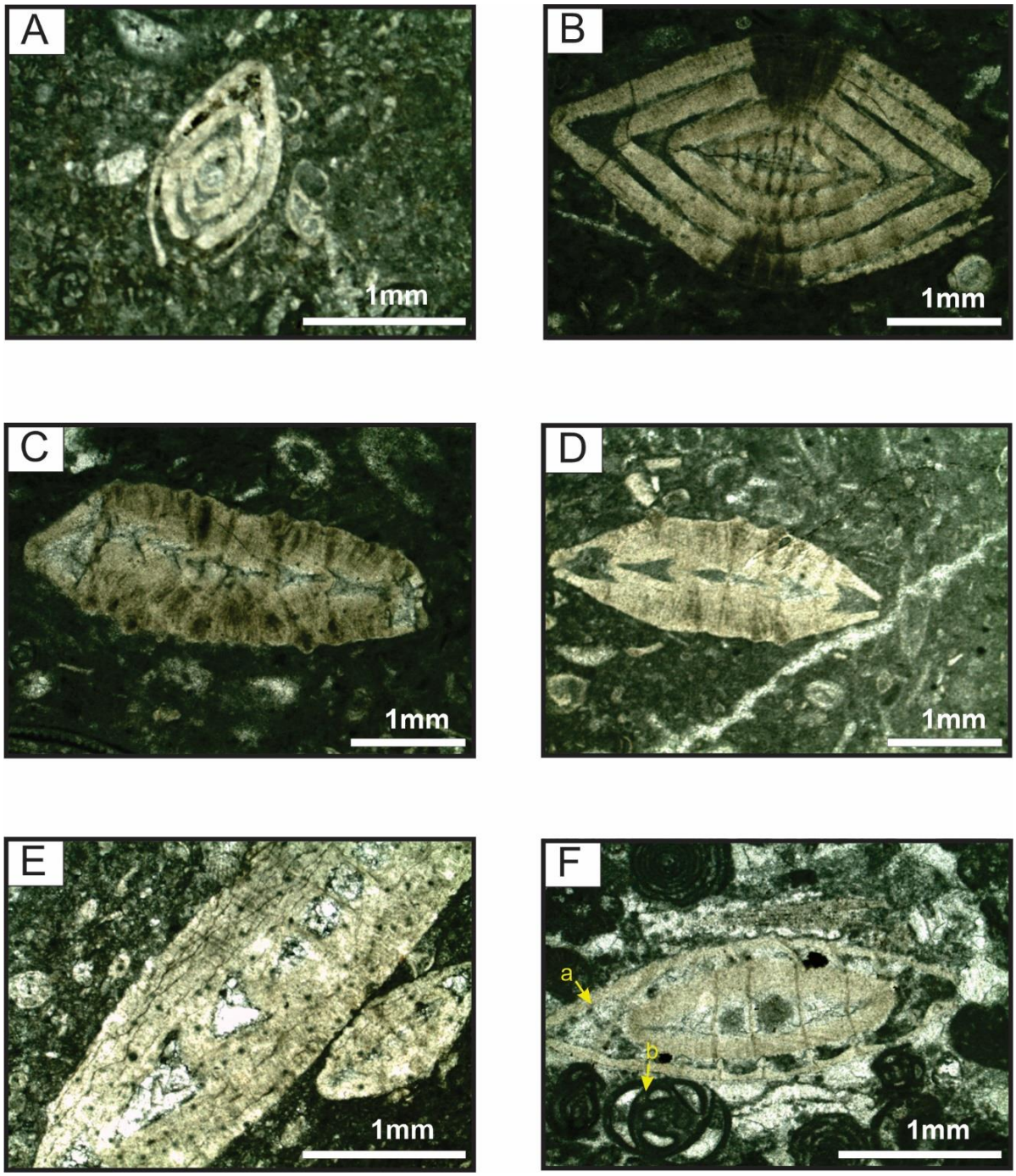

Fig. 4: Photomicrographs shows microfossil (axial sections) from Nammal Formation and Sakeasar Limestone; A) *Nummulite atacicus*, B) *Nummulites mammillatus*, C) *Assilina sp.*, D) *Assilina spinosa*, E) *Assilina subspinosa*, and F) a). *Assilina sp*., b). *Milloilds*.

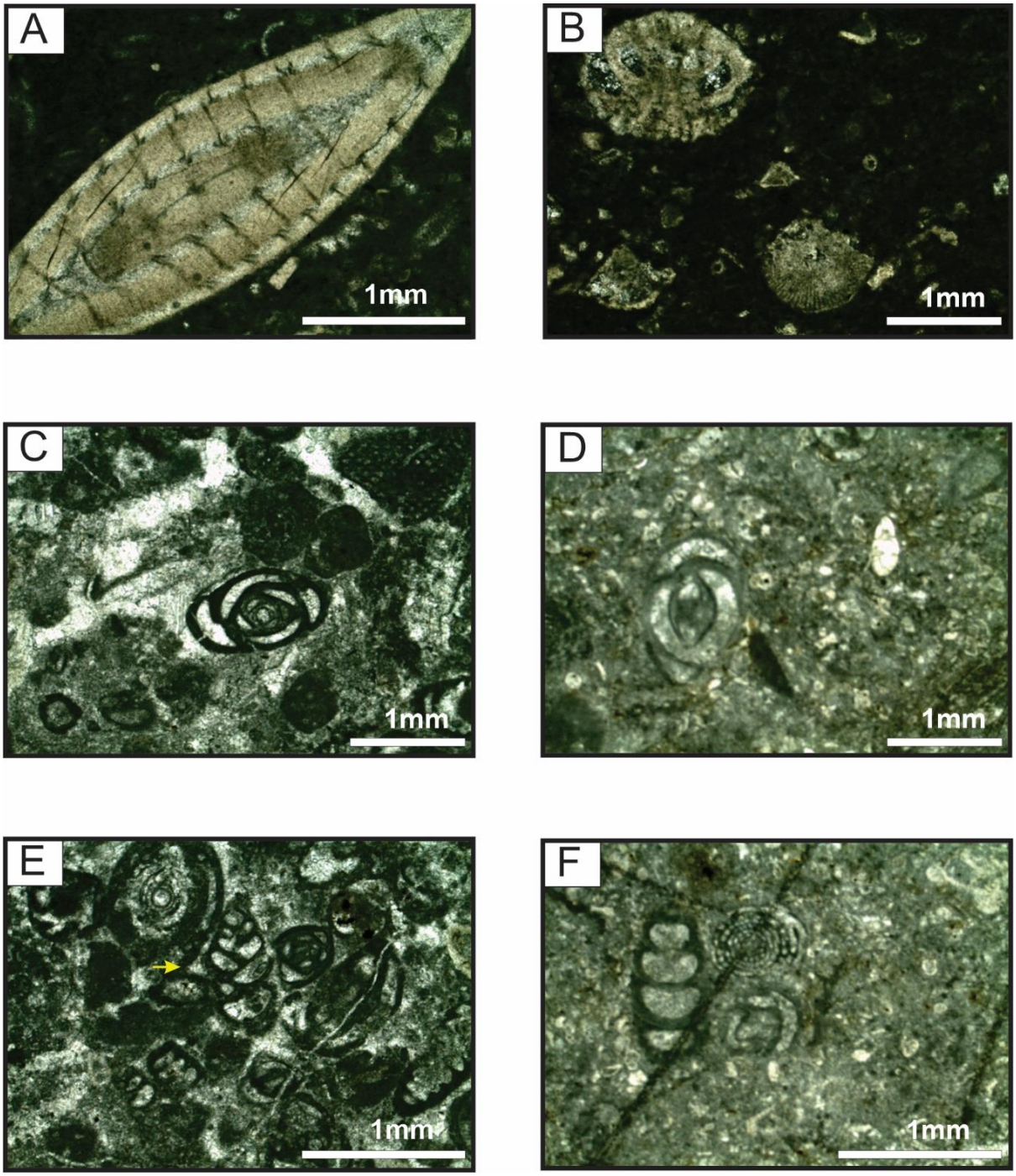

Fig. 5: Photomicrographs shows microfossil (axial sections) from Nammal Formation and Sakeasar Limestone. A) *Assilina sp*., B) *Lockhartia sp*., C) *Quinqueloculina sp*. D) *Spiroloculina sp*. E) *Textularia mississippiensis* F) *Sakesaria sp*.

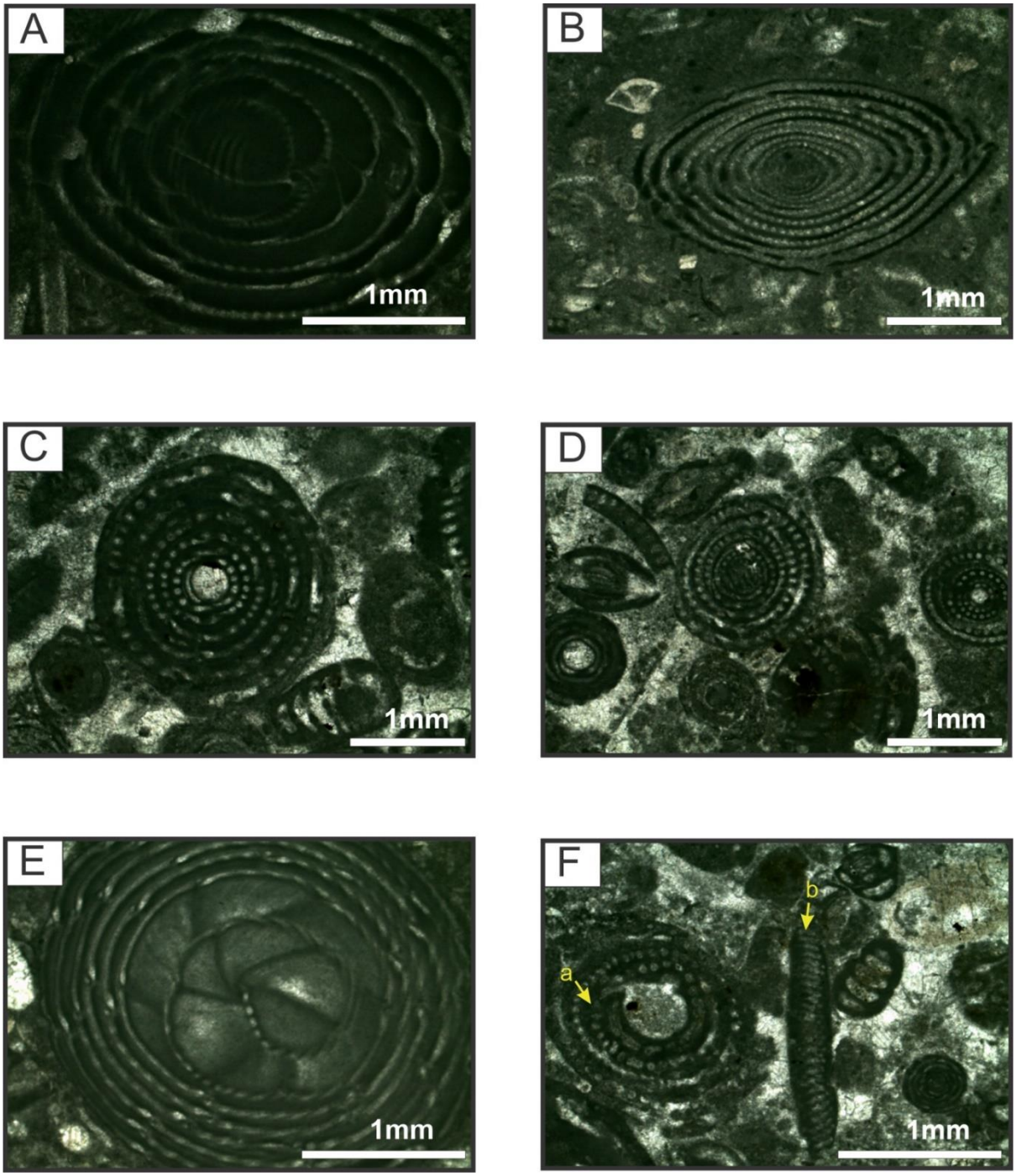

Fig. 6: Photomicrographs shows microfossil (axial sections) from Nammal Formation and Sakeasar Limestone. A) *Alveolina sp*., B) *Alveolina conredi*, C) *Alveolina codolioliformis*, D) *Glomalveolina*, E) *Alveolina pasticillata*, F) a) *Alveolina sp*., b) *Orbitolites.*

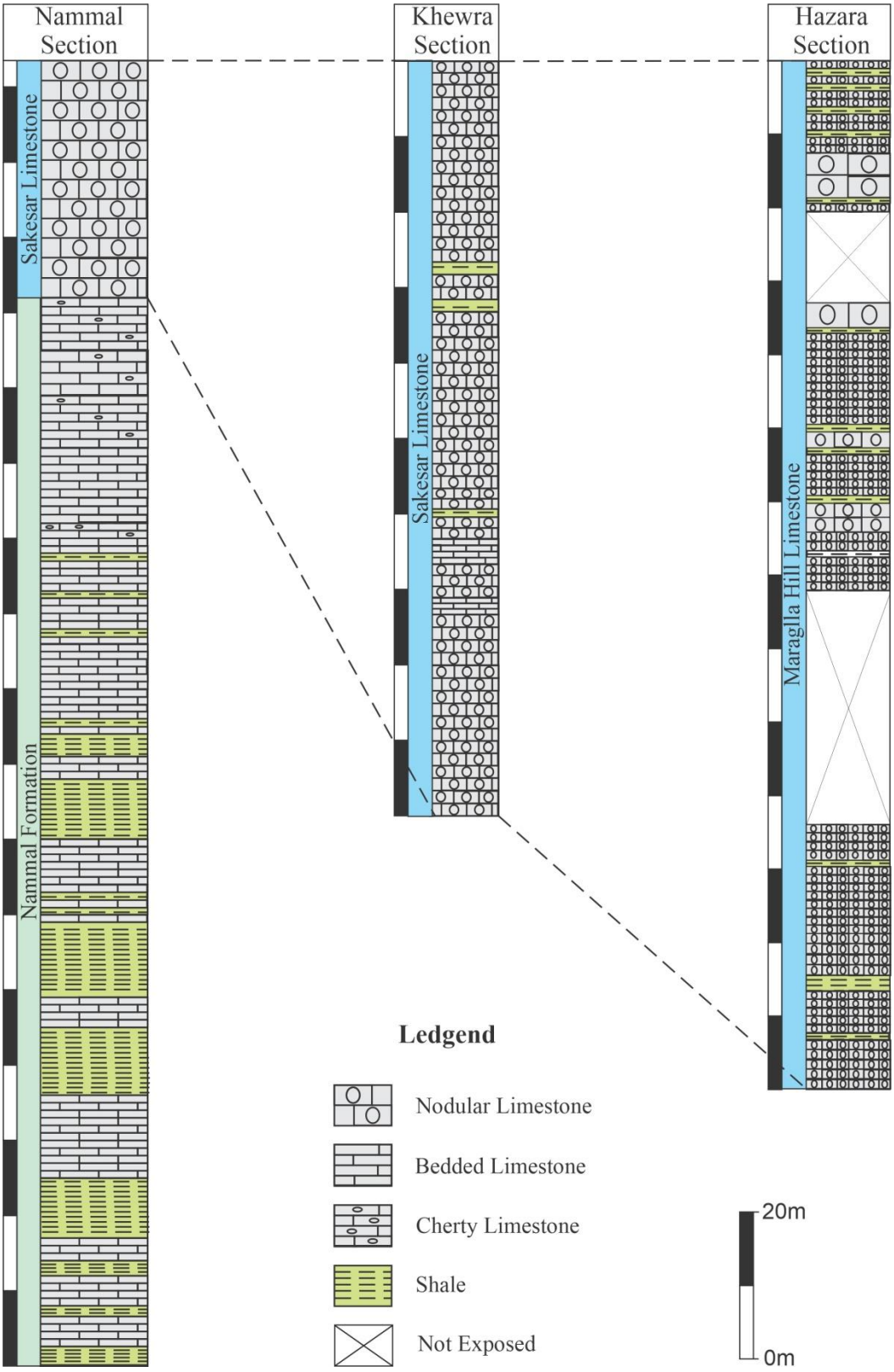

Fig. 7: Lithostratigraphic correlation of Early Eocene carbonates from Nammal, Khewra and Hazara sections.

5. Paleoecology

Most larger foraminifers are not restricted to one type of sediments, and these have their clear preferences. More species of each genus are involved, and that not all necessarily occupy the same ecological niche (Gaemers, 1978). There is only a general impression of the main ecological requirements for some genera of larger foraminifera which are very common in the sequence. *Orbitolites* give preference to the shallow marine environment that protects themselves against tides and waves. *Orbitolites* are present in those limestones are pure deposits. These are also present in those limestones containing sand and clay content. This genus was like epiphytic in nature (Hottinger, 1973). It is mainly associated with the *Alveolinids* and *Miliolids*.

Nummulites are very dominant in the carbonate rocks like limestone. The areas where extensive deposition occurs are usually rare. More of its specimen is present in Marls because these marls were deposited at a low rate than the other marls.

Assilina is dominantly presented in the marly limestone and marl. Average of these were deposited in the greater depths than those where *Operculina* were frequent. *Assilina* is not generally a sand or limestone dweller (Afzal and Shafique, 1997).

Alveolinids are dominantly present in the shallow marine environment where the water is very clear. It dominantly occurs in those deposits rich with lime and consists of different other porcelaneous foraminifers, dominantly *Miliolid* and *Orbitolites*. *Alveolinids* could not live in a brackish environment than the *Miliolids*. *Alveolinids* never occur in environments interpreted as brackish (Hottinger, 1960). According to the analysis performed in this study to identify different species, the Alveolinids are only recorded from the normal saline water, which revealed that it is surely inappropriate to say that Alveolinids are only present in the shelf areas.

6. Discussion And Correlation

The lithostratigraphic units, i.e., the Nammal Formation and the Sakesar Limestone of Early Eocene age from the western and eastern SR, are selected for the current study. Furthermore, these lithic units are compared with the Margalla Hill Limestone of the Hazara area (Fig. 7). The Nammal Formation of Nammal Gorge in SR area consists of thinly to thickly bedded limestone. Limestone is present in the form of small patches, limestone of light-yellow weathered color and light grey to light fresh brown color with subordinate marly shale. Limestone showing massive bedding and conchoidal fractures containing bioclasts about 30 to 35 percent of *Lockhartia sp*., *Nummulites* and *Assilina sp*.

The Sakesar Limestone of Nammal Gorge consists of nodular limestone with solutioning on the weathered surface; nodules size varies from 0.2 to 0.3 meters in diameters. Thickly bedded nodular limestone solutioning is present in the surface of the rock units. The Sakesar Limestone from Khewra Gorge consists of nodular limestone, massively bedded limestone with iron and chert nodules at the top, creamish to light grey, Fossiliferous, nodular limestone, yellowish to creamish color, nodules 20-25cm in diameter and they are generally rounded and floating within a usually micritic matrix. These nodules are hard micritic and less fossiliferous than the surrounding highly fossiliferous material. The color of the matrix and nodule is due to the variation in the number of non-carbonates like Iron Hydro Oxides, sulphides and carbonaceous matter (Flugel, 2004). The massive-bedded limestone with chert nodules portion has a total thickness of about 17 meters. The weathered surface of limestone in this section represents the color scheme of light brown, yellowish and grey to light grey, whereas light grey to yellow and white on the fresh surface. It is hard, massive and chert nodules developed on the top of this unit. The size of the limestone nodules is 18-25cm, and the size of the chert nodule is 5-10cm and frequently varies up to 60cm in length. The size of the forams increases towards the top of this unit. The overall appearance sometimes resembles the conglomerates. The limestone bedding is often wavy to lenticular. The bedding surface shows the lack of concentration of the fossils.

The Stratigraphic equivalent of Nammal Formation and Sakesar Limestone of SR area is Margalla Hill Limestone in Hazara area. The Margalla Hill Limestone consists of grey to dark grey, massively nodular limestone. Limestone is like cliff-forming and clusters of forams, present on the weathered surface. In the Hazara area, its thickness is 140m (Swati et. al., 2013) while the thickness of this sequence in the SR and Surghar Range varied from 143m thick beds of Nammal Formation and 40-100m Sakesar Limestone.

The Margalla Hill Limestone is dominantly nodular limestone with slightly insignificant marly limestone and shale intercalation. The broken fresh surfaces show dark grey to grey, and pale grey color shows on the weathered surface. The weathered surface shows an abundance of larger forams, ranging in size from 3-7mm. The limestone consists of nodules, the range of nodules is from 13cm-24cm in length and up to 33cm in breadth. The nodules are covered by argillaceous material. The massively bedded limestone consists of calcite veins (Munir, 2003). The unit was measured from Hazara by (Munir, 2003) and its thickness was reported as 25-159 meters in the area. The formation is visible from a distance due to high cliff-forming ridges and escarpments behaviour.

The fossils examined from the thin section studies of Nammal Formation and Sakesar Limestone in Khewra (eastern) and Nammal (western) sections are: *Nummulites atacicus*, *Nummulites mammillatus*, *Alveolina globusa*, *Alveolina ovulum*, *Alveolina elliptica*, *Alveolina sp*. *Alveolina indicatrix*, *Assilina granulosa*, Assilina *spinosa,* Assilina *subspinosa*, Assilina *sp*. Lochartia *sp*. *Milliolids*, *Quinqueloculina*

sp. Textularia sp. Nodusaria, Sakesaria, Green Algae. These all microfossils confirm the early Eocene age of the formations.

On the other hand, the fossils which are reported from Margalla Hill Limestone in Hazara section (Munir, 2003) are: *Nummulites mammillatus, Nummulites atacicus, Assilina granulosa, Assilina subspinosa, Assilina spinosa, Assilina laminusa, Operculina patalensis, Ranikothalia sindensis, Lockhartia tipperi, Lockhartia conditi, Rotalia trochidiformis, Alveolina sp. Pseudophragmina stephensoni, Discocyclina dispensa, Rotalia perovalis, Discocyclina ranikotensis, Alveolina ellipticus* and *Alveolina pasticillata*.

The correlation based on microfossils from Nammal Formation, and Sakesar Limestone from Nammal Gorge section and Khewra Gorge section with the Hazara section shows that all the Early Eocene fossils recorded from eastern and western SR were found in the Margalla Hill Limestone from Hazara area except *Sakesaria* sp. which is index fossil of Sakesar Limestone. *Ranikothalia sindesis* and *Pseudophragmina stephensoni* reported from Margalla Hill Limestone by (Munir 2003) have not been found from SR by the author. Otherwise, almost all Early Eocene species from SR and Hazara area are the same, indicating that Sakesar Limestone is stratigraphic equivalent in SR of Margalla Hill Limestone in the Hazara area.

7. Conclusion

The detailed field study, samples analysis and micro-paleontological studies of early Eocene rocks of eastern and western SR yield the following conclusions.

1. Different benthic foraminifera are reported from the Nammal Formation and Sakesar Limestone which are: *Nummulites atacicus*, *Nummulites mammillatus*, Assilina *spinosa*, *Assilina subspinosa*, *Assilina granulosa*, *Alveolina globula*, *Milliolids, Quinqueloculina, Textularia, Nodoseria,* and green *algae*.
2. Based on petrographic studies and the presence of benthic forams shows that the depositional environment of the Nammal Formation is shallow to deep marine, whereas deposition of Sakesar Limestone represents shallow marine settings.
3. The age of the Nammal Formation and Sakesar Limestone inferred from the foraminifera index is Early Eocene.

Reference

Ashraf, M.,Bhatti, M., 1991. Nannofossil biostratigraphy of the Patala and Nammal Formations of Khairabad East, Western SR, Pakistan. Hydrocarbon Development Institute of Pakistan (HDIP), Unpublished report.

Butt, A.A., 1987. The Upper Cretaceous bios-stratigraphy of Pakistan: A synthesis. Geologie Mediterranean XIX, 4, 265-272.

Cushman, J. A., 1922. The foraminifera of the Vickbsburg Group. U. S. Geol. Surv. Prof. Paper, 133,11-71.

Davies, L.M., 1932. The fossil fauna of the Samana Range and some neighbouring areas; Pt1, An Introductory note. Geol. Surv. India, Mem. Paleont. Indica, New Series, 15, 1-13.

Davies, L.M., Pinfold, E.S., 1937. The Eocene beds of the Punjab SR. Geol. Surv. India, Mem., Paleont. Indica, New Series, 24, 1-79.

Archiac, E.J.A.D., Haime, J., 1853. Description des Animaux Fossile du group Nummulitique del'Inde. Paris, Qto., 2, 373.

Orbigny, A.D. d', 1826. Tableau méthodique de la classe des Céphalopodes. Crochard.

Defrance, E., 1824. Upper Cretaceous foraminifera from the Carlsbad area, San Diego County, California. Journal of Paleontology, 488-513.

Fatmi, A.N., 1973. Lithostratigraphic units of Kohat-Potwar Province, Indus Basin, Pakistan. Mem. Geol. Surv. Pakistan, 10, 1-80.

Fichtel, L.V., Moll, J.P.C. Von, 1798. Testacea microscopic aliaque minuta exgeneribus Argonauta et Nautilus, ad nautran picta et descripta. Microscopische and andere Klein Schalthierre aus den Geschlechtern Argonnaute und Schiffer, 7, 123.

Flugel, E., 2004. Microfacies analysis of limestones. Springer-Verlag, Berlin, Heidelberg, New York, 633.

Gaemers, P.A.M., 1978. Biostratigraphy, Palaeoecology and palaeogeography of the mainly marine Ager Formation (Upper Paleocene-Lower Eocene) in the Tremp Basin. Central-South Pyrenees, Spain, 14-25.

Gardezi, S.A.H., Ahmad, S., Ikram, N., Rehman, G., 2021. Geological constraints on the Western Kohat foreland basin, Khyber Pakhtunkhwa, Pakistan: Implication from 2D and 3D structural modelling. Iranian Journal of Earth Sciences, 13(2), 61-76. 10.30495/ijes.2021.678954.

Gee, E.R. 1945. The Age of the Saline Series of the Punjab and of Kohat. Nat. Acad. Sci. India Proc., Sec. B, 14(6), 269-310.

Gee, E.R., 1935. Notes on Mesozoic/Tertiary Stratigraphy of the (former) Punjab, N.W.F.P. Sulaiman Region. The Geologist, 1(q), 2-5.

Gill, W.D., 1953. Facies and fauna in the Bhadar beds of the Punjab, SR, Pakistan. Jour., Paleont. 27(6), 824-844.

Grant R.E., 1966. Late Permian trilobites from the SR, West Pakistan. Palaeontology, Oxford, 9(1), 64-73

Haque, A.F.M.M., 1956. Foraminifera of the Ranikot of the Laki of the Nammal Gorge, SR, Pakistan. Geol. Surv. Mem. Paleont. Pakistanica, I, 300.

Hottinger, L., 1973. Alveoloinids, Cretaceous-Tertiary

Larger Foraminifera. Esso Prod. Res. Europ. Lab. EPR-E-4 SP, 74, 84.

Hottinger, L., 1960. Über paleocaene un eocaene Alveolinen.Doctoral dissertation, Bucjdruckerei Birkhäuser, 89-99.

Hussain, B.R., 1967. Saiduwali member, a name for the lower parts of the Permian Amb Formation, West Pakistan. Univ. Studies (Karachi) Sci. and Technology, 3, 4, 88-95.

Ikram, N., Gardezi, S.A.H., Ahmad, S., Rehman, G., Khalid, A., 2020. Two and Three-Dimensional Structural Modelling of Central Kohat Plateau, Northwestern Himalaya, Pakistan. In: Biswal, T.K., Ray, S.K., Grasemann, B. (Eds), Structural Geometry of Mobile Belts of the Indian Subcontinent. Cham: Springer International Publishing 131-151. 10.1007/978-3-030-40593-9_6.

Kazmi, A.H., Abbasi, I.A., 2008. Stratigraphy and Historical Geology of Pakistan. National Centre of Excellence in Geology, University of Peshawar, Pakistan, 279, 331.

Kazmi, A.H., Rana, R.A., 1982. Tectonic map of Pakistan. GSP, Quetta, Pakistan.

Kazmi, A.H., Jan, Q.M., 1997. Geology and Tectonics of Pakistan. Graphic Publishers, Karachi, Pakistan, 1-27.

Khalid, A., Ali, F., Rehman, G., Ikram, N., Hussain, S.B. and Sajjad, A., 2020. Structural analysis and restoration of the Tolanj Anticlinorium, North Eastern Kohat Basin, Khyber Pakhtunkhwa, Pakistan. Journal of Himalayan Earth Science, 53(1).

Khan, M.A., Raza, H.A., 1986. Geology of Petroleum in Kohat-Potwar depression, Pakistan. Bull. Amer. Assoc. Petrol. Geol., 70(4), 396-414.

Kummel, B., Teichert C., 1970. Stratigraphy and paleontology of the Permian-Triassic boundary beds, SR and trans-Indus ranges, West Pakistan. In: Kummel B., Teichert C., (eds.), Stratigraphic boundary problems: Permian and Triassic of West Pakistan. University of Kansas, Special Publication, Lawrence, 4, 1-110.

Lamarck, J.B., 1801. Système des animaux sans vertèbres, ou tableau général des classes, des ordres et des genres de ces animaux. Déterville, Paris.

Lamarck, J.B., 1804. Critical taxonomic study and nomenclatural revision of the Lituolidae based upon the prototype of the family, Lituola nautiloidea. Contributions from the Cushman Foundation for Foraminiferal Research, 3(1952), 35-56.

Leymerie, A.F.G.A., 1846. Memoire surle terrain a Nummulites (epicretace) des Corbieres et de la Montagne Noire. Geol. Soc. France, Mem. Ser. 2, I(2), 337-373.

Munir, M.H., 2003. Biostratigraphy and Paleoecology of upper Cretaceous to Paleogene of Hazara and Azad Kashmir. Unpub. Ph.D thesis instt. Geol. Uni. Punj. Lahore, Pakistan, 316.

Sameeni, S.J., Butt, A.A., 1998 Alveolinid biostratigraphy of the Kohat Formation, Northern Pakistan. Internat. Symp.

Sameeni S.J., Hottinger L., 2003. Elongate and larger alveolinids from Choregali Formation, Bhadrar area, SR, Pakistan. Pakistan Journal of Environmental Science, 3, 16-23.

Schwager, C., 1883. Die Foraminiferen aus den Eocaenablagerungen der lybischen Wüste und Aegyptens. Band 30, 79-154.

Shah, S.M.I., 1977. Stratigraphy of Pakistan. GSP mem, 12.

Shahzad, A., Munir, M.H., Yasin, M., Umar, M., Rameez, S., Samad, R., Altaf, S., Sarfraz, Y., 2017. Biostratigraphy of Early Eocene Margala Hill Limestone in the Muzaffarabad area (Kashmir Basin, Azad Jammu and Kashmir). Pakistan Journal of Geology. 1(2), 16-20.

Sowerby, J. de C., 1840. Description of fossils from the Upper Secondary Formation of Cutch. Trans. Geol. Soc. London. V2, 12-13.

Swati, M.A.F., Haneef, M., Ahmad, S., Naveed, Y., Zeb, W., Akhtar, N., Owais, M., 2013. Biostratigraphy and depositional environments of the Early Eocene Margalla Hill Limestone, Kohala-Bala area, Haripur, Hazara Fold-Thrust Belt, Pakistan. Journal of Himalayan Earth Sciences. 46(2), 65-77.

Waagen W. 1895. (Ser. XIII.) SR fossils. Fossils from Ceratite Formation. Memoirs of the Geological Survey of India, Palaeontological India, Calcutta, (series XIII), II(I), 1-324.

Yeats, S.R., Hussain, A., 1984. Timing of Structural events in the Himalayan foothills of Northwestern Pakistan. Bull. Geol. Soc. Amer. 99, 161-176.

KASHMIR JOURNAL OF GEOLOGY (KJG)
www.kjg.ajku.edu.pk

Microfacies analysis and depositional environment of the Cambrian Ambar Formation, Peshawar Basin, Pakistan

Rafique Ahmad[1,*], Fahad Ali[1], Bilal Sadaqat[1], Taqweem ul Haq Ali[1], Abdul Mateen[1], Muhammad Idrees ur Rehman[1], Mutahir Siddique[1], Hammad Ullah[1]

[1]Department of Geology, Bacha Khan University, Charsadda, KP, Pakistan.

*Corresponding author:
rafique.ahmad@bkuc.edu.pk

Received: 16 February 2021
Accepted: 15 December 2021
Published Online: 27 December 2021

Abstract

The Cambrian Ambar Formation is composed of massive dolomite, dolomitic limestone, limestone, quarzitic dolomite, and sandy limestone. It is exposed in the Swabi and Turlandi areas, the northeastern part of the Peshawar Basin. The present study deals with the sedimentological and petrographical aspects of the Ambar Formation. Algal laminated beds, dissolution cavities, chop-board weathering, stylolites, quartz, and calcite filled fractures together with open fractures are prominent in the outcrops. Based on microscopic studies, three microfacies are identified: (1) Siliciclastic Mudstone Microfacies (MF-1), (2) Dolomitic Packstone Microfacies (MF-2) and (3) Dolomitic Packstone-Grainstone Microfacies (MF-3) without taking consideration of the lithofacies in a single outcrop exposed in the studied section. The integration of the outcrop and petrographic observations indicate transitional to inner carbonate shelf setting ranging from supratidal to lagoon during the deposition of the Ambar Formation.

Keywords: Cambrian; Ambar Formation; Microfacies; Inner Shelf

1. Introduction

The stratigraphy of the Peshawar Basin is comprised of Neoproterozoic to Silurvian age rocks. The studied strata are least focused on previous works in the context of sedimentology, biostratigraphy, and sequence stratigraphy (Martin et al., 1962; Stauffer, 1968; Pogue and Hussain, 1986; Shah, 2009). The Ambar Formation exposed in the Peshawar basin has been described in the context of stratigraphy (Stauffer, 1968; Pogue and Hussain 1986; Martin et al., 1962; Shah, 2009). (Stauffer (1968) has briefly explained the lithology of the Ambar Formation exposed near the Turlandi area. Martin et al. (1962) mentioned the outcrop of the Ambar Formation in the "Kala Limestone and Dolomite". According to Shah (2009) and present researchers the studied stratigraphic units are comprised of dolomitic limestone, dolomite, calc quartzite with occasional argillite. Chert is also reported as veinlets and nodules within the formation. Dolomite is characterized by algal laminations and stromatolites at the outcrop level. In Swabi area underlying contact between the Ambar formation and Tanawal Formation is unconformable while the overlying contact of the Ambar Formation is also unconformable with the Misri Banda Quartzite in the form of maroon colour shale. The formation is devoid of fossils except debris of microscopic shells within the pisoliths interstices from the Ambar section (Shah 2009). According to Hussain et al. (1991), the Ambar Formation has been assigned the Cambrian age because of its stratigraphic position. The depositional setting of the Ambar Formation is not addressed by any previous work in the past, so the present research work focused on carrying out detailed petrographic analysis in order to present a reliable depositional setting of the Ambar Formation in the Peshawar basin.

1. Geological Setting

The present study investigates Ambar Formation of Cambrian age exposed in Ambar Village, Swabi area of the Peshawar Basin (latitude 34º 03' 02" N; longitude 72º 24' 46" E; Fig. 1).
The field study describes the stratigraphic unit as dolomitic limestone, dolomite, calc quartzite with minor argillite and chert nodules. The dolomite is associated with algal laminations and stromatolites. So, based on the stratigraphic position the Cambrian age is assigned.

Multiple tectonic episodes can be adopted for stratigraphic succession and sedimentology of the Peshawar basin. Erosion of the Ambar Formation, its deposition as a conglomeratic bed at the base of Misri Banda Quartzite, and siliciclasts of the underlying Tanawal Formation represent the late Cambrian events in the region. Quartzitic lithology of the Misri Banda might characterize the erosional products of plutonic felsic rocks which are associated with intrusion of the Precambrian Mansehra Granite (Le Fort, 1975). Tectonics of the Late Cambrian to Early Carboniferous events tell that the sediments deposited in the Peshawar Basin occasionally from regions to the north and gradually eroded craton to the south.

2. Materials and Methods

Current research is based on the study of laboratory analysis and field work. The variation in color, texture, fossil content and lithology are used to collect rocks samples for petrographic analysis. The stratigraphic thickness of the studied formation is measured as per standard procedure with the help of Jacob's Staff (Prothera and Schwab 2003; Fig. 2). The total thickness of the studied strata is approximately 70 meters (Fig. 2). Besides the measurement of the stratigraphic thickness, the field photographs are taken on a high-quality camera (Plate 1A-H).

A total of sixteen thin sections were prepared and analyzed under a polarizing microscope. The studied samples are classified according to the standard classification schemes of Dunham (1962) and Sibley and Gregg (1987). The developed local microfacies types are compared with the standard works of Wilson (1975) and Flugel (2004).

3. Results and Discussion

Three microfacies e.g., siliciclastic mudstone microfacies (MF-1), dolomitic packstone microfacies (MF-2), dolomitic packstone-grainstone microfacies (MF-3) in the Ambar Formation are recognized.

3.1. Siliciclastic Mudstone Microfacies (MF-1)

3.1.1. Outcrop Description

The MF-1 represents the basal part of the Ambar Formation. This thick-bedded limestone is characterized by fractures and rusty appearance on weathered exposure whereas light to dark grey colour on a fresh outcrop. Similarly, pressure dissolution results in solution cavities within the limestone unit. The limestone units appeared in outcrops as fine to medium grained. The bedding is rarely showing any sort of sedimentary structure, fossils assemblages, and other depositional or paleo-climatic indicators (Plate 2A-B, Fig. 2).

3.1.2. Petrographic Description

Lime mud is present as cementing materials which range in percentages from 60-70% while some of the micrites are converting into

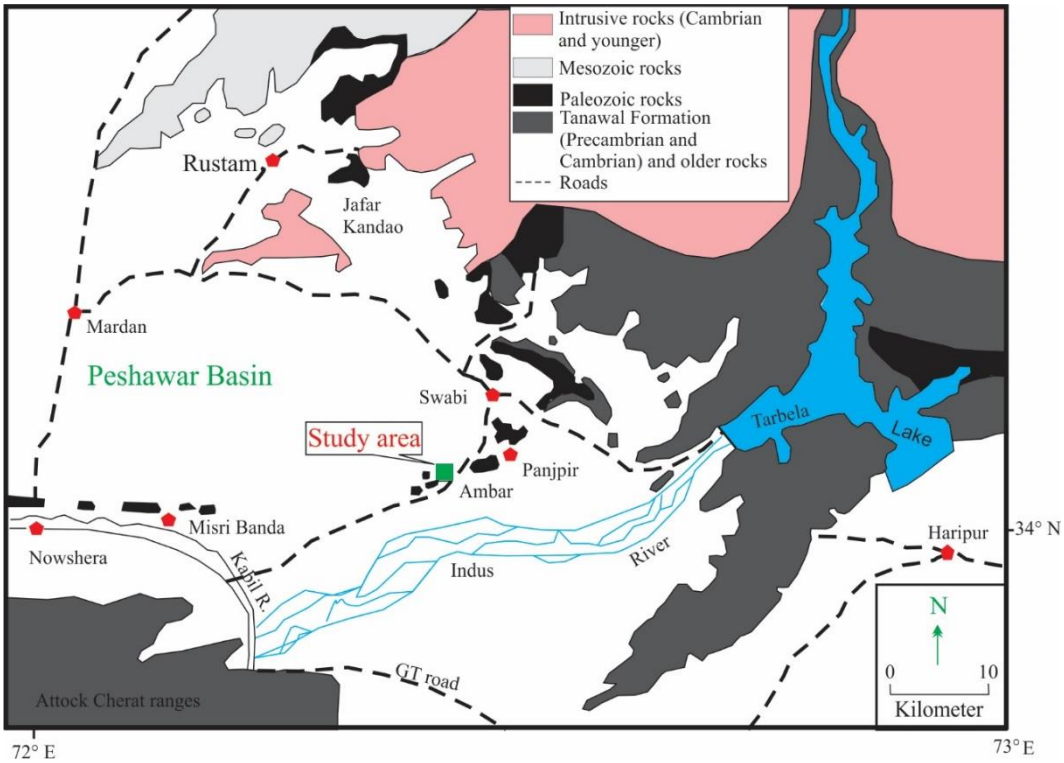

Fig. 1: Generalized geological map of eastern Peshawar Basin, northern Pakistan (Hussain et al., 1991). The study area is marked with a green square.

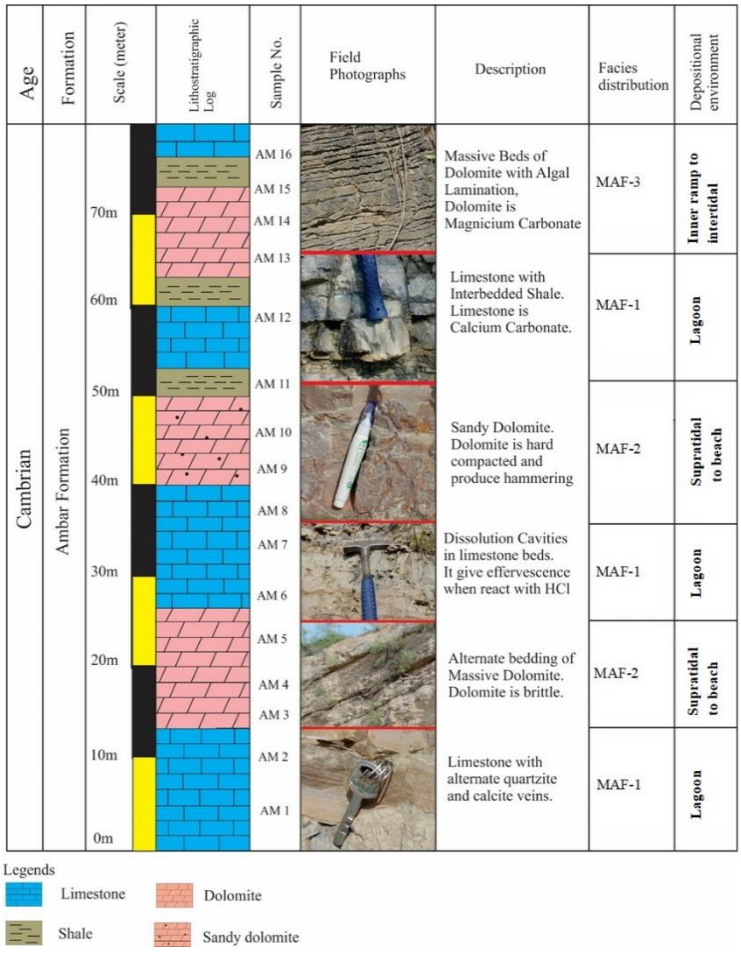

Fig. 2: The lithological log of the Ambar Formation in the Peshawar Basin.

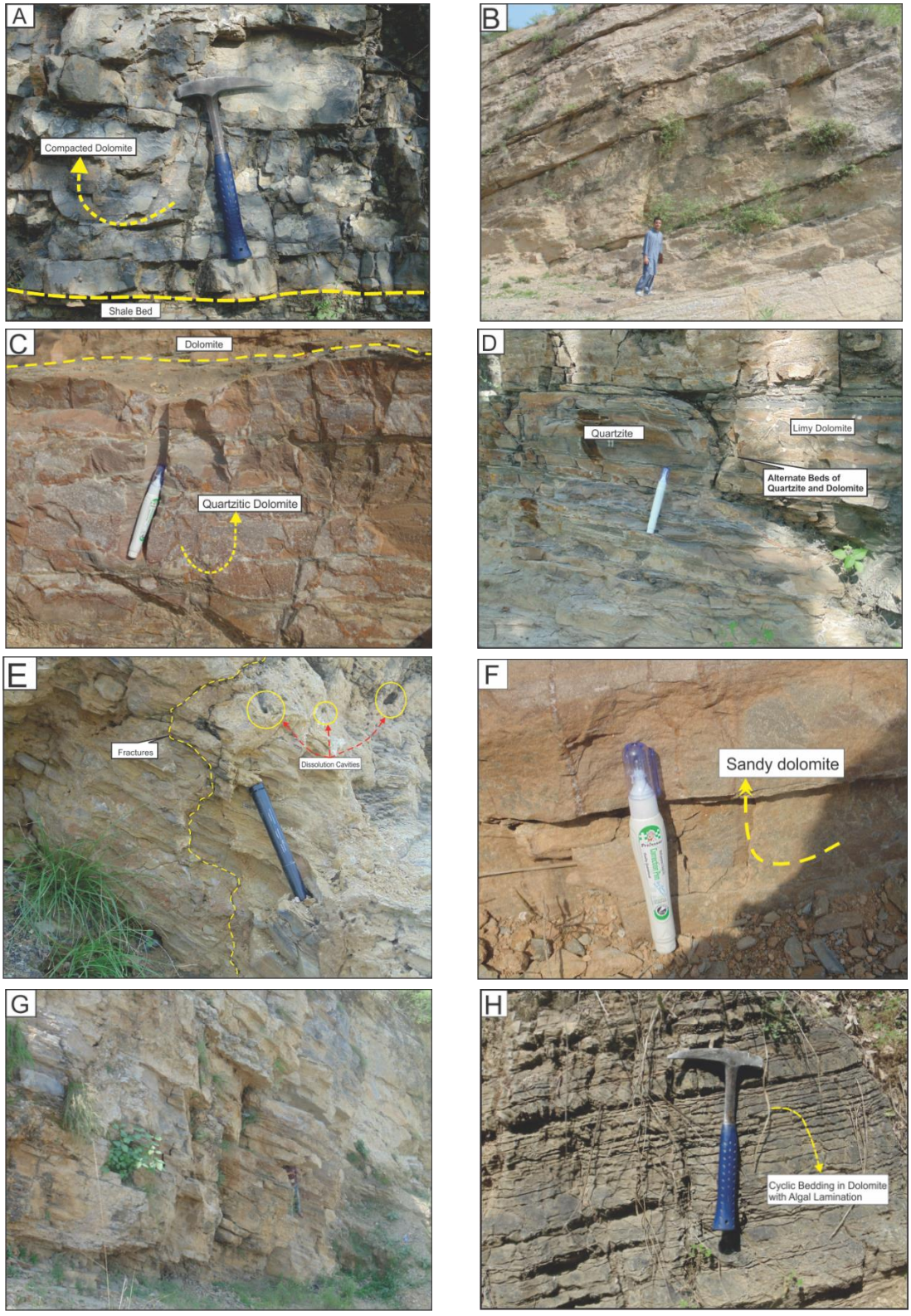

Plate 1: Field photographs show (A) Compact dolomite having interbedded shale (geological hammer for scale); (B) Sandy part of the Ambar Formation; (C) Massive bedded and compact quartzitic dolomite (whitener for scale); (D) Alternate beds of limy dolomite and quartzite (whitener for scale) (E) Meso-fractures and solution cavities within dolomite (a marker for scale); (F) Sandy dolomite beds (lower part of the Ambar Formation), whitener for scale; (G) Measured outcrop of the Ambar Formation; and (H) Rhythmic/Cyclic bedding in dolomite with algal laminations (geological hammer for scale).

microsparites (Plate 2A). The lime mud shows internal arrangements in the form of lamination. Besides this, quartz occurs as angular to sub-angular disseminated grains which constitute ~3% of the rock volume. Further, partial-complete silicification has been noted in the form of micro quartz (Plate 2B). The micritization phenomenon is common which is revealed by the modification of carbonate components (allochems) into micrite through endolithic algae (Flügel, 1982). On the basis of the presence of mud, these microfacies are named siliciclastic mudstone microfacies.

3.1.3. Environmental Interpretation

The MF 1 is devoid of known skeletal and non-skeletal allochems, while a low percentage of detrital grains are present. The absence of allochems, the presence of micritization, and internal lamination indicate a low-energy restricted condition of the high saline geochemical setting. Micritization is the process associated with the boring activity of algae on the allochem surface which is later on filled by lime mud. This phenomenon mostly takes place in low-energy conditions. So, based on these microscopic features, the interpreted depositional settings are low energy lagoons. The lagoon setting is also supported by the microfacies correlation with Standard Microfacies (SMF) 23 of Wilson (1975) and Flügel (2004).

3.2. Dolomitic Packstone Microfacies (MF-2)

3.2.1. Outcrop Description

In outcrop, the MF-2 is dominantly composed of massive beds of greyish dolomite. The dolomite is showing a rhythmic appearance of quartz veins and argillaceous materials (Plate 3A-D; Fig. 2).

3.2.2. Petrographic Description

MF-2 is a mostly prevailing dolomitization phenomenon. Dolomite crystals are fine to medium grained, anhedral-subhedral, and have suture contacts (Plate 3A). Occasionally, the dolomite rhombs have been micritized and devoid of internal structure (Plate 3A, B). The elongated muscovite flakes are distributed randomly throughout thin sections which indicate the continuous clastic input. Peloids are ~0.5mm to 1mm in size and constitute 40 to 45% of this microfacies (Plate 3D). Approximately uniform grain size and partially preserved structures within the peloids show that they are fecal in origin.

Ooids are the third dominant constituents that make up ~15% of the total rock volume and have been micritized up to some extent. Stylolites are also observed which are filled by iron oxides (Plate 3B). In some cases, the documented stylolite is characterized by the precipitation of authigenic minerals (iron oxides) forming stylolitic seams (Plate 3B). This Chemical compaction process causes a strong reduction in rock bulk volume, the thickness of sediments, porosity, and permeability (Wong and Oldershaw 1981; Tucker and Wright 1990 and Flugel 2004).

3.2.3. Environmental Interpretation

This microfacie represents the feature of high energy conditions such as siliciclastic input and ooids. According to Flugel (2004), ooids are important ancient environmental proxies for marine water energy, hotness/warmness, salinity, and water depths. The formation of ooids needs a high-level super-saturation with respect to Ca and CO_3 ions, the presence of nuclei, and high energy agitated conditions (Flugel, 2004). A close relationship existed between ooids formation and water depth. The ooids are formed in shallower water having a higher level of agitation (Jon, 2007). It is commonly believed that most ooid deposits originate in shallow water conditions which are regularly disturbed and agitated over a long time by tides, waves, and/or currents (Flugel, 2004). The presence of siliciclastic input and non-skeletal allochems ooids represent high energy conditions dominated by strong agitated waves and currents. While the existence of dolomite and associated peloids represents a supratidal condition. So, the interpreted geologic setting is shallow ranges from supratidal to beach area.

3.3. Dolomitic Packstone- Grainstone Microfacies (MF-3)

3.3.1. Outcrop Description

The MAF-3 is represented by samples AM 14, 15, and 16. While at the outcrop level these microfacies are dominated by grey coloured sandy dolomite with regular bedding of limestone. The dissolution cavities and butcher chop weathering are well documented in the Ambar Formation. Fractures observed in the studied rocks represent tectonic deformation in the region (Plate 3 A-B; Fig. 2).

3.3.2. Petrographic Description

The MAF-3 is represented by detrital sedimentary particles and the presence of pervasive dolomitization. Detrital sediments are represented by quartz and micas (Plate 4A). The quartz grains are anhedral to sub-hedral (Plate 4A, B) and constitute approximately 5 to 8%. Besides detrital grain and dolomite crystals, thin mud lamination is also noted in this microfacies. The mud is silty and fine grained in nature. Muscovite flakes are present

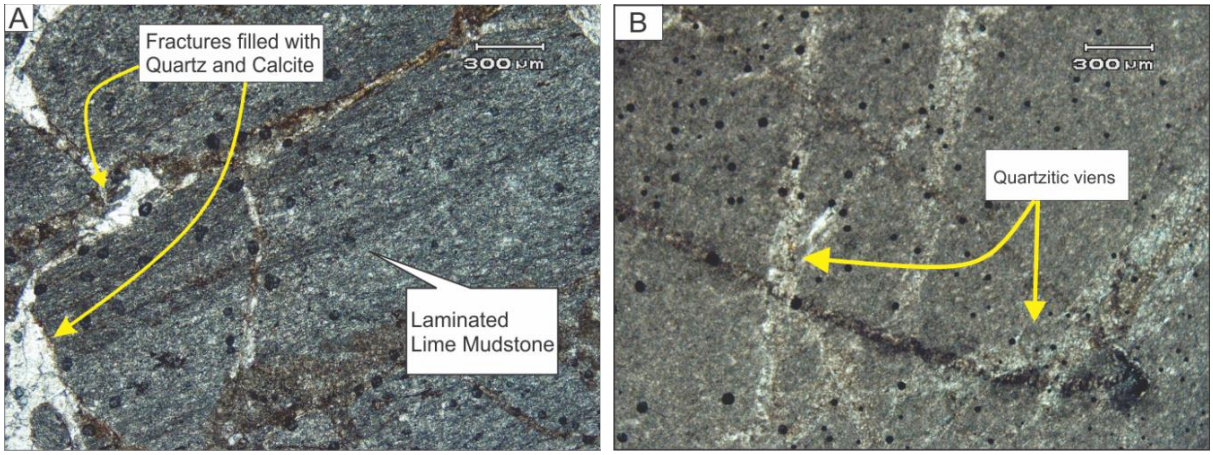

Plate 2 (A-B): Photomicrographs illustrating the details of Siliciclastic Mudstone Microfacies (MAF-1); (A) Fractures are filled with quartz and sparry calcite while the groundmass contains the laminated mud; and (B) Multiple quartz filled fractures (cross-polarized light).

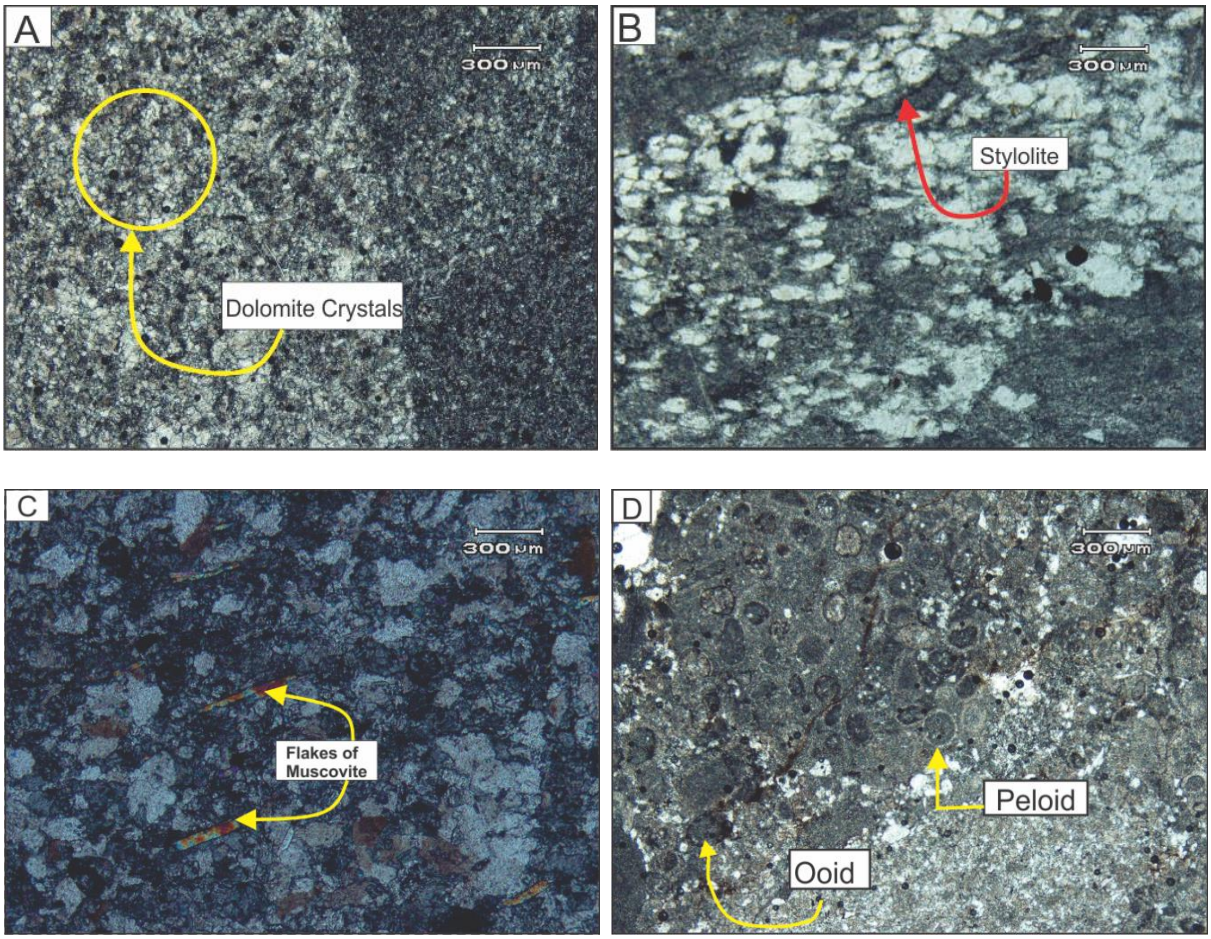

Plate 3 (A-D): Photographs illustrating Dolomitized, Peloidal, Ooidal Packstone Microfacies (MAF-2); (A) Dolomite crystals having suture contacts (Cross Polarized Light); (B) Muscovite flakes showing detrital nature; (C) stylolite; and (D) Ooid and Peloid.

and randomly disseminated throughout the exposed unit of the Ambar Formation (Plate 3C). Further, the iron leaching observed under the polarizing microscope shows oxidizing geologic conditions due to sub-aerial environmental exposure.

3.3.3. Environmental Interpretation

The occurrence of flaky mineral and clastic quartz shows the fluvial input, supplemented by alternate layers of silty material in this rock. On the basis of these results and rounded behaviour

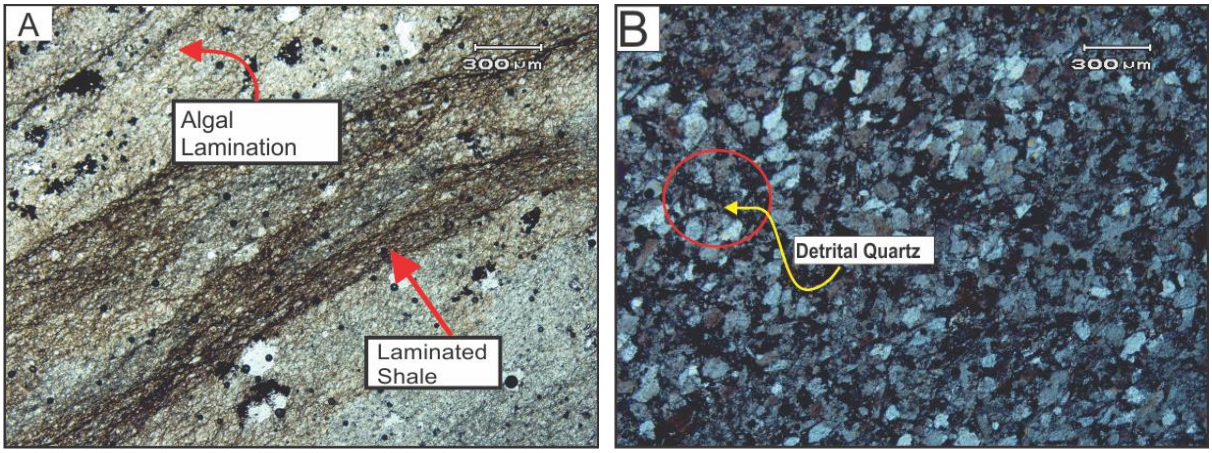

Plate 4 (A-B): Photomicrographs showing Laminated, Sandy Dolomitic Packstone-Grainstone Microfacies (MAF-3); (A) Algal lamination and laminated shale representing clastic input; and (B) Detrital quartz grains having rounded to sub-rounded nature (Cross Polarized Light).

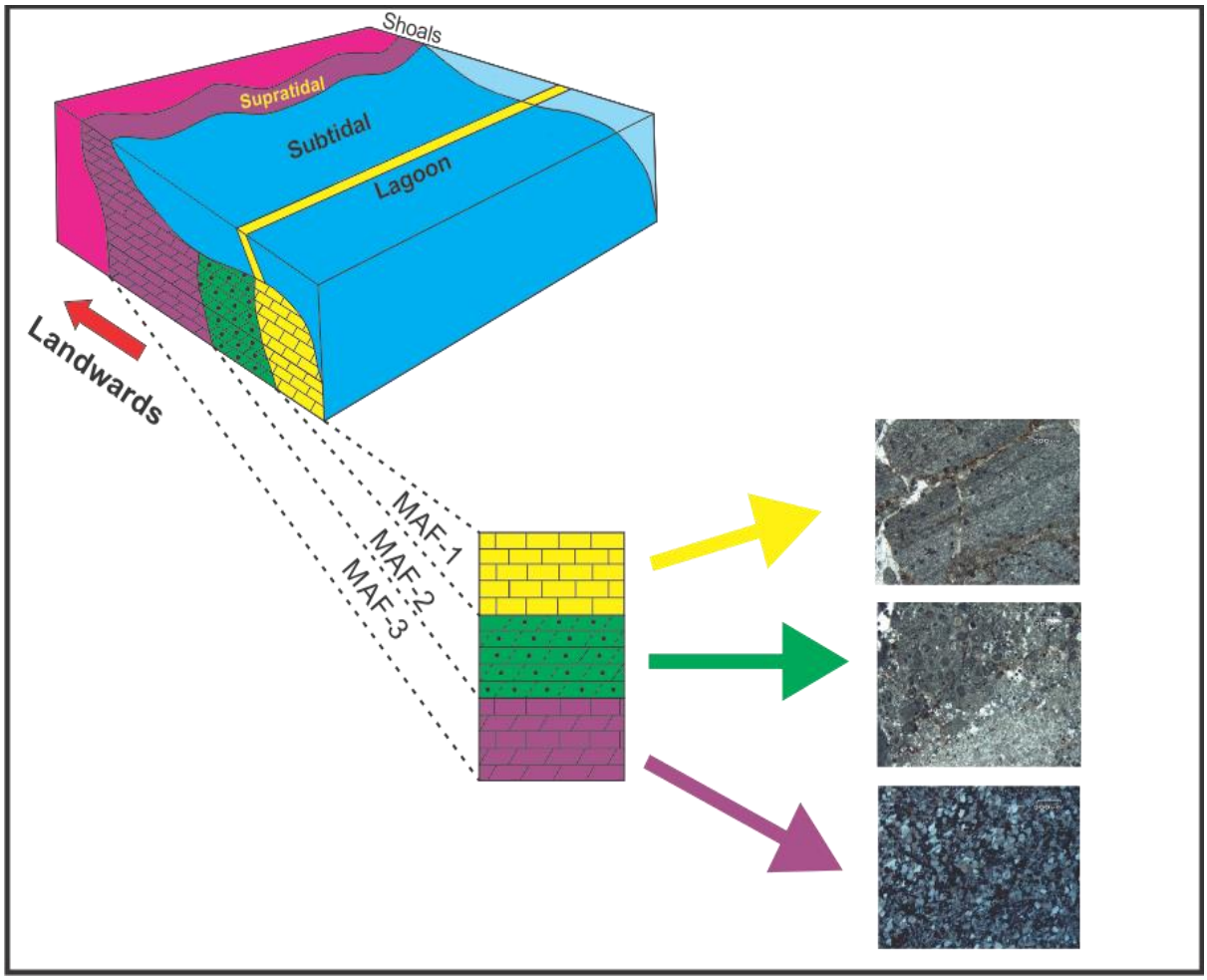

Fig. 3: Schematic depositional model for the Ambar Formation showing sub-environments with their respective microfacies.

of quartz grains, high energy near shoreline marine setting is interpreted as the depositional environment (Boggs 1995), while the presence of algal lamination and silty grain may range from subtidal (inner ramp) to intertidal settings (Scholle and Ulmer-Scholle 2003).

3.4. Depositional Model

The depositional model representing depositional setting for the Cambrian Ambar Formation is comprised of transitional to nearshore inner shelf environment. This interpretation is

grounded on microfacies studies under the polarizing microscope and their vertical continuation at the outcrop level. The lagoonal environment is designated by the limited flora and fauna, which is further supported by micritization that occurs mostly in the low energy environment. Similarly, the supratidal-subtidal depositional environment is suggested by siliciclastic input that demonstrates a highly agitated situation and proceeds to inner ramp condition. The transitional marine condition is characterised as a supratidal environment supported by flaky mineral and clastic quartz, with alternating layers of silty material assisting the process. In such carbonate-dominated settings local changes in topogeography, dissolution cavities, microstylolites, micritization, quartz and calcite veins are common phenomena. The stratigraphic differences from mudstone to packstone, as well as textural variations along constituent grains in various microfacies, reveal changes in energy settings (Fig. 3). The depositional model in current research is compared with the depositional model of Middle Cambrian Lower Zhangxia Formation, Xiaweidian, North China, and Middle Cambrian of Iran (Bayet-Goll et al., 2015; Zhang et al., 2020) showing almost the similar setting of shallow marine environments.

3.5. Conclusion

The detailed analysis from the petrographic characteristics and microfacies analyses leads to the important conclusion of samples from the Ambar Formation.

- In the current study, three microfacies are identified i.e. (1) Siliciclastic mudstone microfacies (2) dolomitized, peloidal, ooidal packstone microfacies (3) Laminated sandy dolomitic packstone-grainstone microfacies.
- The Ambar Formation is inferred to have formed in a carbonate-dominated, transitional to nearshore inner shelf marine, based on the microfacies identified.
- Dissolution cavities, calcite and quartz filled fractures, micritization, stylolites, dolomitization, and silicification are among the digenetic changes documented in the dolomite.

Acknowledgement

We appreciate the logistic and financial support provided by the Department of Geology, Bacha Khan University Charsadda. The authors also thank the Department of Geology, the University of Peshawar for thin section preparation.

References

Ali, K.A., Anwar, J., 1969. Stratigraphic studies of Nowshera reef complexes, Nowshera Tehsil, West Pakistan. Geological Bulletin University of Peshawar, 4, 33-43.

Ali, F., Haneef, M., Anjum, M.N., Hanif. M., Khan, S., 2013. Microfacies analysis and sequence stratigraphic modeling of the Samana Suk Formation, Chichali Nala, Trans Indus Ranges, Punjab, Pakistan. Journal of Himalayan. Earth Science, 46(1), 41-53.

Bayet-Goll, A., Chen, J., Moussavi-Harami, R., Mahboubi, A., 2015. Depositional processes of ribbon carbonates in middle cambrian of Iran (Deh-Sufiyan formation, central Alborz). Facies, 61(3), 9.

Boggs, S., 1995. “Principles of sedimentology and stratigraphy”. Prentice Hall, Englewood Cliffs, New Jersey, 79-93.

Davis, R.G., Ahmad, R., 1963. The orthoconic nautiloids of the Kala Limestone and the portable age of the Swabi formations. Geological Bulletin University of Peshawar, 3, 1-5.

Dunham, R.J., 1962. Classification of carbonate rocks according to depositional textures. Bulletin of American Association of Petroleum Geology, 1, 108-121.

Folk, R.L., 1959. Practical petrographic classification of limestone. Bulletin of American Association of Petroleum Geology, 43, 1-38.

Flugel, E., 1982. Microfacies Analysis of Limestone. Springer-Verlag, Berlin.

Flugel, E., 2004. Microfacies of carbonate rocks, analysis, interpretation and application. Springer, New York, 976.

Fuchs, G., 1975. Contributions to the geology of the north-western Himalayas. Geologische Bundesanstalt, 32.

Hussain, A., Pogue, K.R., Khan, S.R., Ahmad, I., 1991. Paleozoic stratigraphy of the Peshawar Basin, Pakistan. Geological Bulletin University of Peshawar, 104, 85-97.

Jon, 2007. University of Edinburgh, http://www.geologyrocks.co.uk/tutorials/ooid_formation.

Latif, M.A., 1970. Lower Carboniferous rocks near Nowshera, West Pakistan. Geological Society America Bulletin, 81, 1585-1586.

Le Fort, P., 1975. Himalayas: the collided range. Present knowledge of the continental arc. American Journal of Science, 275(1), 1-44.

Loucks, R.G., Longman, M.W., 1982. Lower Cretaceous Ferry Lake Anhydrite, Fairway Field, East Texas. Society of Economic

Paleontologists and Mineralogists, 3, 130-173.
Martin, N.R., Siddiqui, S.F.A., King, B.H., 1962. A geological reconnaissance of the region between the lower Swat and Indus River of Pakistan. Geological Bulletin Punjab University, 2, 1-13.
Pogue, K.R., Hussain, A., 1986. New light on the stratigraphy of the Nowshera area and the discovery of Early to Middle Ordovician trace fossils in N.W.F.P., Pakistan. Geological Survey of Pakistan Information Release, 135, 15p.
Prothera, D.R., Schwab, F., 2003. Sedimentary Geology: An introduction to sedimentary rock and stratigraphy. W.H. Freeman and company, New York.
Sibley, D.F, Gregg, J.M., 1987. Classification of dolomite rock texture. Journal of Sedimentary Petrology, 57, 967-975.
Stauffer, K.W., 1968. Silurian-Devonian reef complex near Nowshera, West Pakistan. Geology Society of America, 9, 1331-1350.
Scholle, P.A., Ulmer-Scholle, D.S., 2003. A color guide to the petrography of carbonate rocks: Grains, texture, porosity and diagenesis. (Memoir 77 (Vol. 77). Tulsa, Oklahoma U.S.A.: The American Association of Petroleum Geologists, 459.
Shah S.M.I., 2009. Stratigraphy of Pakistan. Geological Survey of Pakistan, Memoir, 22.
Teichert, C., Stauffer, K.W., 1965. Paleozoic reef in Pakistan: Science, 150, 1287-1288.
Tucker, M.E., Wright, V.P., 1990. Carbonate sedimentology. Blackwell Scientific Publication London, 10
Tucker, M.E., 2003. Sedimentary Rocks in the Field (3rd edition). Wiley, Chichester.
Wong, P.K., Oldershaw, A.E., 1981. Burial cementation in the Devonian Khyber reef complex, Alberta, Canada. Journal of Sedimentary Petrology, 507-520.
Wilson, J.L., 1975. Carbonate facies in geologic history - 471 pp., 183 Figs., 30 Pls., Springer-Verlag, Berlin Heidelberg, New York.
Zhang, X., Pang, X., Jin, Z., Hu, T., Toyin, A., Wang, K. 2020. Depositional model for mixed carbonate-clastic sediments in the Middle Cambrian Lower Zhangxia Formation, Xiaweidian, North China. Advances in Geo-Energy Research, 4(1), 29-42.

Driving Innovation in the Oil & Gas Industry

VGS

Vizdom GeoScience Suite

- Multidomain Integrated Platorm to perform interpretation on well logs data
- Designed to manage huge fields data
- Perform full-spectrum of interpretatioon workflows for various reservoir types with batch processing capacity
- Petrophysics, Reservoir Petrophysics, Geomechanics/unconventional and Artficial Intelligence
- Commercially Used by various Multinatonal Clients

Vizdom Geoscience Suite

VGS™ is a software platform powered by Vizdom solutions Pvt. Ltd for Petrophysicists, Geologists and Reservoir Engineers to interpret well logs data. Our Software has been designed to manage huge fields, to perform the full-spectrum of interpretation workflows for various reservoir types with batch processing capacity and full extensibility. VGS™ has been widely adopted by the Service Companies, Oil & Gas Operators and Independent Consultants as the best value offering versus cost.

CURRENT OFFERINGS

SINGLE TO MULTI-WELL PETROPHYSICAL SERVICES

- LQC, Depth matching and log editing
- Volumetric Formation Evaluation
- Environmental corrections for all service provider.
- Fluid Typing/ Rock Typing
- Cased hole Analysis (Sigma)
- Porosity Partitioning
- Thin bed Analysis
- MMSW (Multi Mineral FE Sequential Way)
- Log to Core Integration

Unconventional RESERVOIRS FORMATION EVALUATION

- Formation evaluations (A-Z).
- TOC estimation by using OH logs.
- Fracture reservoirs Formation evaluations
- Tight gas /shale gas reservoirs
- Geomechanics
- Overburden estimation.
- Pore pressure estimation by using OH logs with
- Rock failure criteria.
- Y, Bulk, Shear Modulus Estimation by using only
- DTCO and or DTSM

RESERVOIR PETROPHYSICS

- PC Modeling including
- (J-Leverett function, Corey-Brooks
- function, Thomeer function & Lambda function).
- Saturaion Height
- Formation Pressure data Analysis

MACHINE LEARNING

- Principal componenet analysis.
- Multi-Linear Regression
- Neural Network
- Fuzzy logic
- Monte Carlo Analysis

Geology and Geo-science

- Tight gas /shale gas reservoirs Formation evaluations (A-Z).
- Fracture reservoirs Formation evaluations including Fracture Porosity estimation (Unique feature of VGS)
- Carbonate reservoir characterization through MMSW and deterministic model (Unique feature of VGS).
- Thin beds analysis (Bulk analysis Approach)
- TOC estimation by using OH logs.
- Cased hole Water Saturation Analysis (Sigma) including Time laps.
- Prospect Generation.
- 2D/3D Seismic Interpretation.
- Resource assessment.
- Seismic attribute generation/analysis.
- Well/Seismic physical and digital Data Base Management.

PETROPHYSICS MODULE

- MMSW (Multi Mineral Sequential Way FE) Method for better Control on Petrophysical Parameters
- Calculates Volume of Clay/Bound Fluid & Effective Porosity followed by computing Water Saturation
- Contains 22 minerals covering all the Rock Types in the World

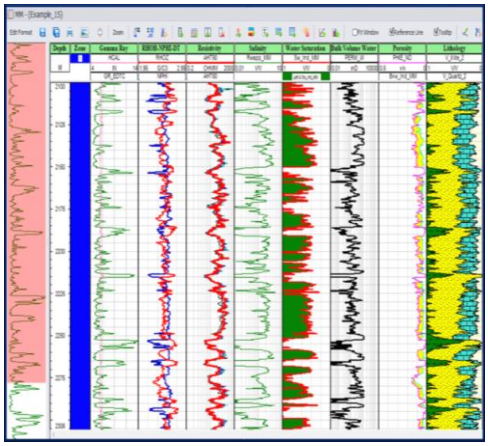

DETERMINISTIC CARBONATE ANALYSIS (UNIQUE IN VGS) AND MULTI WELL CORRELATION

- Deterministic Carbonate Model: A unique feature of VGS especially build for the Geology of Pakistan
- Performs Multi Wells Correlation in a Field
- The Lateral Variations of Facies and Petrophysical Properties of Limestone can be seen by Correlations between the example Wells.

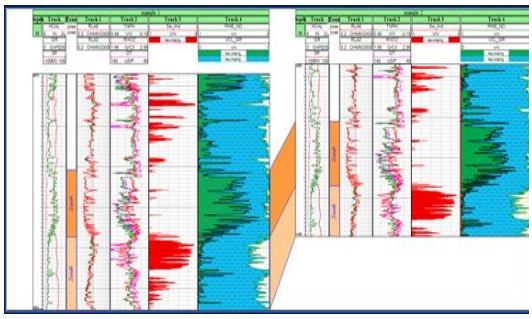

MULTI WELL CROSS PLOT

- Identify (Single to Multi wells) relationships in Well Data in the Same Field and against Same Formations
- Display Multiple Well Data on a Single Cross Plot that helps in Identification Data Patterns, Correlation and Lithologies.

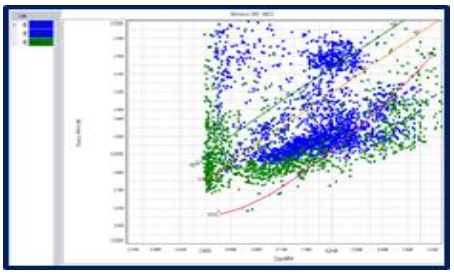

MULTI WELL HISTOGRAM

- Graphically summarize and display the distribution of a processed Data Set
- Display the values of GR, Sonic, SP, Density etc. of different Wells together in the same Plot to Correlate the value of each Log at every point in all Wells

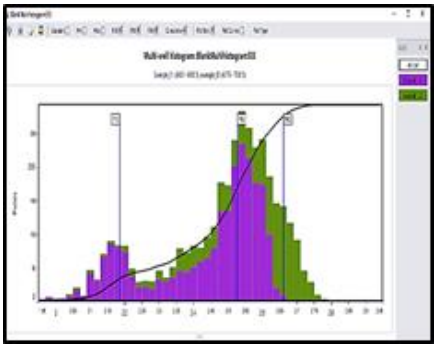

Unconventional SHALE/GAS FORMATIONEVALUATION WITH GEOMECHANICS COMPOSITE PLOT (A UNIQUE FEATURE OF VGS)

- Calculate Total Organic Content (TOC) by Open Hole Logs
- Input: Density, Sonic & Deep Resistivity Logs
- User Input Parameter: Cut Off (GR is used for cut off / no calculation zones); DT Lean Formation
- Allows user to calibrate the Result (Average or Max) TOC with Core Data.
- Output template has user friendly display.
- Calculate Young Modulus, Shear Modulus and Bulk Modulus

- Input: DTCO & Formation Density Logs. (If DTSM measured is available then it will also be used in input otherwise VGS will use VPVS Method or Castangna Method to estimate DT Shear
- Fracture Gradient of the Rock and Pore Pressure is estimated by using Geomechanics module.

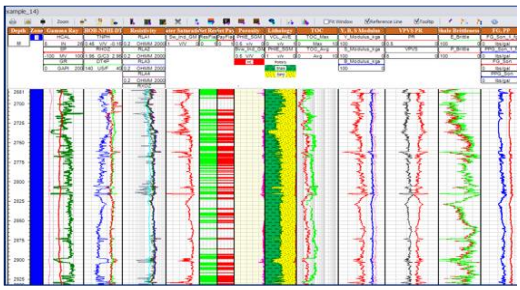

FRACTURE POROSITY MODULE

- This is a unique feature of VGS which can estimate fracture porosity from Openhole log.
- For using the fracture porosity module, the pre-requisite input parameters i.e. Porosity have to be estimated by deterministic or MMSW (VGS) method. Carbonate Fracture Model estimate fractures from OH logs data.
- The block porosity is estimated first. The raw resistivity log RxoZ and Sonic log are the inputs. Alpha processing with Robust 3000 attrition, with 3 seeds Monte Carlo engine is done and the software models fracture porosity.

GEO-MECHANICS MODULES

- As per the published numbers worldwide clients are facing drilling problems and 40% loss time is related to geomechanical issues.
- Most of the geomechanical studies were inconclusive because in most of the old wells shear data was missing
- After Extensive R&D Vizdom solutions used modified Henry Castagna published equation and results were extra ordinary. The Estimated shear vs measured shear matched >96%.
- Only compression sonic data is required as input.
- If Bulk , shear and Young modulus, UCS are required then input is Density and sonic compressional.

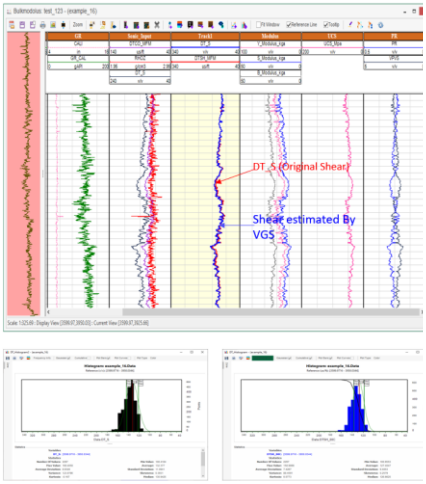

Our Mission

Our Mission is optimization of oil industry cost structure by using state of the art technologies & expertise, supporting our clients to maintain profit margins at any time through our unique solutions & workflows backed by industry known experts.

Our visibility is not limited to Oil & gas sector only, our social responsibilities will always remain high

We are unique

Being first Pakistan's company launching Subsurface & drilling software platforms , VGS & VDS respectively.

Business consulting services , from contract negotiation to 3rd party audits.

We are expert in unconventional (Shale gas/ tight gas) reservoirs , our technical domain experts has worldwide expertise.

Optimization of cost / bbl, improve operational efficiency and increase HC production . We have conducted more than 10 high value projects worldwide, which will be replicated in Pakistan.

Your Success
Is Our Priority!

Vizdom Solutions
Oil and Gas Services

Vizdom Solutions (Pvt) Ltd.

Office:
104-A, Service Road East,
G-13/4, Islamabad, Pakistan

Phone: +92 51 8318671-72

Web: www.vizds.com

CONTACT

Institute of Geology
University of Azad Jammu and Kashmir
Muzaffarabad - 13100
Azad Jammu and Kashmir, Pakistan
Phone: +92-5822-960413
Email: geology@ajku.edu.pk

Principal Contact

Dr. Muhammad Basharat
Institute of Geology
Phone: +92-5822-960413
Email: editorin.chief.kjg@ajku.edu.pk

Support Contact

Fahad Hameed
Phone: +92-346-5550131
Email: editor.kjg@ajku.edu.pk

The Kashmir Journal of Geology (KJG) can be accessible through
www.kjg.ajku.edu.pk

The guidelines for authors are available at
www.kjg.ajku.edu.pk/index.php/journal/AuthorGuidlines

Publisher: Institute of Geology, University of Azad Jammu and Kashmir, Muzaffarabad, Pakistan